

Report FR 11453

LEVEL III

(12)

**DEVELOPMENT OF MAINSHAFT HIGH SPEED
CYLINDRICAL ROLLER BEARINGS FOR
GAS TURBINE ENGINES**

ADA 073381

Pratt & Whitney Aircraft Group
Government Products Division of
United Technologies Corporation
West Palm Beach, Florida 33402

DDC
RECEIVED
AUG 1978
RECEIVED

October 1978

Interim Report for Period 1 April 1977 - 1 October 1978

Approved for Public Release: Distribution Unlimited

DDC FILE COPY

Naval Air Propulsion Center
1440 Parkway Avenue
Trenton, New Jersey 08628
and
Air Force Aero Propulsion Laboratory
Wright-Patterson AFB, Ohio 45433

71

79 08 29 033

UNCLASSIFIED

SECURITY CLASSIFICATION OF THIS PAGE (When Data Entered)

REPORT DOCUMENTATION PAGE		READ INSTRUCTIONS BEFORE COMPLETING FORM
1. REPORT NUMBER	2. GOVT ACCESSION NO.	3. RECIPIENT'S CATALOG NUMBER
4. TITLE (and Subtitle) Mainshaft High-Speed Cylindrical Roller Bearings for Gas Turbine Engines		5. TYPE OF REPORT & PERIOD COVERED Technical Report (Interim) 1 April 1977 to 1 October 1978
7. AUTHOR(s) P. F. Brown, J. D. Robinson L. J. Dobek, J. R. Miner		6. PERFORMING ORG. REPORT NUMBER FR-11453
9. PERFORMING ORGANIZATION NAME AND ADDRESS United Technologies Corporation Pratt & Whitney Aircraft Group Government Products Division West Palm Beach, Florida 33402		8. CONTRACT OR GRANT NUMBER(s) N00140-76-C-2383 AF MIPR-FY-14557600623
11. CONTROLLING OFFICE NAME AND ADDRESS Naval Air Propulsion Center 1440 Parkway Avenue Trenton, New Jersey 08628		10. PROGRAM ELEMENT, PROJECT, TASK AREA & WORK UNIT NUMBERS 62241N WF41-401
14. MONITORING AGENCY NAME & ADDRESS (if different from Controlling Office)		12. REPORT DATE October 1978
		13. NUMBER OF PAGES 12/100
		15. SECURITY CLASS. (of this report) Unclassified
		15a. DECLASSIFICATION/DOWNGRADING SCHEDULE
16. DISTRIBUTION STATEMENT (of this Report) Approved for public release: distribution unlimited		
17. DISTRIBUTION STATEMENT of the abstract entered in Block 20, if different from Report 1 Oct 78		
18. SUPPLEMENTARY NOTES		
19. KEY WORDS (Continue on reverse side if necessary and identify by block number)		
<ul style="list-style-type: none"> ● Cylindrical Roller Bearing ● Dynamics ● Gas Turbine Mainshaft Roller Bearing ● High-Speed Roller Bearing ● Roller Bearing Design and Simulation System ● Roller End Wear 		
20. ABSTRACT (Continue on reverse side if necessary and identify by block number)		
<p>This combined analytical and experimental program is aimed at generating a manual that will permit the design of 3.0 MDN cylindrical roller bearings. The roller bearing analysis will be correlated with the results from a series of bearing tests designed to determine, by statistical methods, the effect of geometrical variables on bearing performance. An existing quasi-static design optimization system was previously upgraded and the basic analyses for use in developing a program to predict the dynamic behavior of roller bearing components was completed. A study</p>		

DD FORM 1 JAN 73 1473

EDITION OF 1 NOV 65 IS OBSOLETE

UNCLASSIFIED

S N 0102-LF-014-6601

SECURITY CLASSIFICATION OF THIS PAGE (When Data Entered)

342 67

UNCLASSIFIED

SECURITY CLASSIFICATION OF THIS PAGE (When Data Entered)

identified a total of thirty separate bearing parameters that can influence roller skewing and skidding. Two groups of 124 mm roller bearing designs were then prepared using statistical design techniques and incorporating parameters from the list of thirty. Fabrication of full-scale bearing hardware was completed and testing was completed. Results indicate that roller end wear is significantly affected by roller corner radius runout.



S/N 0102- LF-014-6601

UNCLASSIFIED

SECURITY CLASSIFICATION OF THIS PAGE (When Data Entered)

SUMMARY

This combined analytical and experimental program is aimed at generating a manual that will permit the design of cylindrical roller bearings capable of operating reliably at 3.0 MDN.

The analytical effort during Phase I focused on three main areas. The first area was concerned with upgrading a roller bearing optimization analysis and computer program. This was based on a quasi-static approach and was completed and reported on in Section IV of the first interim report covering the period 1 October 1975 to 1 April 1977.

The analytical effort for this reporting period has been primarily concerned with two areas; the continuation of work on the dynamic simulation and prediction system, and the development of the computer program. Initial work associated with these two areas was described in Sections V and VI of the first interim report. During this reporting period, several force models were refined. The module STATIC was completed and incorporated into TRIBO 1. Model validation test cases were run for the CADYN module. In addition, improvements were made to models in RODYN and SYSDYN which allow a more accurate analysis of roller and cage dynamics.

The experimental portion of this program is aimed at evaluating the influence of geometric, tolerance, design, and operational parameters on the skidding and skewing wear characteristics of 124mm roller bearings operating at speeds of 1.0 to 3.0 MDN. During the period of the first interim report a study was completed in which a total of 30 separate bearing parameters that influence roller skew and skid were identified. Two groups of bearing designs, labeled N and AF, were then prepared using statistical design techniques and incorporating parameters from the list that could be varied in a sensible manner. The Group-N bearings consist of eight separate designs which permit the quantification of the influence of seven individual bearing parameters on roller skid and skew. The Group-AF bearings consist of five bearing designs which enable four additional parameters to be studied. Bearing test hardware was procured and testing initiated. During this report period testing was completed on both the Group-N and AF bearings. Five of the nine Group-N bearings performed in a stable manner over the entire range of conditions tested while the remaining bearings failed due to excessive roller wear. Four of the five Group-AF bearings tested performed in a stable manner. The fifth bearing failed during testing as a result of an inner ring fracture. Also, a 3.0 MDN prototype bearing was designed during this report period and will be evaluated in a 60 hour rig test. Fabrication of the prototype bearing is in progress.

TABLE OF CONTENTS

	<i>Page</i>
1. INTRODUCTION.....	1
1.1 Background.....	1
1.2 Program Approach.....	3
1.3 Program Scope.....	3
2. CONCLUSIONS AND RECOMMENDATIONS.....	5
2.1 Conclusions.....	5
2.2 Recommendations.....	5
3. DEVELOPMENT OF THE DYNAMIC SIMULATION AND PREDICTION SYSTEM.....	7
3.1 Roller End Viscous Shear Resistance Model.....	7
3.2 Elastic Impact Contact Model.....	15
3.3 Cage Mass Moment of Inertia.....	16
3.4 Roller Dynamics Wear Model.....	19
4. DEVELOPMENT OF THE COMPUTATIONAL SYSTEM.....	22
4.1 STATIC Program Module.....	22
4.2 CADYN Program Module.....	24
4.3 RODYN Program Module.....	26
4.4 SYSDYN Program Module.....	36
5. FUTURE WORK.....	41
6. PARAMETRIC AND VERIFICATION TESTING - TASK II.....	42
6.1 Summary of Previous Progress.....	42
6.2 Group-N Bearing Parametric Tests.....	49
6.3 Summary of Group-N Bearing Tests.....	56
6.4 Statistical Analysis of Group-N Wear Results.....	60
6.5 Group-AF Bearing Tests.....	67
6.6 Summary of Group-AF Testing.....	77
6.7 Statistical Evaluation of the Group-AF Bearing Wear Results.....	77
6.8 Statistical Analysis of Composite Group: Groups N and AF Wear Results Combined With P&WA Data.....	81
7. SIXTY HOUR DEMONSTRATION TEST - TASK III.....	85
8. PLANNED EXPERIMENTAL PROGRAM.....	86
8.1 Prototype Bearing Test.....	86
8.2 Experimental Evaluation of Bearing No. 10.....	86
8.3 Model Check Bearing Test.....	86
REFERENCES.....	87

LIST OF ILLUSTRATIONS

<i>Figure</i>		<i>Page</i>
1	Eccentric Roller End Wear.....	2
2	Typical Bearing Failure Attributable to Eccentric Roller End Wear.....	2
3	Viscous Shear Model Force and Moment System for Roller End/Guide Flange Interface.....	8
4	Shear Element Due to Relative Sliding.....	9
5	Velocity Distribution Due to Relative Sliding.....	10
6	Shear Stress Resulting from Rotation of Roller Relative to Cage Siderail.....	12
7	Net Forces and Moments on Roller End and Cage Siderail Due to Viscous Shear.....	14
8	Contact Model Determines Impacting Roller.....	17
9	The x-Axis Intersects the Number One Cage Pocket.....	18
10	Front and Rear Cage Pocket Azimuth Angles.....	19
11	Reducing Cage Mass Increases Minimum Film Thickness.....	26
12	CADYN Shows Fluid Shear Increases Minimum Film Thickness.....	27
13	The Roller/Guide Flange Finite Element Breakup Model Uses Triangular Elements Compatible With the Sector Shape of the Interface Region.....	29
14	The Cage Siderail Finite Element Model Also Uses Triangular Elements for the Calculation of the Hydrodynamic Force on It.....	30
15	The Calculation of the Hydrodynamic Forces on the Roller Requires a Knowledge of the Components of the Velocity Vector at Each Node in the Finite Element Breakup.....	31
16	Film Thickness Varies Due to Roller Skew and Guide Flange Layback Angle.....	31
17	Coordinate System Used to Locate Roller Unbalance.....	33
18	The Traction Force, \bar{F}_t , Is Applied at an Axial Position, \bar{r} , Located at the Center of Pressure of the Contact Ellipse.....	34
19	The Local x-Axis of the k^{th} Roller Is Oriented Such That Its Euler Angle ψ_k is Equal to the Roller's Angular Location η_k Within the Complement.....	35
20	2-D SYSDYN Shows No Cage Land Contact When Rollers Interact With Cage.....	37
21	CADYN Shows Motion of Cage Unaffected by Rollers.....	38

LIST OF ILLUSTRATIONS (Continued)

<i>Figure</i>		<i>Page</i>
22	2-D SYSDYN Shows Peak Roller Loads as Roller Enters Load Zone.....	39
23	Hydrodynamic Forces Are Sufficient To Prevent Roller/Cage Contact for 2-D Motion.....	40
24	This Basic Bearing Used for Parametric and Verification Testing Has Seen Extensive Use in the TF30 Engine.....	43
25	Group-N Bearings Are Designed To Evaluate Two Levels of Each Parametric Variable.....	44
26	Group-AF Bearings Are Designed To Evaluate Two Levels of Each Parametric Variable.....	45
27	Test of Group-N Bearing No. 4 Shows Increased Skid as Load Is Decreased but With No Skid at Any Load Beyond 2.75 MDN.....	50
28	Group-N Bearing No. 4 Shows No Distress or Unusual Wear After Test.....	52
29	Test of Group-N Bearing No. 5 Shows Increased Skid as Load Is Decreased but With No Skid at Any Load Beyond 2.75 MDN.....	53
30	Group-N Bearing No. 5 Shows No Distress or Unusual Wear After Test.....	54
31	Testing of Group-N Bearing No. 1 Terminated as a Result of Cage Failure...	55
32	Eccentric Roller End Wear Noted on Group-N Bearing No. 3 Prior to Failure	57
33	Testing of Group-N Bearing No. 3 Results in Roller Skew Related Failure at 2.5 MDN.....	58
34	Group-N Bearing No. 8 Cage Failure Results from Roller Skewing.....	59
35	Roller Weight Loss Results from an Increase in Roller Corner Radius Runout	63
36	Roller Weight Loss Results from a Decrease in Roller End Squareness.....	64
37	Roller Weight Loss Results from a Decrease in Inner Race Taper.....	65
38	Roller Weight Loss Results from a Decrease in Roller Flat Offset.....	66
39	Roller Static Skew Angle Increase Results from an Increase in Roller Corner Radius Runout.....	68
40	Group-AF Testing Shows That Increasing Load Has a Slight Effect on Bearing Heat Generation Whereas Increasing Oil Flow Significantly Increases Bearing Heat Generation.....	70
41	Group-AF Bearing No. 22 Shows No Distress or Unusual Wear After Test....	71

LIST OF ILLUSTRATIONS (Continued)

<i>Figure</i>		<i>Page</i>
42	Inner Ring of Group-AF Bearing No. 21 Fractures During Testing at 2.75 MDN	73
43	Increasing Oil Flow of Group-AF Bearing No. 23 Increases Rig Horsepower and Decreases Outer Ring to Inner Ring Temperature Differential.....	74
44	Group-AF Bearing No. 23 Shows No Distress or Unusual Wear After Test....	75
45	Group-AF Bearing No. 24 Shows No Distress or Unusual Wear After Test....	76
46	Group-AF Bearing No. 25 Shows No Distress or Unusual Wear After Test....	78
47	Group-AF Bearing Testing Indicates Similar Heat Generation and Outer Ring to Oil Inlet Temperature Differential for All Designs.....	79
48	Group-AF Bearing Testing Indicates Similar Rig Horsepower and Outer Ring to Inner Ring Temperature Differential for All Designs.....	80
49	Roller Bearing Variables Experimentally Evaluated in Full-Scale Bearing Tests.....	82

LIST OF TABLES

<i>Table</i>		<i>Page</i>
1	CADYN Test Results.....	25
2	FERFI Test Results.....	33
3	Group-N Bearings — Manufacturing Inspection Data.....	46
4	Group-AF Bearings — Manufacturing Inspection Data.....	47
5	Group-N Bearings — Pretest Wear Related Measurements.....	47
6	Calibration and Endurance Test Program.....	48
7	Group-N Bearings — Pretest Rig Related Inspection Measurements.....	50
8	Roller Weight and Skew Angle Wear Data for Group-N Bearings.....	60
9	Group-N Bearings — Roller Weight Change.....	61
10	Group-N Bearings — Roller Static Skew Angle Change.....	62
11	Roller Wear Results from Group-N and P&WA Tests.....	63
12	Pretest Roller Wear Related Measurements for the Group-AF Bearings.....	69
13	Pretest Rig Related Inspection Measurements for the Group-AF Bearings....	69
14	Roller Weight and Skew Angle Wear Data for Group-AF Bearings.....	81
15	P&WA Parametric Bearing Designs Tested.....	83
16	Effect of Independent Roller Bearing Variables on Wear.....	84
17	Limits of the 3.0 MDN Prototype Bearing Design Compared to Baseline Bearings.....	85

1. INTRODUCTION

1.1 Background

The higher thrust-to-weight ratios required for advanced aircraft turbine engine designs demand increased rotational speed of the turbines and compressors. The design and development of such turbomachinery is often complicated by bearing considerations. The rotor and rotor support systems are generally characterized by high shaft speeds to achieve maximum gas dynamic performance, minimum size, and minimum weight; flexible bearing support structures for light weight and minimum disruption of the flowpath by interdiction of struts and vanes; and large shaft diameters for high bending and torsional stiffness. These factors result in bearing specifications which require high bearing DN levels and high misalignment capability. It is anticipated that speed levels to 3.0 MDN (million DN) will be required for engines in the 1980-1990 time frame.

Considerable effort has been expended by investigators on upgrading the performance of high DN ball thrust bearings, and this effort has produced many tens of thousands of hours of operating time at 3.0 MDN under laboratory conditions. Ball thrust-bearing technology has evolved to where material considerations determine the life limits of the design. However, the technology base needed for the design of optimum roller bearings to meet high DN requirements is not well defined. In many cases, roller bearing performance has been the limiting factor in the design of high speed rotor systems because of a lack of understanding of certain aspects of roller bearing behavior. There is good reason for this. The increased susceptibility of roller bearings to fail has surfaced in relatively recent times. Ever increasing engine rotational speeds have driven bearing speeds up to DN levels which serve to intensify the influence of geometric variations and other parameters on roller dynamics. Evidence accumulated in the field, and data obtained in development tests, indicate that bearing performance is very sensitive to roller instabilities.

These instabilities occur frequently in high DN bearings and cause roller skewing. The characteristic failure mode which identifies roller skew is rapid eccentric wear on the end surfaces of some or all of the rolling elements of a bearing. Figure 1 shows the eccentric wear pattern on one end of a roller, with the other end having a similar pattern but 180 degrees out of phase. This condition can exist undetected until bearing failure occurs. Figure 2 shows a typical example of bearing failure precipitated by eccentric end wear of one roller element.

Related to skewing, and apparently influenced by many of the same forces which induce it, is roller skidding. When rollers skid, the resulting damage is particularly severe on the rolling contact surfaces and, subsequently, has an adverse effect on bearing durability. Currently, skidding is considered to be of secondary importance compared to roller end wear. This conclusion is based upon considerable field service experience. Data indicate that roller end wear failures predominate. The mechanisms that cause skidding are more readily understood, and inherent in this understanding is the suggestion for its control. It is well known that roller skidding occurs when bearing radial loads are light and rotational speeds are high. A concept commonly used to supplement the external load is a two-point radial preload design. This basic preload system, which is achieved by machining the outer ring OD in an out-of-round oval shape combined with a slight interference fit in the bearing housing, adds enough load to keep the rollers "in gear" around most of the bearing's circumference. However, as speeds increase, the ability to maintain control of the internal clearance needed to ensure operation free of skidding damage becomes increasingly dependent upon accurate knowledge of the internal heat generated by the bearing. This factor, coupled with the cooling system design, determines the operating temperature level of the bearing and, more importantly, the temperature gradient from the inner to the outer raceway. Thus, an accurate knowledge of the heat generated is a necessity if adequate control of operating clearance is to be achieved so that roller loading is maintained at a level that successfully inhibits roller skidding.



Figure 1. Eccentric Roller End Wear

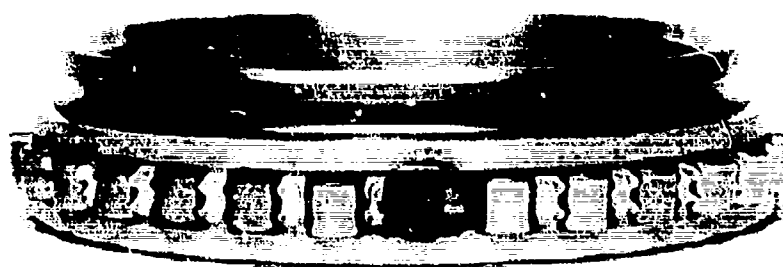


Figure 2. Typical Bearing Failure Attributable to Eccentric Roller End Wear

Of course, there are other modes of engine roller bearing failure beside those attributable to end wear and skidding. Some of these modes are identifiable with the cage and others may be due to roller edge loading causing premature fatigue spalling. However, it appears highly likely that if the basic roller end wear problem — as influenced by skewing action — can be avoided, a large measure of the solution to other root problems can be effected. This becomes largely self-evident upon study of the long list of geometric, dimensional, tolerance, quality, and operational parameters which influence and control roller tracking forces. A design system which provides identification and regulation of these factors will provide a means for establishing the entire bearing design. For these reasons, this system must go beyond a quasi-static analysis and must address roller bearing dynamic behavior.

1.2 Program Approach

As indicated, future engine design requirements dictate roller bearing DN levels to 3M. Therefore, to achieve this DN level, roller bearing technology must be upgraded in time for its utilization in engines slated for operation in the 1980-1990 time frame. The schedule to develop bearings to meet the 3 MDN requirement calls for an extension of the present state-of-the-art of bearing design and requires considerable analytical and experimental effort to investigate the effects of increased DN levels on many critical design parameters. In addition to the conventional parametric studies involving fatigue life, stresses, temperature, fits, clearances, alignment, lubrication and rotor dynamic response, special attention must be given to roller skidding and skewing motions which have been identified as likely problem areas for high DN operation. Proper analysis of these effects requires development of a new computer program which considers the complete dynamic motion of each element in the roller assembly.

Effort under this program is being directed toward formulating a viable generalized roller bearing analytical design system that considers a number of geometrical and operational parameters. This development program is based on an integrated analytical/experimental effort. The resultant design system, in the form of a complete computer program, is intended to provide the bearing design engineer with a useful tool for studying the static as well as dynamic characteristics of high DN roller bearings for future aircraft engine mainshaft applications. The design system will be useful in conducting analytical experiments under simulated operating conditions. A parametric study utilizing a reliable analytical design system could establish basic design criteria, help to separate the important variables from the unimportant ones, predict the effect of each controllable design factor, and could substantially reduce the number of costly test programs in the early phase of new bearing development. It could also be used to assist in the diagnosis of roller bearing failures in service engines.

1.3 Program Scope

The work being performed under this contract includes both analytical and experimental activity. Under Task I, a computer program which describes the roller bearing dynamics, loads, stresses, deflections, deformations, thermal conditions, heat generation, lubrication, and operating parameters will be developed. In Task II, experimental rig tests will be conducted on a group of 124 mm bore roller bearings to define the influence of geometric and operating variables and to verify the accuracy of the computer program. The computer program will be refined as necessary to reflect the test results. Also, results from other planned experimental testing which will address a separate group of roller bearing variables will be used to further refine the model. In Task III, the information developed under Tasks I and II will be used to design and fabricate a prototype bearing and conduct a demonstrator rig test having a goal of 60 hours operation over a range of DN values from 2.2 to 3.0M. In Task IV, the results of Tasks I through III will be incorporated into a design manual for high-speed cylindrical roller bearings. The manual will include the computer program developed in Task I and modified during subsequent

tasks. These tasks also include parametric testing on an additional group of roller bearings containing different bearing variables than those studied in Task II. The test results from this added testing will be used to further refine the analytical model developed under Task I. The work also includes installation of the computer program at the Wright-Patterson Air Force Base computer facility.

2. CONCLUSIONS AND RECOMMENDATIONS

2.1 Conclusions

The program development process continues to yield new insights into methods of analysis and bearing dynamic behavior. Some of the more important are:

- Extensive refinement of the program and replacement of previously developed subroutines with more effective versions has resulted in improvements in both accuracy and efficiency. This program improvement process has been facilitated by the modular organization of the program.
- Preliminary results from the computer analysis indicate that a large number of contacts between the roller and/or the cage and/or guide flanges is to be expected. As a result it is concluded that the method employed for handling the contact model will have a significant impact on overall program running time.
- Modeling the actual deformation resulting from the dynamics of impact at the guide flange is not feasible due to the excessive computation time required which is a direct result of the need to use extremely small time steps. The alternative approach calculates the post impact velocities without resorting to time-consuming computation methods.
- Cage web flexibility does not significantly affect the roller to cage web impact load magnitude for point contacts near the web root. Line contact between the roller and web does have an effect on cage web stress. This mode of contact, however, is unlikely to occur for general three-dimensional roller motion.

Conclusions that can be drawn based on experience accumulated in the experimental portion of this program are:

- Test time and conditions produced roller end wear of sufficient magnitude to allow statistical correlation to the test parameters.
- Although a wide range of roller wear was experienced for the parametric test bearings, similar thermal characteristics were measured for each bearing.
- Extreme amounts of roller slippage result in unusual thermal behavior of the bearing nor did it result in skid damage or distress in this test environment and duration.
- Increasing coupled roller corner radius runout has the most significant effect on increasing roller wear and resultant skew angle limits.
- Increasing roller end clearance and L/D ratio have a significant but lesser effect than corner radius runout on roller wear and skew angle increase. The effect in both instances is to increase roller wear.

2.2 Recommendations

Based upon the above conclusions the contractor makes the following recommendations:

- It is recommended that additional methods for reducing computation time be sought and applied to TRIBO 1.

- Upon completion of the program as presently defined, it is recommended that sensitivity studies be performed to determine the effect of certain assumptions and the influence of program iteration tolerances on running time. This knowledge would allow program running time to be minimized.
- Bearing temperature monitoring should not be relied upon as a method to detect roller wear.
- Roller corner radius runout should be maintained at the lowest possible level in high-speed roller bearings.
- The lower levels of both roller L/D ratio and end clearance that were evaluated should be incorporated in future high-speed cylindrical roller bearing designs.

3. DEVELOPMENT OF THE DYNAMIC SIMULATION AND PREDICTION SYSTEM

The fundamental elements in the dynamic simulation and prediction system consist of analyses to determine all forces acting on the bearing cage and rollers, including those due to contact between the inner ring and the cage, the rollers and the cage, and the rollers and the inner race, as well as analyses to determine dynamic behavior of the cage/roller system under the action of the external forces.

The first interim report described analyses for determining certain forces that act on the roller and presented preliminary methods for calculating roller-to-race contact forces and roller-to-cage contact forces. The equations of motion and the general coordinate systems were discussed for both the rollers and the cage.

The following sections describe analyses of the remainder of the roller/cage forces that are of significance as well as refinements and updates for analyses of some of the forces previously discussed.

3.1 Roller End Viscous Shear Resistance Model

In the first interim report, consideration was given to the fluid shear forces and moments imposed on the roller cylindrical surface as a result of its proximity to the cage web. The interaction of the roller end surfaces with the cage and guide flange also produces forces and induces moments on the roller due to shearing of the interposed lubricant film. The magnitude of these forces and moments is influenced by the type of lubrication acting at these interfaces; that is full film, boundary, or dry. Because hydrodynamic normal forces tend to keep the surfaces separated, the current analysis assumes that full film lubrication is the predominant form of lubrication existing during high-speed operation. The forces and moments generated are therefore due to viscous shearing of the oil. The damping effects of these viscous shear forces on the roller ends can significantly affect the roller dynamic motion. In addition, a portion of the total bearing internal heat generation is due to the energy dissipated in overcoming this viscous shear resistance.

The net relative velocity between the roller end and either the guide flange or cage siderail is treated in this analysis as being the result of a combination of both translational motion of the roller center due to rotation about the bearing axis and rotation of the roller about its own center. The viscous shear forces and their line of action are dependent upon the roller angular velocity ω_r , the lubricant film thickness h , and viscosity μ , as well as the geometry of the surfaces. Shear forces arising from centripetal acceleration of the lubricant due to cage and roller rotation are not considered. The approach used in this analysis is to superimpose the solution for Couette flow between parallel plates on the solution for a free rotating disk in a viscous fluid (Ref. 1). How this was done in the present analysis will be illustrated first for the interface between the roller end and the inner race guide flange, and then for the interface between the roller end and the cage siderail.

3.1.1 Roller End to Guide Flange Interface

Figure 3 shows a schematic of the roller end and guide flange interface, where the roller has been fixed in space and the guide flange moves past it with a relative translational velocity. Lubricant flowing through this region is subjected to shearing due to both roller angular velocity and roller-to-flange relative sliding. It has been assumed that these effects can be considered independently with the total effect of velocity then determined by superposition. It is further assumed, for the purpose of this analysis, that the lubricant viscosity is constant, the flow is laminar, and that the shear stress in the interface is unaffected by variations of local film thickness caused by roller skewing.

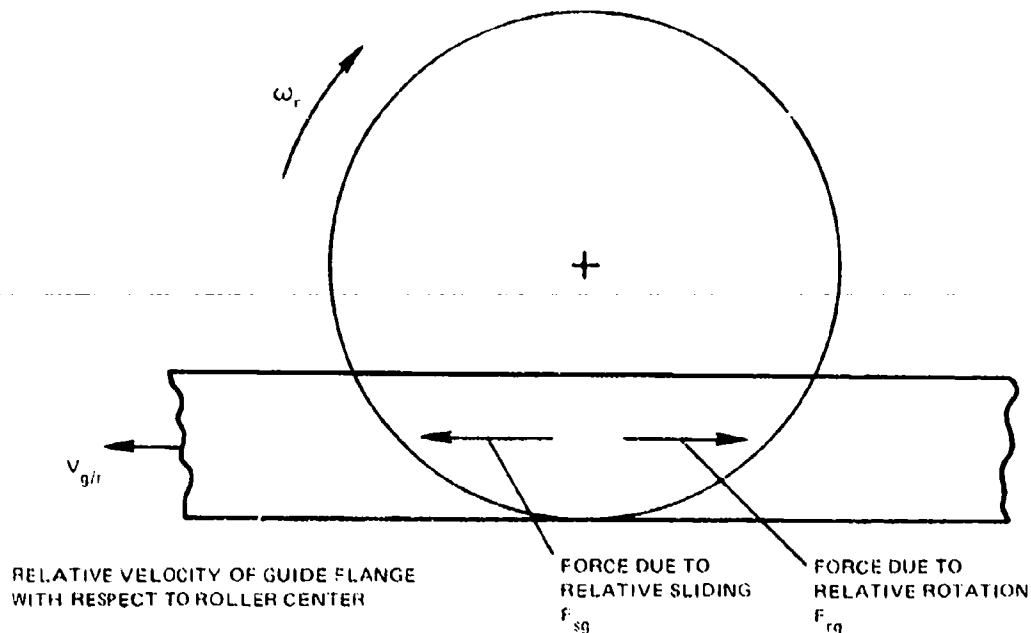


Figure 3. Viscous Shear Model Force and Moment System for Roller End/Guide Flange Interface

With these assumptions taken into account, the total shear stress acting on one end of the roller due to the guide flange can be expressed by:

$$\tau_{tr} = \tau_{rg} + \tau_{sg} \quad (1)$$

where:

- τ_{tr} = total shear stress between roller and guide flange
- τ_{rg} = component of shear stress due to roller rotation relative to the guide flange
- τ_{sg} = component of shear stress due to roller sliding relative to the guide flange.

Shear Stress Due to Roller Rotation Relative to the Guide Flange, τ_{rg}

Discounting edge effects, an analysis of the turning moment on a disk rotating in a viscous fluid is available in the classic text by Schlichting (Ref. 1). This equation is applicable when the fluid boundary layer due to disk rotation is small with respect to the gap. This condition is generally satisfied due to the very high roller angular velocities encountered in typical bearing applications. However, to provide a reasonable estimate of the shear stress on a roller due to interaction with the guide flange, the reference analytical approach had to be modified to approximately reflect the effect of the appropriate sector-shaped shear area as illustrated in Figure 4.

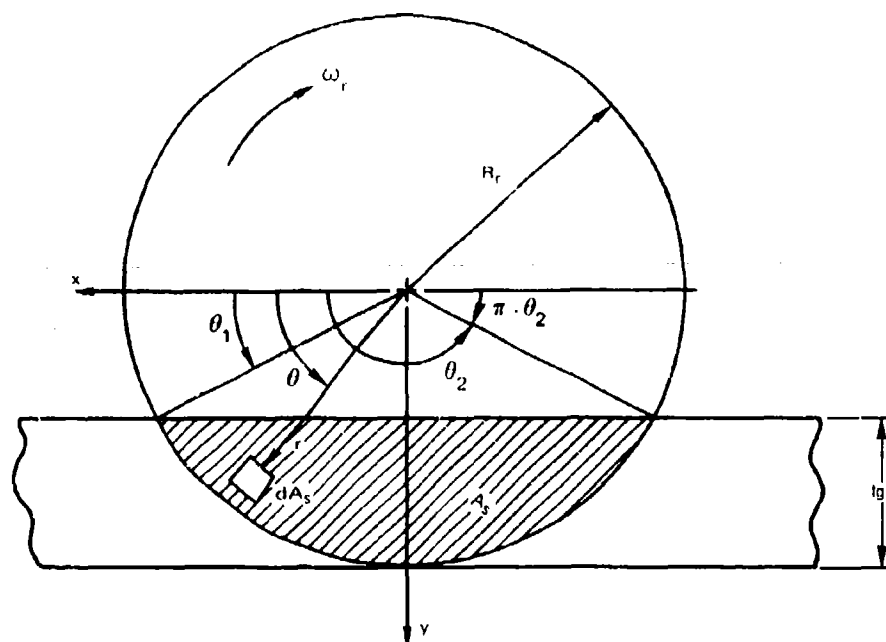


Figure 4. Shear Element Due to Relative Sliding

According to the analysis presented in Ref. 1, the variation of shear stress in the radial direction for a rotating disk is

$$\tau_{rk} = 0.616 \rho \left(\frac{\gamma}{g} \right)^{1/2} \omega_r^{3/2} r \quad (2)$$

where:

- ρ = density, lb/in.³
- γ = kinematic viscosity, in.-sec
- ω_r = angular velocity, rad/sec
- r = radius variable, in.
- τ_{rk} = shear stress, lb/in.²
- g = gravitational constant, in./sec²

In general, the force F_{rk} , and moment M_{rk} , on the roller can be obtained from the following relationships:

$$F_{rk} = \int_{A_s} \tau_r dA_s \quad (3)$$

and

$$M_{rk} = \int_{A_s} \tau_r r dA_s \quad (4)$$

Substitution of Eq. (2) into Eq's (3) and (4) leads to the following integral expressions;

$$F_{rk} = 0.616 \rho \left(\frac{\gamma}{g} \right)^{1/2} \omega_r^{3/2} \int_{\theta_1}^{\theta_2} \int_{\frac{R_r - t_g}{\sin \theta}}^{R_r} r^2 dr d\theta \quad (5)$$

and

$$M_{rx} = 0.616 \rho \left(\frac{\lambda}{g} \omega_r^2 \right)^{1/2} \int_{\theta_1}^{\theta_2} \int_{R_i}^{R_o} \frac{R_i \cos \theta}{\sin^2 \theta} r^2 dr d\theta \quad (6)$$

These integral equations can be solved closed form for the total force and moment acting on the roller end face:

$$F_{rx} = \frac{0.616 \rho \left(\frac{\lambda}{g} \omega_r^2 \right)^{1/2}}{3} \left[R_o^3 (\pi - 2\theta_1) - (R_i - R_o)^3 \left(\frac{\cos \theta_1}{\sin^2 \theta_1} + \frac{1}{2} \ln \left(\frac{\tan \left(\frac{\pi - \theta_1}{2} \right)}{\tan \left(\frac{\theta_1}{2} \right)} \right) \right) \right] \quad (7)$$

$$M_{rx} = \frac{0.616 \rho \left(\frac{\lambda}{g} \omega_r^2 \right)^{1/2}}{4} \left[R_o^4 (\theta_2 - \theta_1) - (R_i - R_o)^4 \left(\frac{2 \cos \theta_1}{3 \sin^2 \theta_1} + \frac{4}{3} \cot \theta_1 \right) \right] \quad (8)$$

Shear Stress Due to Roller Sliding Relative to the Guide Flange, τ_{sr}

Because of the kinematics of the roller/guide flange system a large component of sliding is present between the two surfaces. Since the variation of the sliding velocity in the radial direction is small, we can consider the flow in the gap between the roller end and the guide flange to be primarily one-dimensional, i.e., in the bearing circumferential direction. Thus the problem can be reduced to one similar to Couette flow between two flat plates with no pressure gradient present along the direction of flow. A schematic representation of this system is shown in Figure 5.

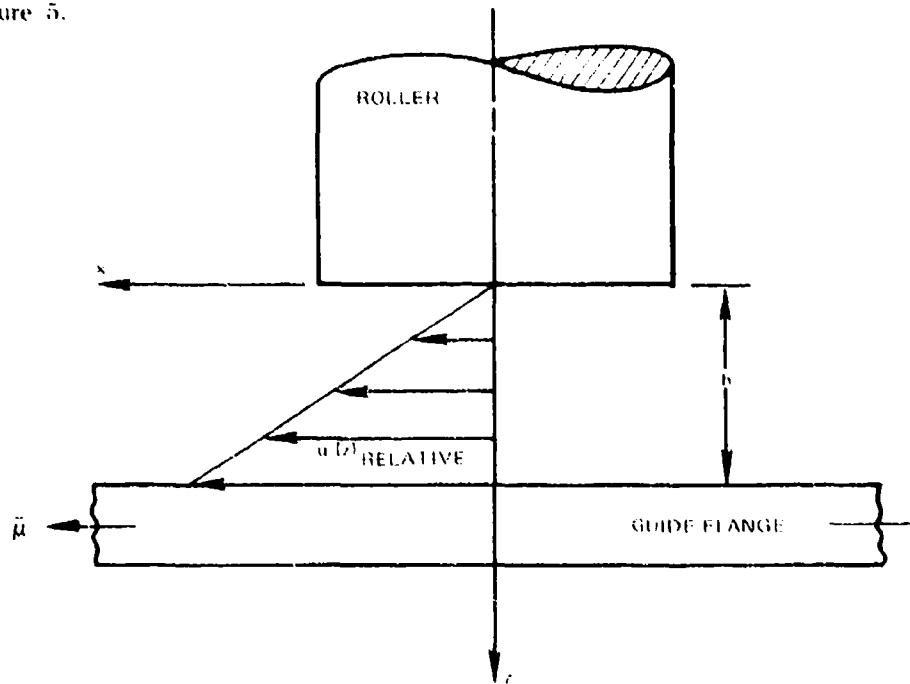


Figure 5. Velocity Distribution Due to Relative Sliding, $\mu(z)$

The expression for the shear stress in this case is given by:

$$\tau_{sk} = \mu \frac{\partial u(z)}{\partial z} \quad (9)$$

The circumferential relative velocity gradient,

$$\frac{\partial u(z)}{\partial z}$$

is simply

$$\frac{\partial u}{\partial z} = \frac{\bar{u}}{h} \quad (10)$$

where \bar{u} is the relative sliding velocity between the guide flange and the roller.

Direct substitution for the sliding shear stress yields:

$$\tau_{sk} = \frac{\mu \bar{u}}{h} \quad (11)$$

The basic integral expressions relating force and moment to the applied shear stress, equations (3) and (4), can again be utilized to obtain:

$$F_{sk} = \int_{A_s} \tau_{sk} dA_s = \frac{\mu \bar{u}}{h} \int_{A_s} dA_s \quad (12)$$

$$M_{sk} = \int_{A_s} \tau_{sk} r dA_s = \frac{\mu \bar{u}}{h} \int_{A_s} \tau_{sk} r dA_s \quad (13)$$

The effect of the sector-shaped slider geometry of the roller end face must once again be taken into account by choosing appropriate limits for the surface integrals (12) and (13). That is:

$$F_{sk} = \frac{\mu \bar{u}}{h} \int_{\theta_1}^{\theta_2} \int_{\frac{R_r - t_{gr}}{\sin \theta}}^{R_r} r dr d\theta \quad (14)$$

$$M_{sk} = \frac{\mu \bar{u}}{h} \int_{\theta_1}^{\theta_2} \int_{\frac{R_r - t_{gr}}{\sin \theta}}^{R_r} r^2 dr d\theta \quad (15)$$

Solving (13) and (15) for the force and moment on the roller respectively:

$$F_{sk} = \frac{\mu \bar{u}}{2h} [R_r^2 (\pi - 2\theta_1) - (R_r - t_{gr})^2 (2 \cot \theta_1)] \quad (16)$$

$$M_{sk} = \frac{\mu \bar{u}}{2h} \left[R_r^2 (\pi - 2\theta_1) - (R_r - t_{gr})^2 \left(\frac{\cos \theta_1}{\sin^2 \theta_1} + \frac{1}{2} \ln \left(\frac{\tan \left(\frac{\pi - \theta_1}{2} \right)}{\tan \left(\frac{\theta_1}{2} \right)} \right) \right) \right] \quad (17)$$

The total shear force on the roller due to the guide flange, F_{tr} , is then the summation of the rotational and sliding components and acts in the circumferential direction.

$$F_{tr} = F_{trr} + F_{sr} \quad (18)$$

The total moment about the local roller z-axis is:

$$M_{tr} = M_{trr} + M_{sr} \quad (19)$$

3.1.2 Roller End to Cage Siderail Interface

Consideration of the effect of oil film shearing in the roller end/cage siderail interface poses a problem similar to that for the roller end and guide flange interface presented in the preceding section. Since the shear on the roller end will also affect the cage dynamic motion, the computed shear forces must be added to both the individual roller and to the overall cage force and moment system. The roller rotates about its own axis with respect to the cage and is also free to move circumferentially and radially with respect to the cage.

As was the case for the roller/guide flange contact, the total shear force and moment is computed approximately by summation of the rotational and sliding components. Figure 6 shows the shear stress resulting from rotation of the roller with respect to the cage siderail. Since shear variations due to roller skewing are not considered, it can be inferred from the figure that the contribution of the roller rotation to the net roller radial force will be zero since shear stress components on either side of the y-axis are equal in magnitude and opposite in sign.

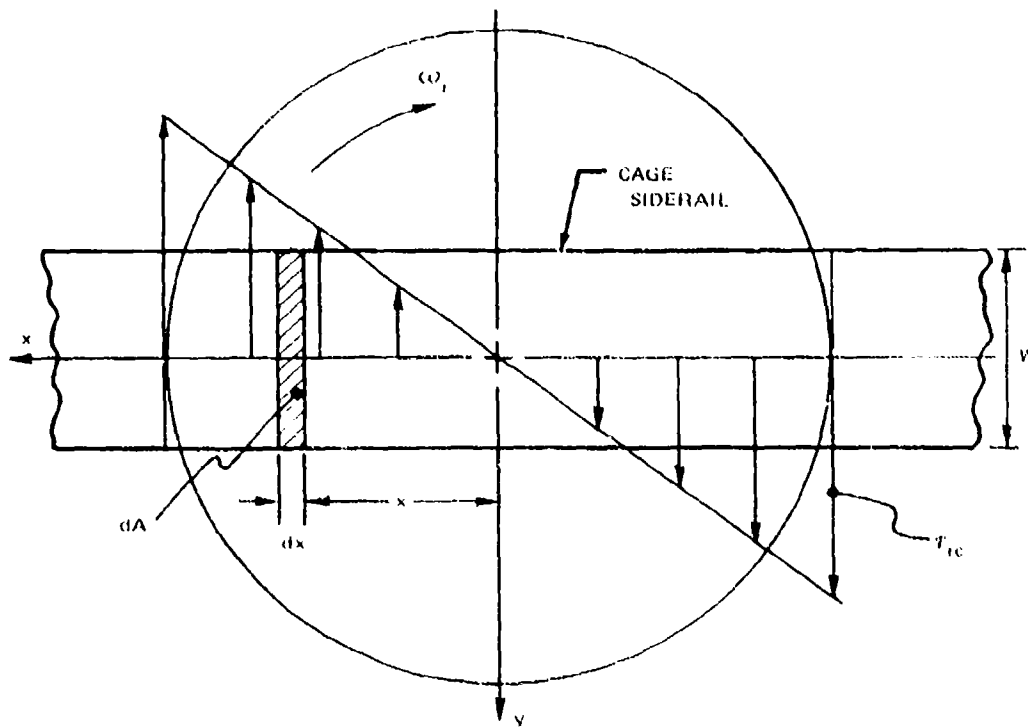


Figure 6. Shear Stress Resulting from Rotation of Roller Relative to Cage Siderail

In addition, because of the small clearances between the cage bore and the inner ring lands, the effect on shear due to any cage eccentricity with respect to the roller pitch diameter can be neglected. The total moment on the roller due to shear drag with the cage is then due solely to roller angular velocity, ω_r .

The shear stress equation for a rotating disk is again modified to reflect the effect of the contact zone which, for the roller/cage interface, is approximately rectangular. Following an analytical procedure similar to that for the roller/guide flange contact we can develop the expression for the roller drag moment due to its angular velocity as:

$$M_{rc} = \int \tau_{rc} x dA \quad (20)$$

$$M_{rc} = \int W x dx$$

where

$$\tau_{rc} = 0.616 \rho \left(\frac{\gamma}{g} \right)^n \omega_r^{2.2} x$$

and all terms are as previously defined in equation (2). Therefore,

$$M_{rc} = 0.616 \rho \left(\frac{\gamma}{g} \right)^n \omega_r^{2.2} W \left(\frac{3R_r^2}{2} \right) \quad (21)$$

The radial and circumferential components of the shear force acting on the roller due to a relative sliding velocity between the roller and cage are calculated using the same type of Couette flow analysis as was used for the roller/guide flange contact.

The radial component:

$$F_{(ac)_r} = \int \tau_{(ac)_r} dA \quad (22)$$

$$F_{(ac)_r} = \frac{\mu W R_r}{h} \cdot V_{(s)_r}$$

The circumferential component:

$$F_{(ac)_c} = \int \tau_{(ac)_c} dA \quad (23)$$

$$F_{(ac)_c} = \frac{\mu W R_r}{h} \cdot V_{(s)_c}$$

where:

$F_{(ac)_r}$ = shear force due to sliding relative to the cage in the radial direction

$F_{(ac)_c}$ = shear force due to sliding relative to the cage in the circumferential direction

The total shear force on the k^{th} roller end can now be completely identified by summing the components in the radial and circumferential directions due to both the guide flange and the cage. The only radial shear force component is that due to roller velocity relative to the cage (eq. 22)

$$F_{r1k} = F_{r2k}$$

The total circumferential shear force is found by summing equations (18) and (23)

$$F_{\theta 1k} = F_{\theta 2k} + F_{\theta 3k} \quad (24)$$

The total moment about the local roller z -axis is found by summing equations (19) and (21)

$$M_{z1k} = M_{z2k} + M_{z3k} \quad (25)$$

Each roller exerts an equal and opposite drag force and moment on the cage, the directions of which depend on the sense of the instantaneous relative sliding velocity between the roller and cage. These net forces on the k^{th} roller and k^{th} cage pocket are as shown in Figure 7. The overall effect on the cage can be represented by a summation of the individual contributions of all the rollers which then identifies the total radial and circumferential shear force acting on the cage due to interaction with the roller ends.

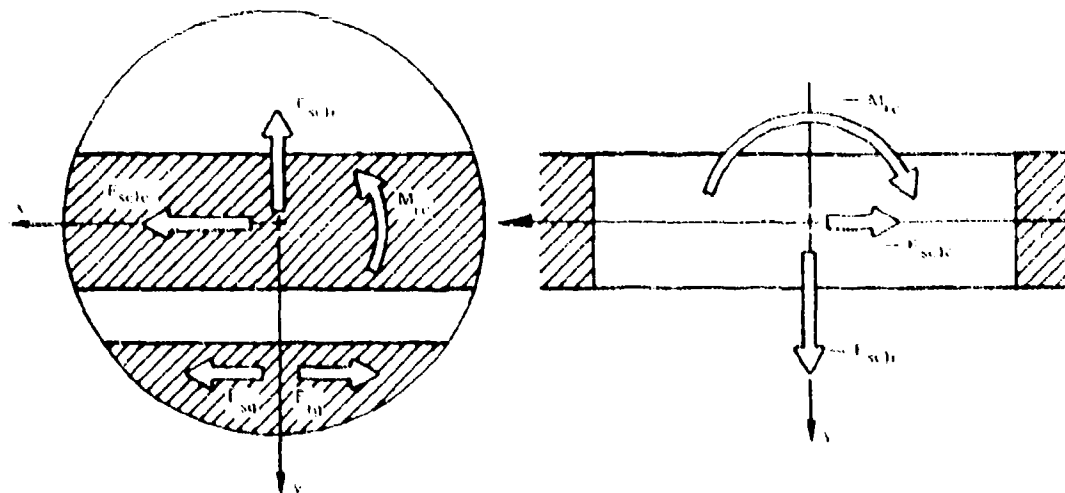


Figure 7. Net Forces and Moments on Roller End and Cage Siderail Due to Viscous Shear

Total Radial Component:

$$F_r = \sum_{k=1}^n F(K)_r \quad (26)$$

where

n = Number of rollers

Total Circumferencial Components:

$$F_c = \sum_{k=1}^n F(K)_c \quad (27)$$

Total Moment about cage z-axis:

$$M_z = \sum_{k=1}^n M(K)_z - R_c \sum_{k=1}^n F(K)_c \quad (28)$$

3.2 Elastic Impact Contact Model

The movement of a roller at any time may be with sufficient velocity that contact with the constraining surfaces may be classified as an impact. Analytical methods have been developed in the subject program to deal with impacts occurring between a roller and the inner ring guide flange constraints as well as between a roller and the cage web constraints.

A contact is said to exist when the separation distance between a roller and the guide rail or the cage web becomes either negative or less than some previously defined minimum separation distance. This minimum separation distance can be described physically as the film thickness below which hydrodynamic lubrication theory is no longer valid and boundary type lubrication effects predominate.

The elastic impact model described in the first interim report was intended to consider both the deformation and restitution phases of roller and cage impacts. This approach, while theoretically valid, was prone to certain computational disadvantages.

The occurrence of an impact with a corresponding metal to metal contact represents an extremely rapid change in the system of forces acting on the roller, and as such, represents a virtual discontinuity for the mathematical system. The impact forces and moments are functions of both the displacement and stiffness of the roller and the body it is in contact with, and may undergo large changes in magnitude in a very short time. Under these conditions, the integration time step required to solve the equations of motion becomes prohibitively small.

3.2.1 General Solution Technique

To avoid an undesirable penalty in execution time, an improved analytical method was devised to eliminate the necessity of calculating the impact force variation during the deformation phase of the impact, but yet still allow a real-time simulation of the post-contact motion of each body. At each time step, each roller in turn is checked to determine its separation distance with respect to the raceway guide flanges and cage web. All rollers indicating a contact situation are identified. These rollers are then analyzed to determine which of them contacts the

constraint first. The system integrates a time step is then adjusted so that the velocity and position of that roller which contacts the constraint first is determined at the instant of contact. The program now freezes the position of all rollers and enters the contact mode.

The peak force and contact duration are then calculated from the Hertz theory for centrally impacting spheres (Ref. 2). The peak force corresponding to maximum local deformation is assumed to exist at the start of the contact analysis, and to decay with time as a cosine function,

$$F(t) = F_{\text{peak}} \cos(\omega t), \quad (20)$$

finally dropping to zero at the end of the restitution period which is assumed to be equal to one-half of the theoretical contact duration. During this contact mode, the response of the roller-cage system is determined by integrating the equations of motion in the usual manner. At the end of the restitution period, the roller is no longer in contact with the constraint and the program leaves the contact mode.

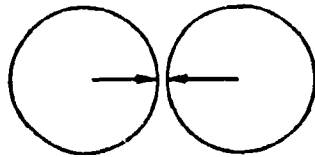
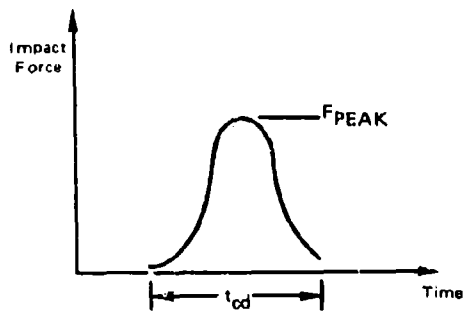
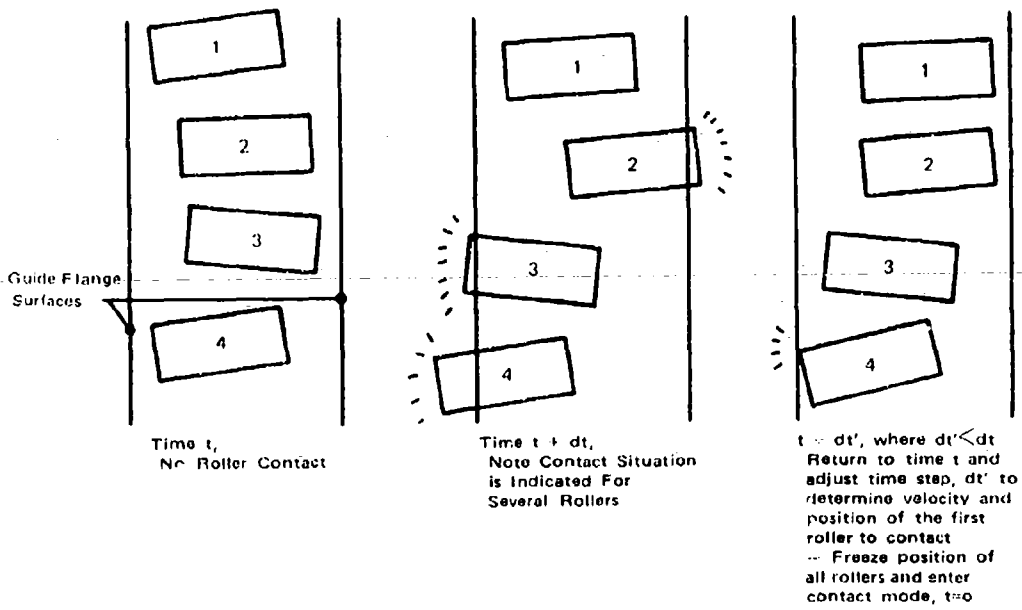
The above procedure is summarized in Figure 8 and is applied as described to impacts of the roller with the guide flanges and with the cage web.

3.2.2 Effect of Cage Web Flexibility

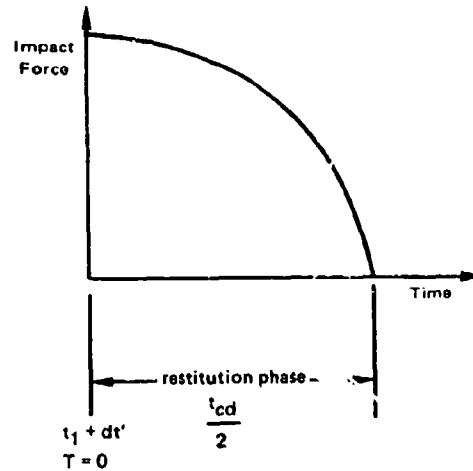
An analysis to determine the effect of cage web flexibility on contact force variation and contact time duration has been completed. Depending on the roller skew angle at the instant of contact, the impact force may be assumed to act as either a point load near the root of the cage web (where the cage web joins the siderail), or as an evenly distributed force over the roller-to-web contact length. This latter assumption of line contact occurs only when there is zero relative skew between the roller and the cage, which is considered rather unlikely. Results of the analysis indicate that cage web flexibility can significantly affect the magnitude of the peak force for line type contact, but that web flexibility has a negligible effect for the more likely occurring point contacts. Therefore, it is advantageous from an execution time standpoint to utilize the more approximate, rigid cage web method of analysis. This is based on the assumptions that only point type contacts occur and that the bearing geometry and materials are similar to those that have been employed in the parametric test program.

3.3 Cage Mass Moment of Inertia

As a convenience for the user, an analysis for the determination of the cage mass moments of inertia about the body fixed x, y, and z axes was derived, incorporated in the program, and is presented here. The analysis assumes that the cage pockets are evenly spaced, with the x axis radiating from the center of the cage through the center of pocket number 1 at 3 o'clock as shown in Figure 9. Furthermore, it is also assumed that the local x, y, and z axes are the principal axes. This is normally true for conventionally designed cages with an even number of pockets. The assumption is approximately correct for cages with an odd number of pockets, since the number of rollers in a mainshaft gas turbine engine bearing is sufficiently large so that the effect of this assumption on the mass moment of inertia becomes negligible.



Calculate peak force and contact duration, t_{cd} , from Hertz theory for centrally impacting spheres.



Assume the force varies as above for the restitution phase of the impact over a time interval equal to $\frac{1}{2}$ of the theoretical Hertzian contact duration.

Figure 8. Contact Model Determines Impacting Roller

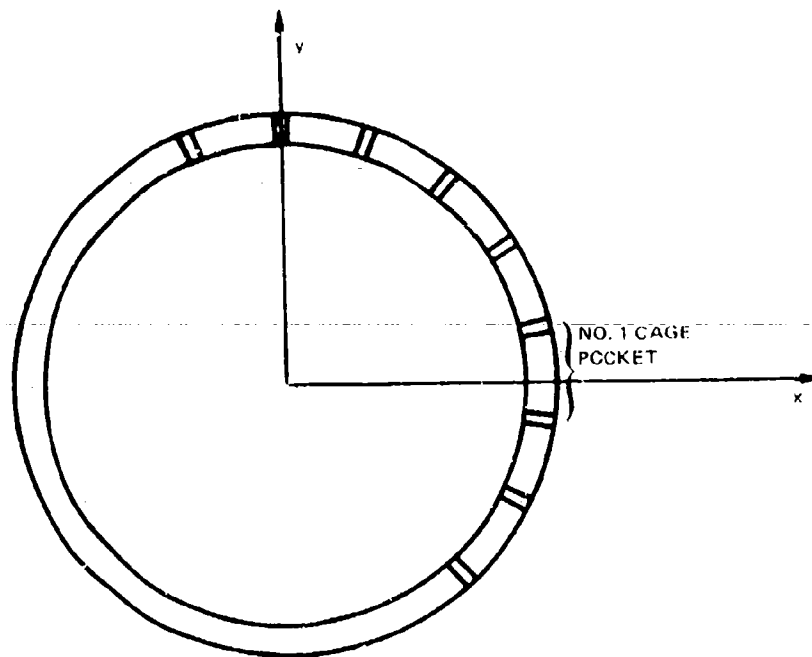


Figure 9. The x-Axis Intersects the Number One Cage Pocket

The equations for the mass moments of inertia are as follows:

$$I_{xx} = \frac{1}{12} \frac{\pi \rho_c W_c}{g} (r_2^2 - r_1^2) [3(r_2^2 + r_1^2) + W_c^2] + \frac{1}{16} \frac{\rho_c W_p}{g} (r_2^2 - r_1^2) \sum_{q=1}^n \{ (r_2^2 + r_1^2) [2(\theta_{q2} - \theta_{q1}) - \sin(2\theta_{q2}) + \sin(2\theta_{q1})] + \frac{2}{3} W_p^2 (\theta_{q2} - \theta_{q1}) \} \quad (30)$$

$$I_{yy} = \frac{1}{12} \pi \frac{\rho_c}{g} W_c (r_2^2 - r_1^2) [3(r_2^2 + r_1^2) + W_c^2] + \frac{1}{16} \frac{\rho_c}{g} W_p (r_2^2 - r_1^2) \sum_{q=1}^n \{ (r_2^2 + r_1^2) [2(\theta_{q2} - \theta_{q1}) - \sin(2\theta_{q2}) + \sin(2\theta_{q1})] + \frac{2}{3} W_p^2 (\theta_{q2} - \theta_{q1}) \} \quad (31)$$

$$I_{zz} = \frac{1}{4} \frac{\rho_c}{g} (r_2^2 - r_1^2) \left[2\pi W_c + W_p \sum_{q=1}^n (\theta_{q2} - \theta_{q1}) \right] \quad (32)$$

For the q^{th} cage pocket:

$$\left. \begin{aligned} \theta_{q1} &= \frac{2\pi}{n}(q-1) - \frac{S}{r_o + r_i} \\ \theta_{q2} &= \frac{2\pi}{n}(q-1) + \frac{S}{r_o + r_i} \end{aligned} \right\} \text{ See Figure 10} \quad (33)$$

- n = No. of cage pockets
- q = q^{th} cage pocket
- ρ_c = Cage mass density (lb/in³)
- W_c = Total width of cage (in.)
- r_o = Cage outer radius (in.)
- r_i = Cage inner radius (in.)
- W_p = Width of cage pocket (in.)
- θ_q = Azimuth angle of q^{th} cage pocket (rad)
- S = circumferential length of cage pocket at pitch radius (in.)

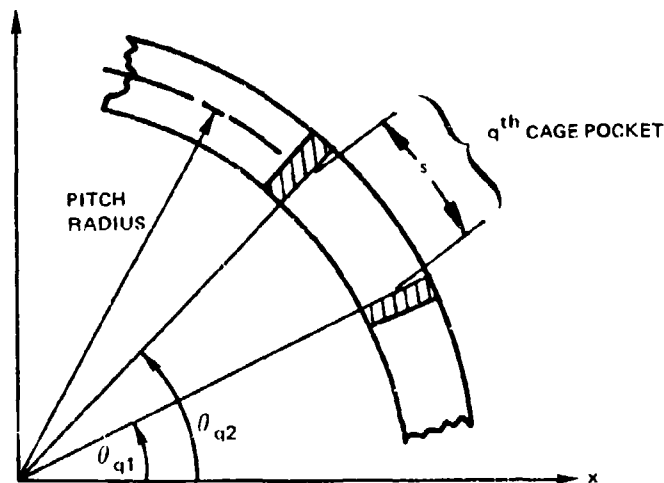


Figure 10. Front and Rear Cage Pocket Azimuth Angles

3.4 Roller Dynamic Wear Model

Accurate prediction of roller end wear due to dynamic interaction with the cage and guide flanges presents a difficult analytical dilemma from two standpoints. The mechanism of dynamic wear is quite complex and requires rigorous treatment if an accurate wear profile is to be generated. The analysis, however, must be efficient and quickly solvable via the computer if reasonable run times are to be possible.

A linear wear model was selected to represent the wear mechanism between the roller end and the guide flange since the relative sliding velocities are quite moderate and are typically in the 200-300 ft/sec range. This type of model, which has been used to compute wear in journal bearings and similar sliding devices (Ref. 3) has to be modified to reflect both geometry differences as well as the transient loading conditions inherent in the roller end/guide flange contact zone. The general form of this model is expressed as:

$$W = f(K, P, S)$$

The specific form of this model employed in the subject analysis is the linear version; namely

$$W = KPS \quad (34)$$

where

- W = wear volume (in³)
- K = empirically determined wear coefficient (in³/in.-lb)
- P = load (lb)
- S = sliding distance (in.)

Whereas the load P usually represents a steady-state load, the TRIBO 1 wear model redefines P in terms of a Hertzian impact load for point contacts (Ref. 4).

$$P = 0.7064 (V_n^3 M_r^2 B^{-1} E_r^2)^{1/5} \quad (35)$$

where

- V_n = normal approach velocity (in./sec)
 - M_r = mass of roller (lb)
 - B = roller corner radius parameter, 1/2R_{corner} (in.⁻¹)
 - E_r⁻¹ = equivalent elastic modulus of roller and guide flange (psi⁻¹)
- $$= \left(\frac{1 - \nu_1^2}{\pi E_1} + \frac{1 - \nu_2^2}{\pi E_2} \right)$$

ν₁, ν₂ = Poisson's ratio of roller and guide flange

The sliding distance, S, is considered as a function of roller and guide flange velocity components in the radial and circumferential directions as well as the dynamic contact duration time, Δt. It is assumed that the roller angular velocity remains constant during the contact.

The sliding velocity is given by

$$V_{\text{sliding}} = (V_c^2 + V_r^2)^{1/2} \quad (36)$$

where

- V_c = relative circumferential roller velocity component (in./sec)
- V_r = relative radial roller velocity component (in./sec)

The Hertzian contact duration time for a point contact (Ref. 4):

$$\Delta t_c = 5.198 (V_n^{-1} M_r^2 B E_r^{-2})^{1/5} \quad (37)$$

Thus the sliding distance is:

$$S_{\text{sliding}} = (V_c^2 + V_r^2)^{1/2} \Delta t_c \quad (38)$$

This concept has been utilized as the basis for the incremental wear model, wherein a wear increment, W_i, is calculated from the following equation whenever a contact occurs in the dynamic system.

$$W_i = K P_i S_i \quad (39)$$

The total wear is then the sum of the individual increments:

$$W_{\text{total}} = \sum_{i=1}^n K P_i S_i \quad (40)$$

which by substitution is

$$W_{\text{total}} = \sum_{i=1}^n \frac{K V_{\text{rel}} M_{\text{rel}} (V_c^2 + V_p^2)^{1/2}}{g} \quad (41)$$

4. DEVELOPMENT OF THE COMPUTATIONAL SYSTEM

The computational system consists of the algorithm which determines all roller and cage forces and integrates the roller and cage equations of motion to determine their respective positions and velocities as a function of time.

The overall computer program, TRIBO 1, is organized on a modular basis and is built on four major subprograms, or modules, namely; STATIC, CADYN, RODYN and SYSDYN. Each of these modules will be discussed with its own input and output capability and each can be run as a separate program apart from TRIBO 1. Each module is composed of many subroutines which are used for evaluation of the forces and moments arising from interactions among the bearing raceways, cage, and rollers.

The basic structure and logic of these subprograms was developed and reported in the 1st interim report. Work since then has resulted in extensive refinement, and in some cases, replacement, of some of the above mentioned subroutines. This effort has resulted in certain revisions that reduce computer time and others that reduce computer core requirements. Also, extensive revisions to the program input/output subroutines have been made resulting in greater clarity and convenience for the user. In addition, model validation was effected through comparison with a closed form analytical solution, and several parametric studies were run to illustrate particular subprogram capabilities.

4.1 STATIC Program Module

STATIC is the subprogram which provides the means for quasi-static roller bearing design optimization. The related analysis and program capability were discussed in the first interim report in Sections IV and VI respectively.

Work performed during this reporting period was directed towards improving program computational efficiency for STATIC and updating several related roller optimization subroutines. Also, the STATIC subprogram module was incorporated into the overall TRIBO 1 program.

4.1.1 Improved Computational Efficiency of STATIC

The flexible ring bearing analysis used within the subprogram STATIC was developed from an earlier version of the deck, which was based upon an assumption that the inner and outer bearings rings were rigid. The flexible ring analysis utilized this rigid ring analysis to provide initial values of roller deflections for the flexible ring iterative procedure. Subsequent experience has indicated that it is not necessary to obtain the rigid ring solution as the first step in finding the flexible ring deflections. The elimination of this first step in the analysis has resulted in up to a 30% reduction in computer time for some test cases.

Additional development work on the static roller optimization analysis, called subroutine OPTIMA, has resulted in increased capability in handling extremes of both misalignment and outer-ring out-of-roundness.

4.1.2 Improvements to the Roller Optimization Module

The roller optimization module has been updated with the addition of two subroutines. The first subroutine deals with the calculation of the influence coefficients for the inner and outer rings and support structures. The second subroutine provides a way to take into account the effect of raceway undercuts on the optimum combination of roller flat length and crown radius.

As explained in Section IV of the first interim report, the influence coefficients are used to account for the effects of ring and support structure flexibility on the bearing internal roller load distribution and hence on bearing life. In actual aircraft engine applications the inner and outer ring support structures may have rather complex cross sections and the influence coefficients corresponding to the application of a point load may have to be determined by means of either a finite element analysis or a shell analysis. While it may be desirable to consider the effects of ring/support flexibility, the use of either of these procedures, to calculate influence coefficients however, is generally not necessary in a preliminary design since the support structure geometry is normally not defined sufficiently to warrant the effort involved.

The new subroutine allows consideration of flexibility effects without requiring a structural analysis. The required "A" influence coefficient submatrix can be calculated within the program for an assumed ring and support geometry. The calculation logic is based on the assumption that the ring and structure can be replaced by a single equivalent ring with a rectangular cross section supported by a sinusoidally varying shear load (Ref. 5). The influence coefficients, A_{qj} , defined as the radial deflection of the q^{th} roller location due to a unit load at the j^{th} location, are then prescribed by the following formula.

$$A_{qj} = \frac{\delta_q}{P_j} = \left[\frac{1}{2} (\pi - \phi_q) \sin \phi_q + \left(\frac{\pi^2}{6} - \frac{\pi}{2} \phi_q + \frac{1}{4} \phi_q^2 - \frac{3}{S} \right) \cos \phi_q - 1 \right] \frac{R^3}{2\pi EI} \quad (42)$$

where

δ_q = radial deflection of the q^{th} roller location, in.

P_j = unit load at the j^{th} roller location, lbf

q = circumferential location of the q^{th} roller, rad.

R = radius to the neutral axis of the equivalent rectangular cross section support structure, in.

E = equivalent Young's modulus of support structure, psi

I = effective polar moment of inertia of support structures, in⁴

It is emphasized that these internally calculated influence coefficients should only be used in the preliminary design stage. Once the supporting structures are defined, the finite element analysis should then be used to determine the influence coefficients.

The second subroutine added to the roller optimization module allows for the consideration of the effect of raceway undercuts on the optimization of the roller flat length and crown radius. The inner raceway undercuts facilitate machining operations during manufacture and provide a means of distributing oil to the raceway and guide flange surfaces. The roller must be designed so that the contact area "footprint" does not extend over the edge formed by the breakout of the raceway undercut and the raceway surface. If this should occur, stress concentrations would occur and roller life would be severely reduced.

4.1.3 Incorporation of STATIC into TRIBO 1

The incorporation of the **STATIC** module into the overall **TRIBO 1** program has been completed. With this addition, **TRIBO 1** can now be run in any of the following six modes each of which are independent of the others:

1. **STATIC**
2. **CADYN**
3. **RODYN**
4. **SYSDYN**
5. **STATIC + RODYN**
6. **STATIC + SYSDYN**

This feature is of particular interest since the program now has the capability of running the **STATIC** module in conjunction with either **RODYN** or **SYSDYN**. This **STATIC** module provides the circumferential roller load distribution and details information about the roller-to-raceway contact area, such as its location with respect to the roller center of mass, and its variation due to roller loading. This information is passed to **RODYN** or **SYSDYN** and is used by the traction subroutine to calculate roller traction forces and moments which affect roller motion.

4.2 CADYN Program Module

The development of **CADYN**, the cage dynamics module, has proceeded as planned. A series of test cases have been employed in this work that were designed to validate the program for cage 3-D motion. A parametric study was also undertaken to assess the effects of both cage mass and cage and inner ring interfacial shear forces on the 2-D motion of the cage.

Three-dimensional cage motion was simulated by modeling the motion of a free gyroscope which was allowed to rotate in any direction about a fixed point in space. The choice of the free gyro as a test case allows for the determination of the correctness of the general system dynamics without the need to consider the constraints ordinarily arising from interactions of the cage with the rollers and the ring lands.

With **CADYN**, the cage geometry was input such that it represented the rotor of the gyroscope whose polar axis was the local z-axis. Thus, the moments of inertia about the local x, y, and z axes were $I_{xx} = I$, $I_{yy} = I$, $I_{zz} = I_p$. The gyroscopic motions about the local, x, y, and z axes were determined by solving Euler's equations of rotational motion for the special case of zero external torque. The solution of the resulting differential equations was derived for the special Eulerian coordinate system within **CADYN**, in a manner similar to that presented in Ref. 6.

The resultant angular velocity components are given as follows:

$$\begin{aligned}W_x &= W_{x0} \cos(kt) + W_{y0} \sin(kt) \\W_y &= W_{x0} \sin(kt) + W_{y0} \cos(kt) \\W_z &= \text{Constant} = W \cos \alpha\end{aligned}\tag{43}$$

where

$$K = \frac{I_p - I}{I} \omega_x$$

$$\beta = \arctan \left[\frac{I}{I_p} \tan \alpha \right] = \text{angle between the local z and inertial z-axes (deg)}$$

$$\omega_{x0} = \text{cage angular velocity about the local x-axis at } t = 0 \text{ (rpm)}$$

ω_{y0} = cage angular velocity about the local y-axis at $t = 0$ (rpm)

ω = magnitude of the cage angular velocity vector (rpm)

α = angle between the angular velocity vector and the local z-axis (deg)

For this example the assumed initial conditions are as follows:

$\omega = 1000$ rpm

$\alpha = 27.9^\circ$

$I = 3.0$ lb-in.-sec²

$I_p = 3.0$ lb-in.-sec²

$\beta = 10^\circ$

The results of this test case as obtained from CADYN showed excellent agreement with the exact solutions, as indicated in Table 1.

TABLE 1. CADYN TEST RESULTS

Time, Milli-sec	ω_x (rpm)		ω_y (rpm)		ω_z (rpm)		β (deg)	
	Exact	CADYN	Exact	CADYN	Exact	CADYN	Exact	CADYN
0.0	0.0	0.0	467.59	467.59	883.95	883.95	10.0	10.0
0.6	51.83	-51.83	464.71	464.71	883.95	883.95	10.0	10.0
1.1	94.57	94.57	457.93	457.93	883.95	883.95	10.0	10.0
10.3	441.43	441.43	154.21	154.20	883.95	883.95	10.0	10.0
50.3	52.51	52.53	464.63	464.63	883.95	883.95	10.0	10.0

Much information about the relative influence of certain variables on overall cage dynamic behavior can be obtained by performing parametric studies as an integral part of the program development process. The results of such studies provide data on the computation time requirements of particular analyses and can assist in the determination of whether the amount of computer time spent in solving for a given parameter is justified.

Two parametric studies were undertaken using CADYN. In the first study, the effects of reduced cage mass on the uncoupled cage motion were observed. The dynamic behavior of a cage with one fifth the mass of the standard cage was examined over a range of unbalances from 0 to 10 gm-cm. From the resulting plots of cage motion, it was determined that a reduction in cage mass results in a larger film thickness between the cage and the inner ring land riding surface over the range of unbalances considered, as shown in Figure 11.

The second CADYN study examined the effect of the fluid shear forces, as well as the hydrodynamic normal forces, on the cage film thickness. Two cases were run for comparison. One case included the effects of shear forces on the cage, the other had the shear forces and moments suppressed. As seen in Figure 12, the shear forces and moments have a significant effect on the cage motion and final steady state film thickness. These results clearly show that the shear forces cannot be neglected in the analysis.

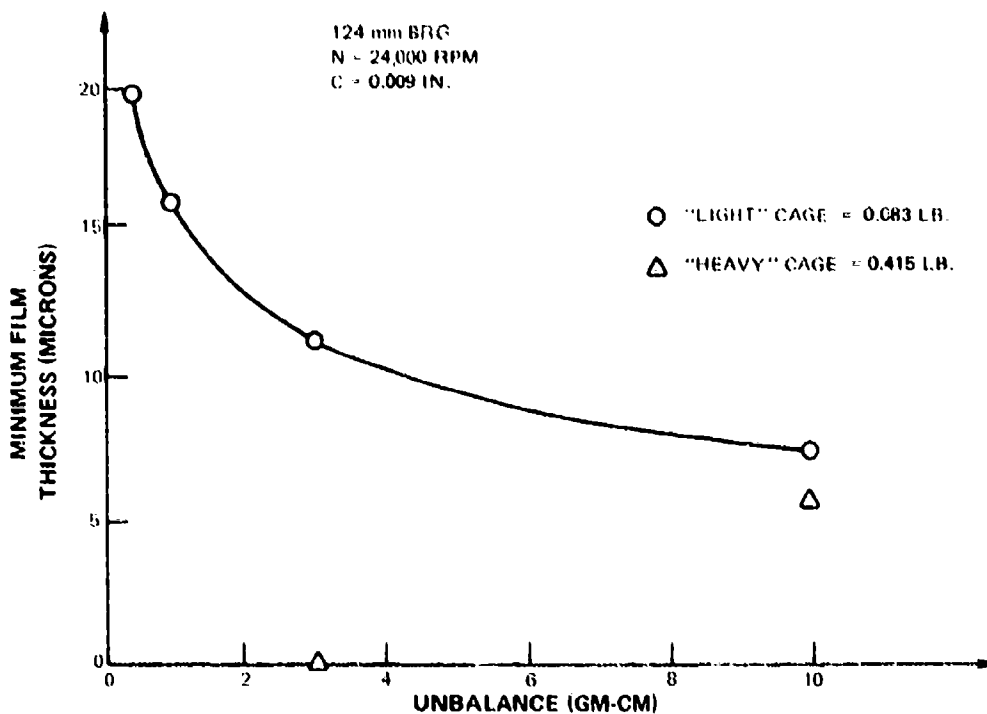


Figure 11. Reducing Cage Mass Increases Minimum Film Thickness

4.3 RODYN Program Module

RODYN is the subprogram designed to evaluate the dynamic behavior of bearing rollers when uninfluenced by interactions with the cage. This module contains all roller equations of motion and all subroutines relating to the determination of forces resulting from interactions between the rollers and both the inner and outer rings.

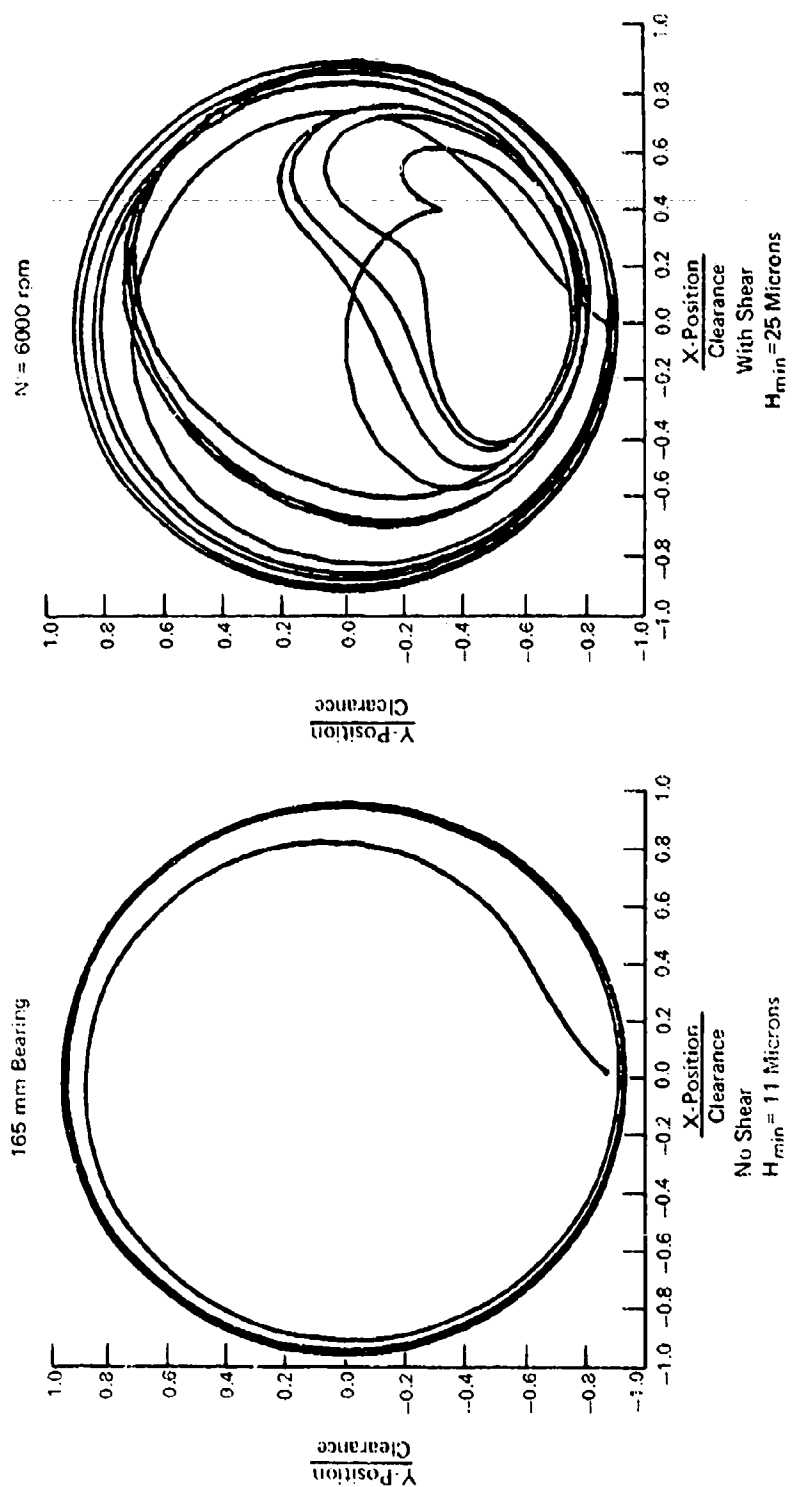
Work performed during this reporting period centered primarily on the development of the additional force and moment subroutines discussed in the following sections. A discussion of input/output improvements is also included.

4.3.1 Roller/Guide Flange and Roller/Cage Siderail Hydrodynamic Contact Model Development

The finite element analysis developed to model the hydrodynamic behavior of the lubricant film between the roller and the guide flange and between the roller end and cage siderail has been incorporated into the main TRIBO 1 Program.

This analysis, called FERFI, was originally created and tested as an independent program in keeping with the modular concept of TRIBO 1 development. The inclusion of this program as a subroutine of TRIBO 1 required the development of additional supporting modules in order to provide all the necessary input.

A preprocessor, designated BRKUP, was developed to automatically assign the finite element grid to both the guide flange and cage siderail interfaces. The element arrangement, node



FD 160192
790703

Figure 12. CADYN Shows Fluid Shear Increases Minimum Film Thickness

No.'s and node coordinates for each interface are stored internally within the program, based upon user input geometry. A typical breakup is shown for the guide flange, Figure 13, and for the cage, Figure 14.

An accurate description of the local roller velocity relative to the guide flange and the cage is also required as input to FERFI. The relative velocity at each node in the breakup has to be defined in terms of its radial, tangential and axial components as identified in Figure 15. These velocities are calculated in another module, ROLVEL. The ROLVEL subroutine is called at every time step in order to provide FERFI with the most up-to-date information.

Description of the interface is completed by calculating the film thickness distribution between the interacting surfaces in subroutine ROISEP. The film thickness distribution within the roller/guide flange interface, as represented in Figure 16 is affected by roller axial translation, roller skew and guide flange layback angle. The roller/cage siderail interface film thickness distribution is a function of both cage and roller axial translation and skew. The film thicknesses (separation distances) at each node are calculated as a function of these variables at each time step. A description of the actual calculations used in FERFI was given in Section V.C.3 of the first interim report.

A variety of test cases were prepared in order to confirm the proper function of the FERFI module and its associated support modules within TRIBO 1. One of these test cases, presented below, calculates the pressure distribution over a flat circular surface as it normally approaches a plane wall at a constant velocity. This example was chosen because a closed form solution is available (Ref. 7) for this monotonic squeeze film problem by direct integration of the Reynold's equation. The geometry and operating conditions used in this model test case are as follows:

Radius of the circular pad,	$r_0 = 1.0$ in.
Instantaneous film thickness,	$h = 0.001$ in.
Approach velocity,	$\dot{h} = 10.0$ in./sec
Lubricant viscosity,	$\mu = 4.6 \times 10^7 \frac{\text{lb-sec}}{\text{in.}^2}$

As is indicated in Table 2, excellent agreement for the hydrodynamic pressure distribution was obtained between the finite element method and the exact solution.

4.3.2 Force and Moment Due to Roller Unbalance

The analysis of the forces resulting from roller unbalance was derived in a manner similar to that used in the cage unbalance analysis. As indicated in the first interim report, the expression for this unbalance force, F_{rk} due to the j^{th} unbalance mass, in the k^{th} roller is given

$$F_{rk_{\text{unbal}}} = \sum_{j=1}^p m_{jk} \frac{d^2 \dot{R}_{rjk}}{dt^2} \quad (44)$$

where

$$\frac{d^2 \dot{R}_{rjk}}{dt^2} = \frac{d^2 \ddot{R}_{rjk}}{dt^2} + \alpha_{rk} \times r_{rjk} + \omega_{rk} \times (\omega_{rk} \times r_{rjk}) \quad (45)$$

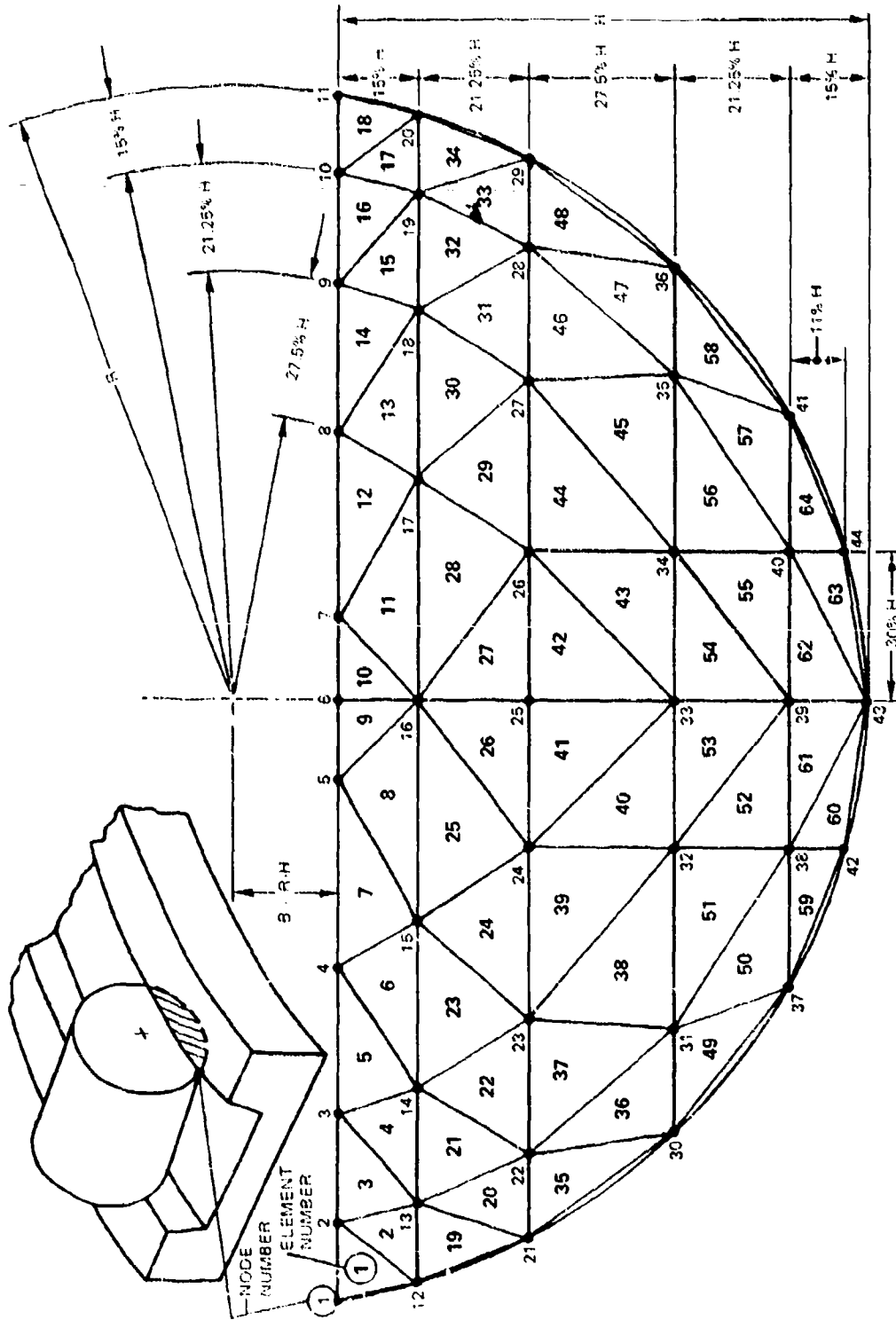


Figure 13. The Roller/Guide Flange Finite Element Breakup Model Uses Triangular Elements Compatible With the Sector Shape of the Interface Region

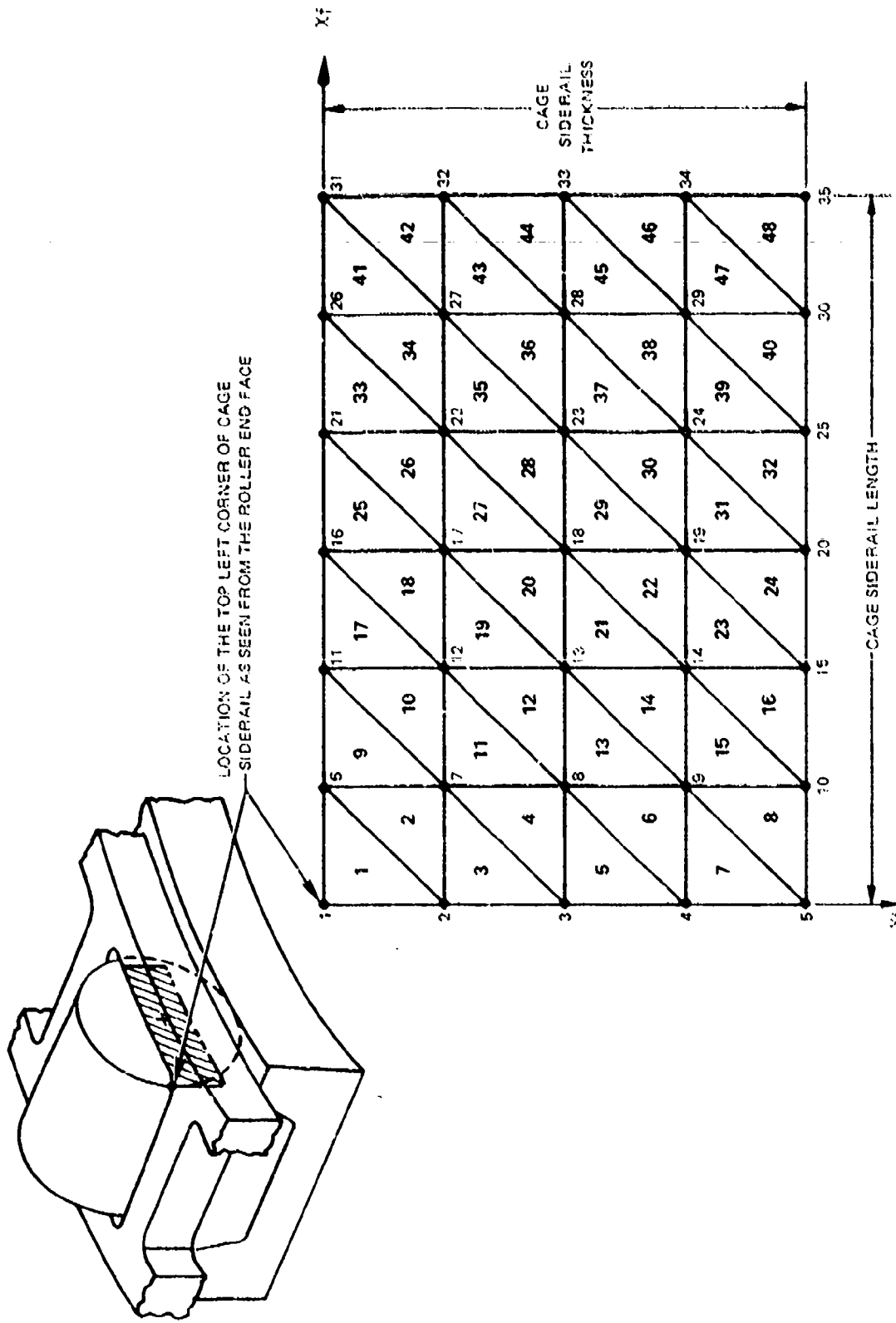


Figure 14. The Cage Siderail Finite Element Model Also Uses Triangular Elements for the Calculation of the Hydrodynamic Force on It

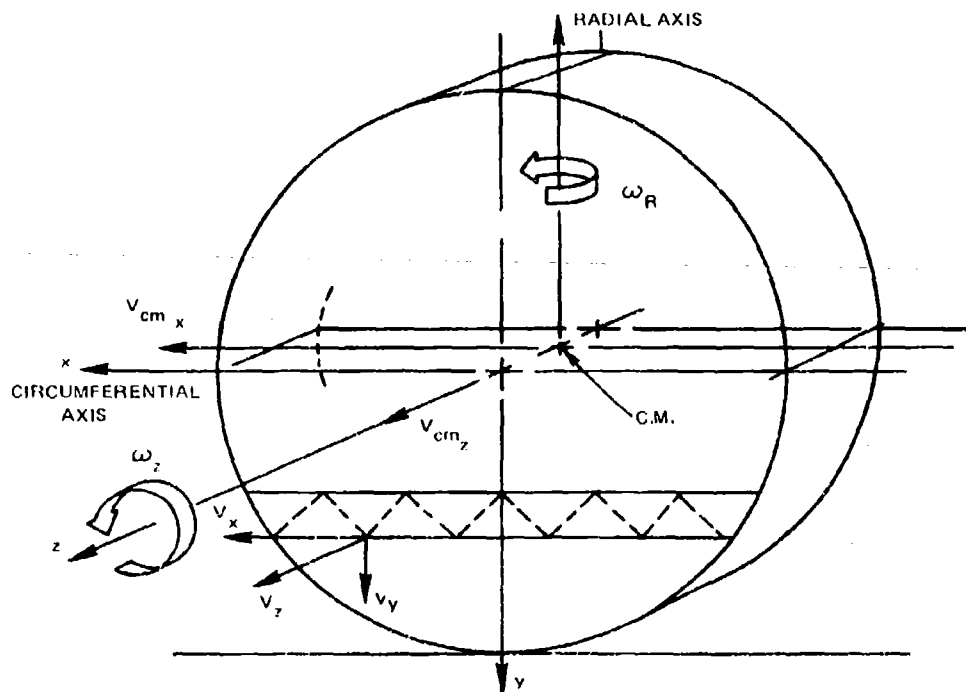


Figure 15. The Calculation of the Hydrodynamic Forces on the Roller Requires a Knowledge of the Components of the Velocity Vector at Each Node in the Finite Element Breakup

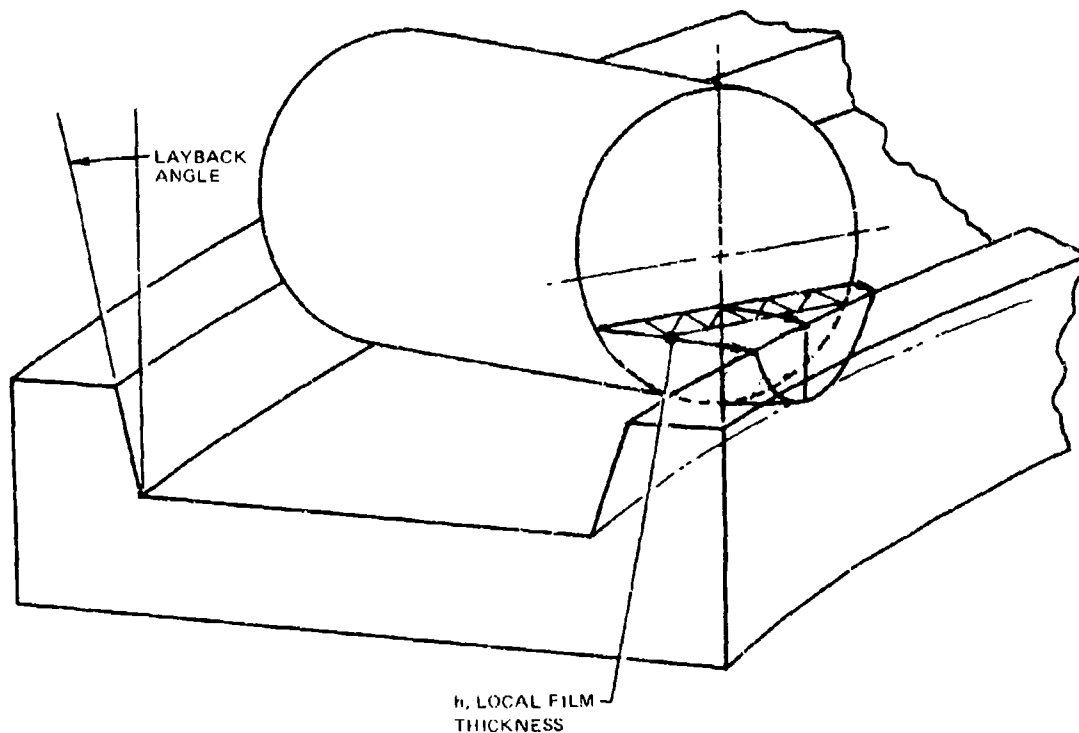


Figure 16. Film Thickness Varies Due to Roller Shew and Guide Flange Layback Angle

$$\frac{d^2 \mathbf{R}_{rk}}{dt^2} = (\ddot{\mathbf{R}}_{rk} - R_{rk} \ddot{\theta}) \mathbf{I}_{rk} + (R_{rk} \ddot{\theta} + 2 \dot{R}_{rk} \dot{\theta}) \mathbf{I}_{rk} + \ddot{Z} \mathbf{K} \quad (46)$$

P = number of unbalance masses in the roller

and the position vectors \mathbf{R}_{rk} and \mathbf{r}_{rjk} , as shown in Figure 17, represent the location of the k th roller center in the vertical frame, and the location of the j th unbalance mass with respect to the roller center.

The out-of-plane motion of the roller is then affected by the unbalance moment created by the cross-product of the position vector, \mathbf{r}_{rjk} , and the unbalance force, \mathbf{F}_{rk_unbal} as given below

$$\mathbf{M}_{rk_unbal} = \mathbf{r}_{rjk} \times \mathbf{F}_{rk_unbal} \quad (47)$$

The calculation of this moment is of great interest since it is felt that the component of this unbalance moment about the roller radial axis is one of the primary causes of roller skewing.

4.3.3 Skewing Moment Induced by an Asymmetric EHD Traction Distribution

The introduction of shaft misalignment results in roller "footprints", i.e. roller contact areas on the inner and outer raceway surfaces, which are nonsymmetrical with respect to the roller circumferential axis. When this situation occurs, the calculated EHD traction force is displaced from its axial position at the middle of the roller length to a location where the contact moment about a circumferential axis through that point would be zero. (See Figure 18). This new point, \mathbf{r}_{ik} , is calculated based upon information obtained from *STATIC* concerning the total roller contact load and the contact moment about the circumferential axis through the middle of the roller length.

Thus, for the i th raceway surface on the k th roller;

$$\mathbf{r}_{ik} = \frac{\mathbf{M}_{ik}}{P_{ik}} \quad (48)$$

$$i = \begin{array}{l} 1 \text{ outer raceway} \\ 2 \text{ inner raceway} \end{array}$$

\mathbf{M}_{ik} = contact moment (in.-lbf)

P_{ik} = contact load (lbf)

After calculating all of these moment arms, a curve is fit through the plot of their magnitudes for the inner and outer surfaces as a function of circumferential location, η . This procedure enables the program to obtain values for the moment arm, in a manner similar to that used for the traction force, for each roller as it travels around the raceway surfaces. The skewing moment for each roller is then calculated to be the sum of the products of the moment arm and its associated traction force on the inner and outer raceway surfaces.

$$\mathbf{S}_k = \sum_{i=1}^2 (\mathbf{r}_{ik} \times \mathbf{F}_{tik}) \quad (49)$$

TABLE 2. FERFI TEST RESULTS

Radial Location (r/r_o)	Pressure (Exact) (psi)	Pressure FERFI (psi)	% Error
0.0	13,800	13,800	1.3
0.15	13,490	13,470	0.1
0.3625	11,987	11,610	3.1
0.6375	8,192	8,139	0.6
0.8500	3,830	3,866	0.9
1.0	0.0	0.0	0.0

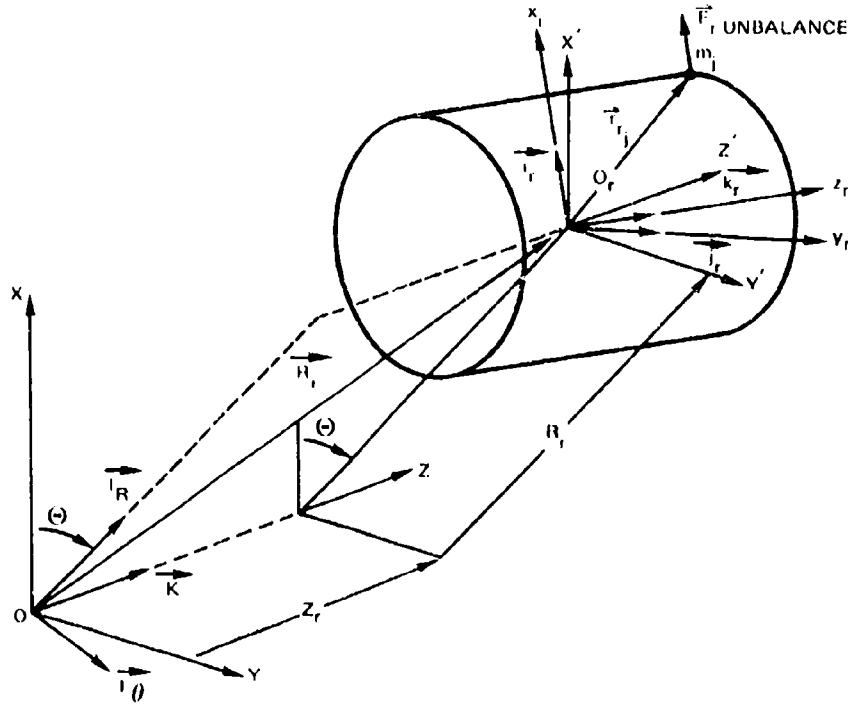


Figure 17. Coordinate System Used to Locate Roller Unbalance

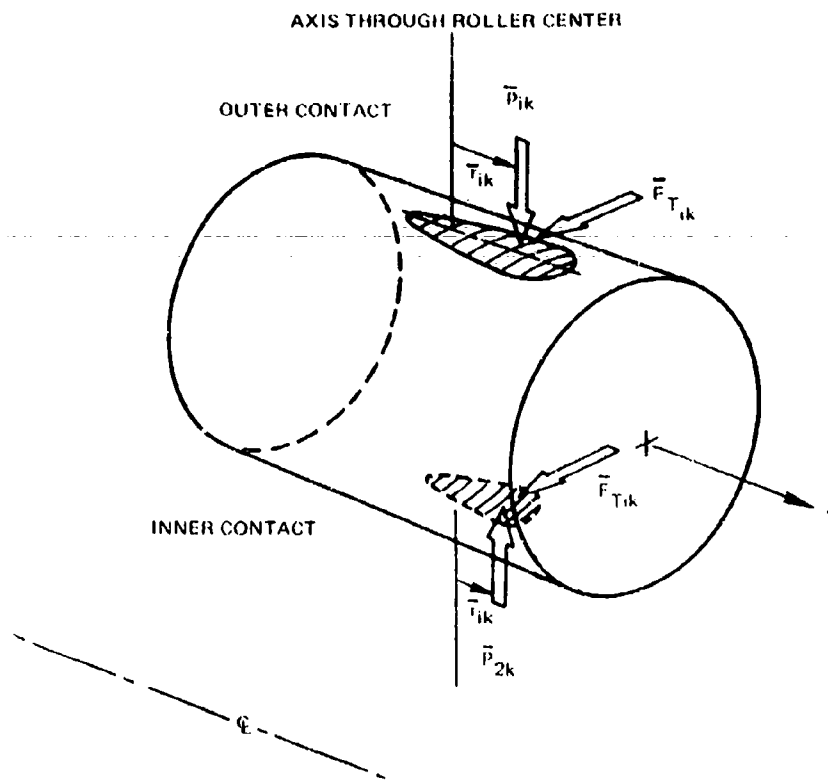


Figure 18. The Traction Force, F_T , Is Applied at an Axial Position, \bar{r} , Located at the Center of Pressure of the Contact Ellipse

4.3.4 RODYN I/O Improvements

Several new input and output features have been incorporated in RODYN, the roller dynamics program. This work was done to improve convenience for the user in the set-up and running of the deck. New output routines were also developed to highlight the most important of the various output data generated by the many analyses within the program. Both sets of improvements combine to provide an increase in overall cost effectiveness of the program by reducing the probability for error and reducing the time required for interpretation on the part of the user.

There were three areas of improvement in the input section. The first consisted of the establishment of roller sets. Each input roller set contains any number of identical rollers within the complement, the rollers in the set being identified by their position with respect to roller No. 1 at the 3 o'clock position. The rollers in the last set need not be identified since the program assigns all previously undefined rollers to this set. This feature is especially useful when there is only 1 roller in the complement which is different than the others. That one roller is identified by number in the first set, while the remaining rollers are automatically assigned within the second set.

The second improvement that was made concerned the initial conditions imposed on each of the rollers. Default values for the position of the center of mass, angular orientation, translation velocities, and angular velocities have been internally set for each roller. The default value is that quantity assigned automatically to the subject parameter by the program if the user does not care to make an independent assignment. Each roller is positioned at the pitch radius, evenly spaced

around the circumference and centered midway between the inner ring guide flanges. The angular orientation is set such that the roller local z-axis or polar axis is in the same direction as the inertial Z axis, i.e. no skewing initially exists. The orbital velocity of the center of the roller, η , is initially set equal to the no-slip orbital speed. Similarly, the angular velocity of the roller about its own center is also set according to the no-slip condition. Finally, the initial orientation of the roller is set such that the local x axis is colinear with a line drawn from the center of the bearing through the center of the roller as depicted in Figure 19. This is accomplished by fixing the roller's Euler angle ψ equal to the roller's inertial angular position η . The benefit derived from doing this is to make it easier to interpret the roller output data.

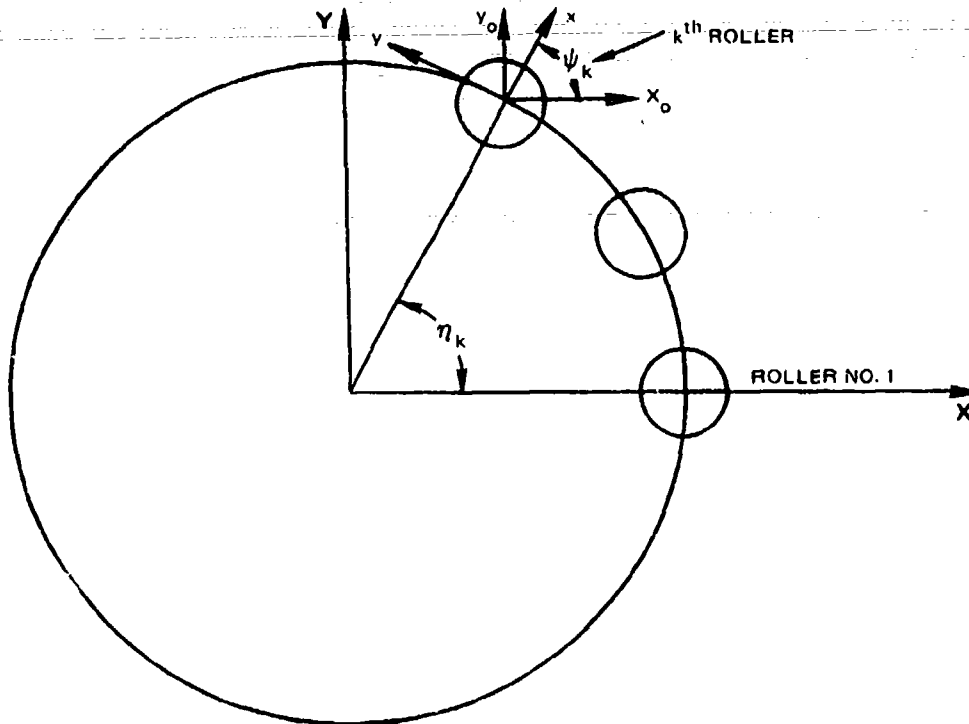


Figure 19. The Local x-Axis of the k^{th} Roller Is Oriented Such That Its Euler Angle ψ_k is Equal to the Roller's Angular Location η_k Within the Complement

The last new input feature incorporated in the RODYN module provides the user with the option of suppressing any of the individual force routines in the program. Thus, if it becomes evident that for a particular application, one of the forces plays an insignificant role in the determination of the roller motion, that calculation may then be eliminated for subsequent, similar runs. This option provides the user a corresponding savings in computer run time.

The RODYN output format has also been revised so that the most important of the calculated data can be highlighted. This work has been accomplished in both the print and plot routines. In the output printout, the user now has the capability of eliminating output data for any number of rollers, thereby focusing attention on information pertaining to only a particular number of rollers. In addition, the type of data printed for those rollers can be shortened considerably by selecting only certain types of output data. This is done by setting up groupings of various output data. Each numbered group, containing a set of output parameters, is assembled in a table and presented to the user at input. The user then selects any number of output data groups, according to his needs. In a similar manner, output plots of particular parameters may be selected at input by the user.

4.4 SYSDYN Program Module

Modeling the dynamic behavior of the complete roller bearing system is accomplished within TRIBO 1 by activation of the SYSDYN program module. SYSDYN utilizes the CADYN and RODYN analyses in combination with additional subroutines designed to account for the interactions that occur between rollers and cage. The forces and moments imposed on the rollers due to the cage and vice versa are transmitted through the interfaces at the circumferential cage web and the cage siderail. Forces and moments developed at these interfaces arise from either hydrodynamic pressure generated in the interposed lubricant film or through actual metal-to-metal impact. The development of the roller-cage web impact model was discussed previously in this report in Section 3.2. The roller-cage web hydrodynamic contact model was described in the first interim report in Section V.C.2.

Three-dimensional roller and cage motion as predicted by SYSDYN can be very complex. Simplification of the 3-D coupled system by restricting motion to two dimensions is valuable for the purpose of confirming the basic program logic and analyses, and efforts on the development of the SYSDYN module have been primarily directed towards this end. Expansion of the model to include 3-D motion is proceeding as well, contingent upon successful completion of the 2-D program validation tests. A number of general improvements have also been made to the SYSDYN module to upgrade efficiency and enhance user convenience.

One of these improvements is that the overall input format was broken down into several separate components based upon the combination of sub-programs to be run e.g. STATIC, STATIC plus SYSDYN, SYSDYN alone, etc. Each of these component input formats is now a separate entity, identified by a single flag on the first input card, and reflecting only that information required as input to run the specific subprogram desired. In addition, several other convenience items, such as the capability of inputting cage angular velocities in the cage local frame, as opposed to the inertial frame, were built into the deck.

Interpretation of program output has also been greatly improved by the development of an expanded plotting routine for SYSDYN. The new plotting package can be requested in its entirety or on an individual plot-by-plot basis by the user. Plots include cage angular velocity relative to the non-slip condition, roller circumferential displacement within the cage pocket, roller orbital velocity relative to the non-slip condition, roller circumferential forces, and roller skew angle.

Another significant improvement was made concerning the reorganization of the data base generated by the program. It has been estimated that, due to the increasing size and complexity of the program, two million bytes of computer core storage would be required to analyze a typical bearing with thirty rollers. Since overall computer system efficiency is increased when core requirements are reduced, an effort was made to improve the program's data processing procedures. By removing from core those data that specifically pertain to output printing and plotting and holding them on a separate storage disk, the program is now capable of analyzing a bearing with thirty roller elements using only one half the storage previously needed.

The first coupled system dynamics case chosen to test SYSDYN was run successfully. This model case corresponded to a non-preloaded roller bearing and employed four equally spaced rollers. Using four rollers instead of a full complement allows computer run times to be minimized for the test case.

The system was constrained to operate with two-dimensional motion and was subjected to an externally applied radial load of 1500 lb at 3 MDN. The test case, which was run for 50 milliseconds of real time, encompassed 9 complete roller orbits or the equivalent of 9 complete rotations of the cage. The total CPU time required for running this case was approximately 2 minutes.

One of the output items from this test case identifies the effects of the roller interaction forces on the cage motion during transient motion of the system which is diagrammatically represented in Figure 20. For comparative purposes, Figure 21 shows the motion of the cage under similar conditions, but uncoupled from the effects of the rollers, obtained from a CADYN run for the same cage used in the subject SYSDYN test case. The influence of the four rollers on the displacement of the cage is manifested as a more random motion of cage center of gravity within the clearance circle. Note that since the cage C.G. stays within the clearance circle, roller interactions were not sufficiently severe to cause the cage bore to contact the inner ring lands.

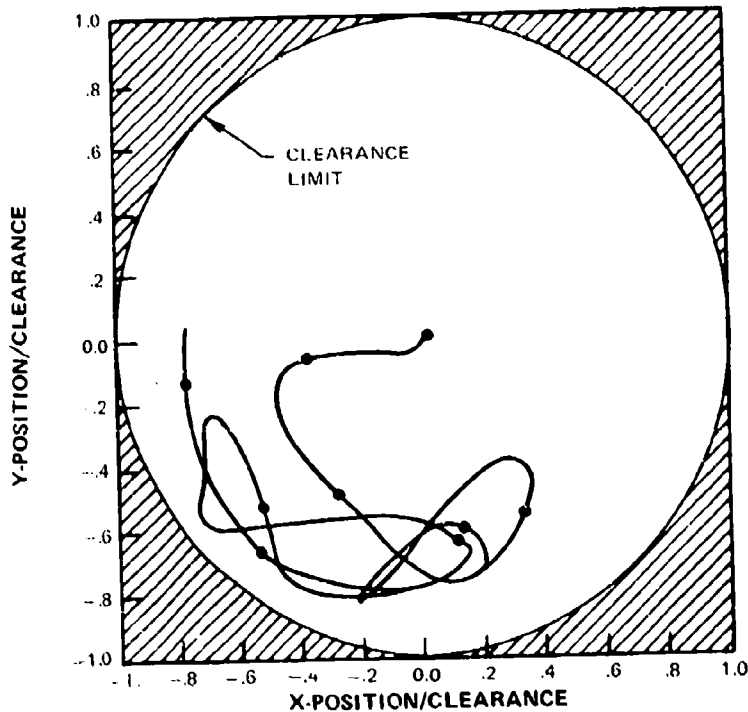


Figure 20. 2-D SYSDYN Shows No Cage Land Contact When Rollers Interact With Cage

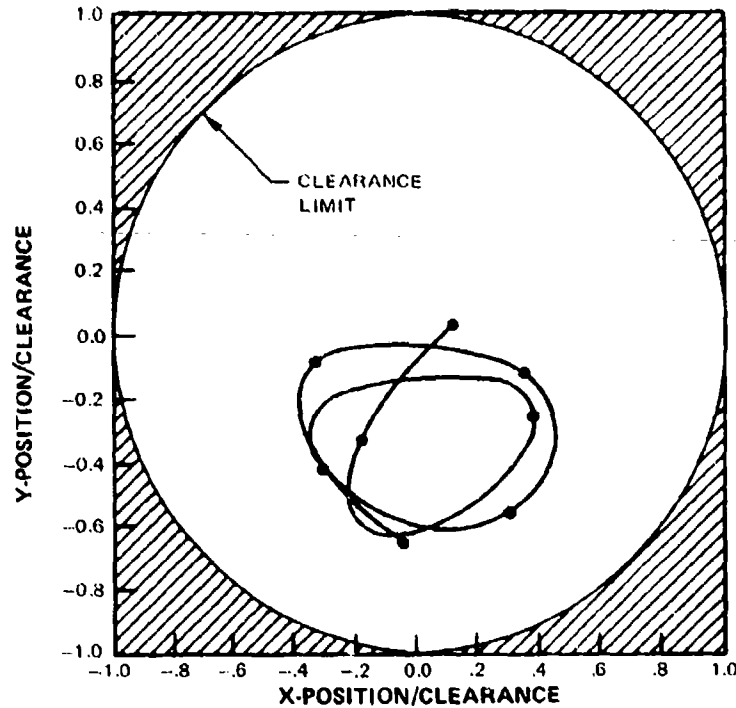


Figure 21. CADYN Shows Motion of Cage Unaffected by Rollers

Figure 22 shows the force history for a typical roller as a function of time. The traction and cage web hydrodynamic forces are seen to be a maximum as the roller passes through the load zone as might be expected. Although no actual roller/cage metallic impacts occurred during the run, as shown in Figure 23, the cyclical nature of the circumferential roller motion within the cage pocket is quite evident. While no definite conclusions can be drawn from the results of this test case due to its simplicity, it is felt that the general trends predicted by SYSDYN are compatible with the physically reasonable dynamic behavior of a real bearing.

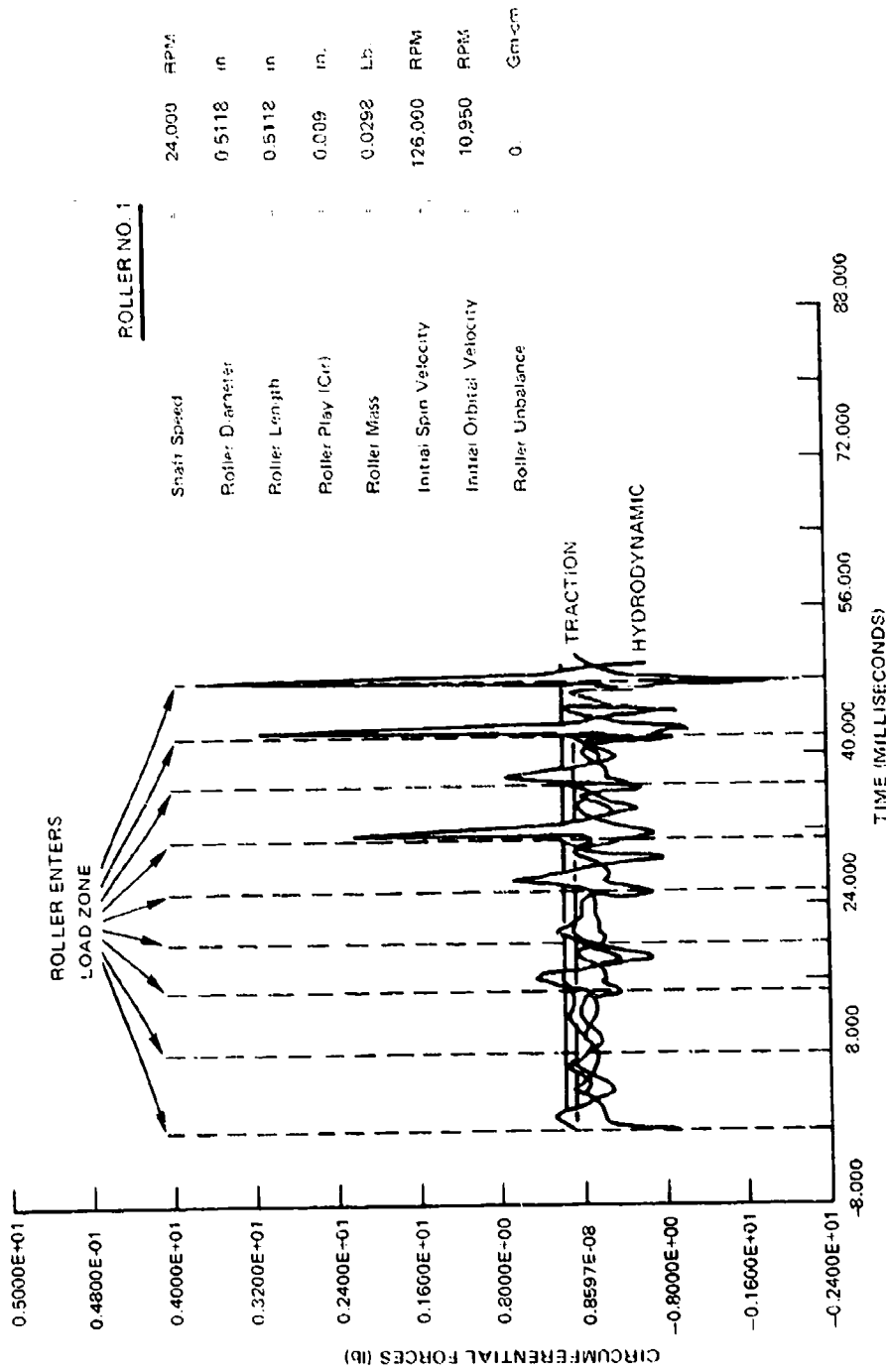


Figure 22. 2-D SYSDYN Shows Peak Roller Loads as Roller Enters Load Zone

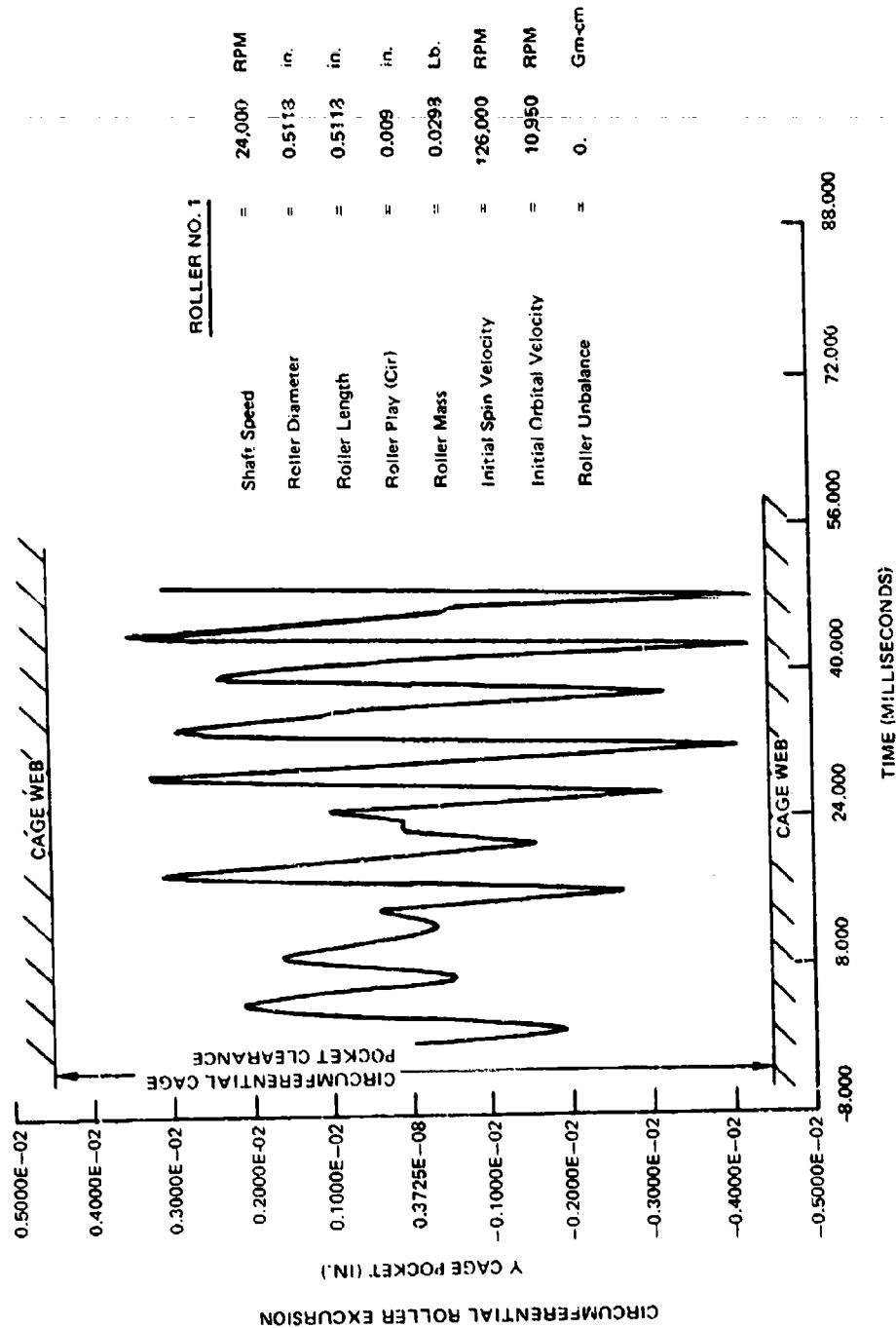


Figure 23. Hydrodynamic Forces Are Sufficient To Prevent Roller/Cage Contact for 2-D Motion

5. FUTURE WORK

Work during the next interim reporting period will focus on the following areas:

1. Continued refinement of analytical models
2. Continued analytical verification of SYSDYN module in the 3-D mode
3. Continued TRIBO I correlation with test data
4. Preparation of design manual.

6. PARAMETRIC AND VERIFICATION TESTING — TASK II

6.1. Summary of Previous Progress

The experimental progress made under Task II of the Contract for the period 1 October 1975 to 1 April 1977 is described in detail in Reference 8. For the sake of completeness a summary of the work accomplished under Task II during that period is presented here.

6.1.1 Parameter Selection and Bearing Design

A total of 30 separate variables that can influence roller skew and skid were identified. These variables were then divided into three categories. Category I included 14 variables considered to have the greatest direct influence on roller end wear. Category II was composed of eight variables considered to have less direct impact on roller wear, and Category III was composed of eight variables judged to have the least direct effect. Two groups of bearings were designed in order to evaluate some of the roller bearing variables from Categories I and II using statistical design experiment techniques.

The basic roller bearing selected for the design of the parametric bearings is shown in Figure 24. This bearing has a bore diameter of 124.3 mm and is used in the No. 5 position of the TF30 model production engine.

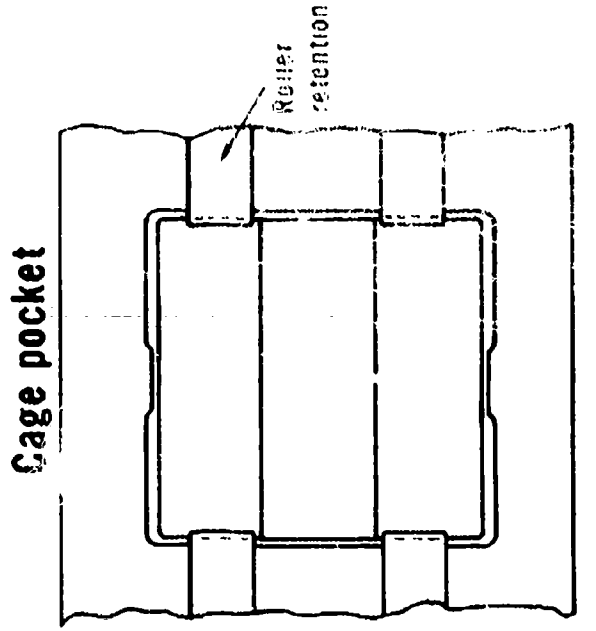
The first group of bearings, designated as Group-N, were designed for evaluation under Task II. Eight designs were prepared incorporating seven parameters selected from Category I. Two levels of variations were selected for each parameter. The parameters selected for test and the actual levels of variation for each of the bearing designs are shown in Figure 25. A total of 10 bearings were manufactured for test, one each of the eight designs and duplicates of No.'s 7 and 8 to provide hardware for repeat testing.

The second group of bearings, designated as Group-AF, were designed for evaluation under Task VI. Five test bearings were designed, Figure 26, incorporating four parameters selected from Category II. As with the Group-N bearing designs, two levels of variation were selected for each parameter. The actual levels of the parameter variation are presented in Figure 26. A total of six Group-AF bearings were procured, one each of the five designs and a duplicate of bearing No. 22 for repeat testing.

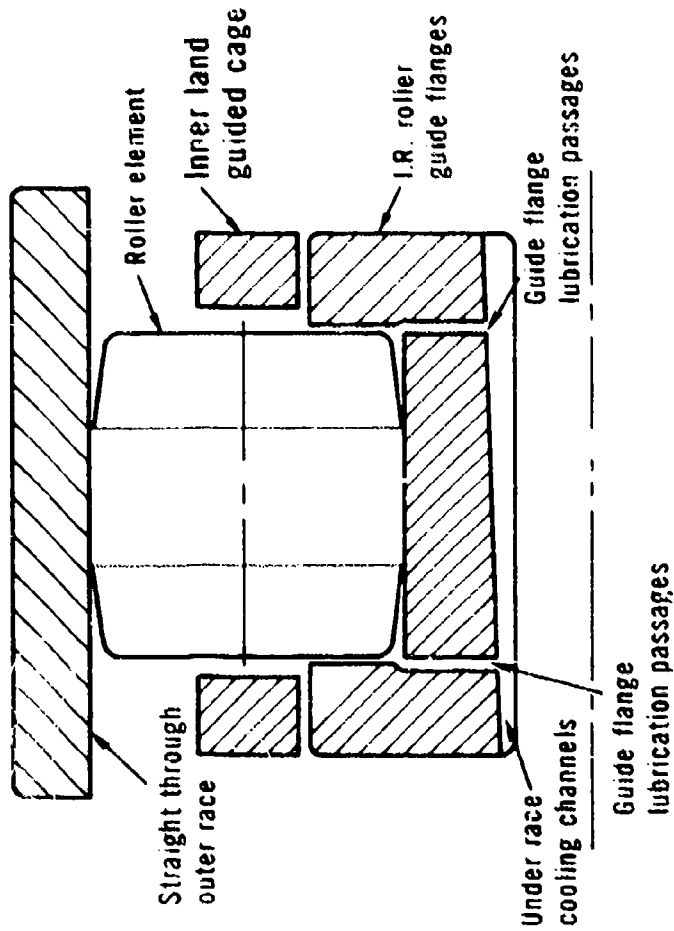
6.1.2 Pretest Inspection and Preparation

For each of the Group-N and Group-AF bearings, detailed dimensional measurements of the bearing components were made and recorded by the manufacturer. This was done to ensure tight quality control as would be required by any statistically planned program and to provide reference data useful to the post-test analysis of the experimental results. A summary of these inspection results is provided in Tables 3 and 4 with the average measurements shown where possible.

Following this inspection work the Group-N bearings were prepared for test. Each outer ring was instrumented with a strain gage to permit measurement of roller pass frequency during dynamic testing in order to determine whether or not the roller elements were skidding. Also, the end faces of every other roller element were copper flashed for the purpose of highlighting any end wear that may occur during testing. In addition, each roller was weighed and measured for static skew angle of turn allowed by the combination of end clearance and the inner ring guide flange geometry. Repeating the weighing after test permits a determination of the amount of roller mass loss attributable to end wear. Repeating the skew angle measurement after test permits an assessment of the combined effect of the wear of both the roller and the guide flanges. The pretest roller weight and static skew angle measurements for the Group-N bearings are found in Table 5.



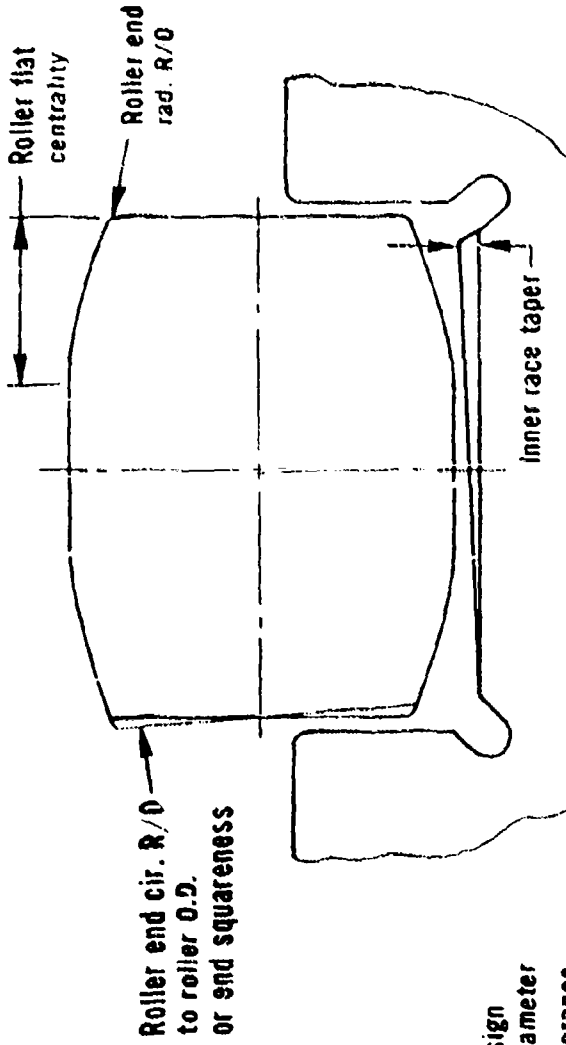
Cage pocket



Inner race bore dia. : 124.3mm
Basic roller size, L/D : 13mm X 13mm
No. of rollers : 28
No. of radial tube holes : 3 per side
Bearing material : **VIM-VAR M-50**

Cage material : **AMS-6414**
Cage plating : **Silver per AMS-2412**

Figure 24. This Basic Bearing Used for Parametric and Verification Testing Has Seen Extensive Use in the TF30 Engine

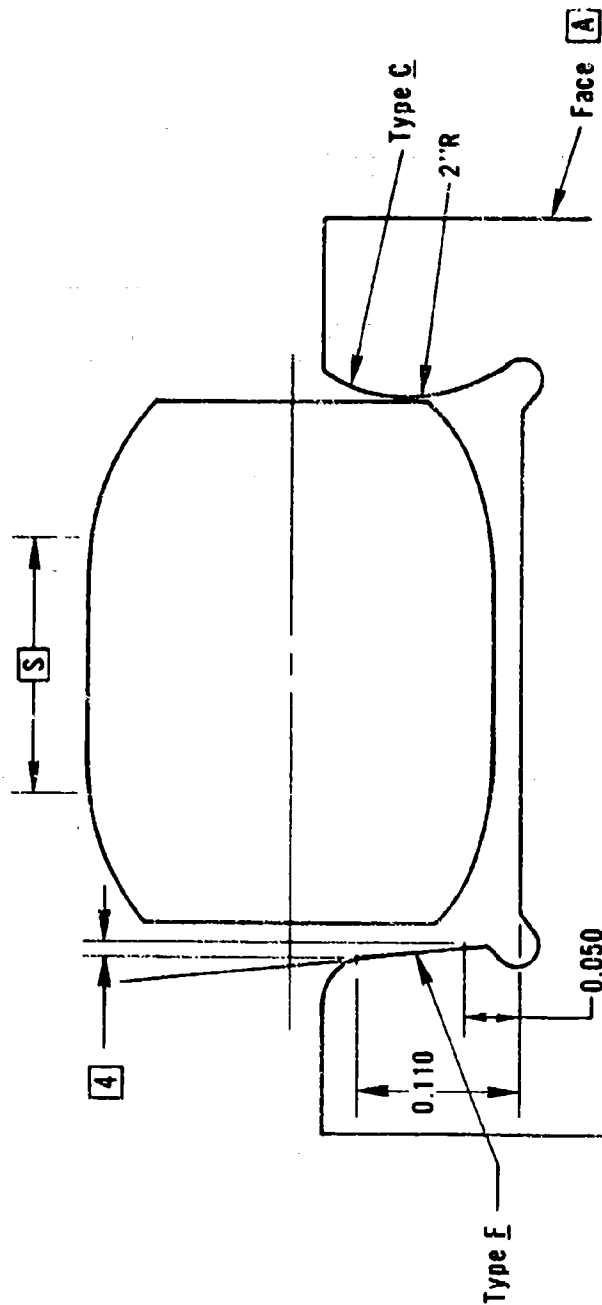


Legend

- Design parameter
- Tolerance parameter

Bearing serial no.	Parameters						
	1 Bearing preload, lbs.	2 Max. coupled roller end radius R/D inch	3 Roller end cir. R/D to roller O.D. inch	4 Inner race taper minutes	5 Roller flat centrality, inch	6 Raceway angular misalignment degree	7 Lubrication oil, lb/min
Baseline	500	0.001	0.000120	0.8	0.010	0	20
1	500	0.005	0.000180	0.8	0.050	0	13
2	500	0.001	0.000050	3.58	0.010	0	29
3	0	0.005	0.000050	3.58	0.010	0.5	13
4	0	0.001	0.000180	0.8	0.050	0.5	29
5	0	0.001	0.000180	3.58	0.050	0	13
6	0	0.005	0.000050	0.8	0.010	0	29
7	500	0.001	0.000050	0.8	0.010	0.5	13
8	500	0.005	0.000180	3.58	0.050	0.5	29
9	Same as No. 7						
10	Same as No. 8						

Figure 25. Group-N Bearings Are Designed To Evaluate Two Levels of Each Parametric Variable



Legend
 □ Design parameter
 □ Tolerance parameter

45

Bearing no.	Parameters			
	Extended roller flat, % of roller length, □ S	IR guide range layback, inch, □ 4	IR guide range contour, Type E	IR guide range import to face, inch, max, □ 2
Baseline	40	0.00025 max.	Type E	0.0004
21	48	0.00025 max.	Type E	0.0004
22	67	0.0009-0.0011	Type E	0.0020
23	67	0.0009-0.0011	Type C	0.0004
24	67	0.00025 max.	Type C	0.0020
25	48	0.0009-0.0011	Type C	0.0020
26	Same as No. 22			

Figure 26. Group-AF Bearings Are Designed To Evaluate Two Levels of Each Parametric Variable

TABLE 3. GROUP-N BEARINGS-MANUFACTURING INSPECTION DATA

	Bearing Number										
	B/I	1	2	3	4	5	6	7	8	9	10
Bearing Assembly											
Cage Clearance, in.	0.0176	0.0177	0.0193	0.0172	0.0175	0.0170	0.0182	0.0179	0.0190	0.0170	0.0182
Roller End Clearance, in.	0.0012	0.0012	0.0010	0.0013	0.0009	0.0010	0.0012	0.0011	0.0011	0.0014	0.0011
Internal Radial Clearance (Unmounted), in.	0.0040	0.0045	0.0044	0.0043	0.0042	0.0044	0.0042	0.0039	0.0046	0.0042	0.0052
Rollers											
Length, in.	0.51175	0.51188	0.51162	0.51168	0.51160	0.51160	0.51190	0.51176	0.51150	0.51169	0.51181
Diameter, in.	0.51166	0.51194	0.51168	0.51170	0.51137	0.51139	0.51140	0.51173	0.51194	0.51174	0.51134
Surface Finish (AA), μ in.	—	3.5	2.5	1.5	6.0	3.25	1.0	2.5	6.7	2.25	5.0
Corner Radius R.O., in.	0.001	0.00370	0.00023	0.00335	0.00017	0.0020	0.00335	0.00024	0.00370	0.00005	0.00350
Crown Radius, in.	24	30	30	30	50	30	30	30	50	30	30
Cylinder Length, in.	0.209	0.203	0.247	0.250	0.191	0.210	0.231	0.244	0.186	0.238	0.172
Cylinder Flatness, μ in.	—	0.010	0.050	0.006	0.051	0.044	0.008	0.004	0.049	0.005	0.060
Cylinder Off-Set, in.	—	160	—	—	95	75	—	—	150	—	145
Crown Profile R.O., μ in.	120	245	45	50	170	155	50	45	185	40	190
End Squariness, μ in.	0.00085	0.00060	0.00060	0.00065	0.00063	0.00048	0.00053	0.00060	0.00053	0.00058	0.00063
Crown Drop, in.	60 min	62.0	63.0	62.5	62.0	62.0	61.0	62.5	—	63	62
Hardness (R _c)											
Outer Ring											
OD Max, in.	6.7561	6.7559	6.7554	—	—	—	—	6.7562	6.7558	6.7563	6.7559
OD Min, in.	6.7350	6.7351	6.7358	—	—	—	—	6.7351	6.7351	6.7352	6.7352
OD Avg, in.	6.7456	6.7455	6.7455	6.7459	6.7458	6.7458	6.7459	6.7457	6.7455	6.7458	6.7456
ID, in.	6.4246	6.4247	6.4247	6.4244	6.4244	6.4249	6.4242	6.4249	6.4243	6.4247	6.4245
Eccentricity, μ in.	25	18	35	13	8	15	18	19	18	18	38
ID Flatness, μ in.	15	12	27	15	18	12	12	12	22	27	24
Surface Finish (AA), μ in.	4.0	4.5	2.5	2.5	1.5	2.0	2.0	4.0	4.0	4.5	5.0
Hardness (R _c)	62.0	63.5	62.5	62.5	62.5	63.0	63.5	63.0	63.5	62.0	62.5
Inner Ring											
Bore Diameter, in.	4.8936	4.8938	4.8936	4.8936	4.8938	4.8937	4.8936	4.8938	4.8936	4.8936	4.8937
OD Overall, in.	5.6773	5.6771	5.6770	5.6772	5.6768	5.6771	5.6772	5.6772	5.6773	5.6771	5.6770
OD Roller Path, in.	5.3956	5.3966	5.3965	5.3968	5.3970	5.3970	5.3964	5.3969	5.3955	5.3966	5.3961
Roller Path Eccentricity, μ in.	18	20	18	20	8	10	20	19	18	18	18
Roller Path Taper, deg/min	0-0	0-0	0-3.42	0-3.58	0-0	0-3.25	0-0	0-0	0-3.00	0-0	0-3.58
Guide Flange Angle, deg/min	0-6	0-3.7	0-3.4	0-6.4	0-5.16	0-5.59	0-6.45	0-4.30	0-3.23	0-4.08	0-2.69
Guide Flange Finish (AA), μ in.	4.9	2.5	3.5	5.0	3.0	3.0	5.0	5.0	3.0	4.0	2.5
Roller Path Finish (AA), μ in.	3.0	2.5	4.5	3.0	3.0	3.0	2.5	4.0	3.0	3.5	3.0
Hardness (R _c)	63.0	63.0	63.0	62.5	62.5	62.5	62.0	62.5	63.0	63.0	63.0
Cage											
ID, in.	5.6977	5.6973	5.6971	5.6974	5.6973	5.6974	5.6968	5.6975	5.6950	5.6973	5.6970
Pocket Squareness, μ in.	450	150	440	130	190	240	350	460	440	120	470
Pocket Parallelism, in.	0.0011	0.0021	0.0012	0.0015	0.0016	0.0013	0.0013	0.0015	0.0011	0.0013	0.0013
Unbalance, gram-centimeter	1.32	1.21	1.44	1.40	1.13	2.03	2.73	1.17	1.40	2.14	1.91
Hardness (R _c)	33.0	33.5	32.5	33.5	33.0	33.0	33.0	33.0	32.5	33.0	33.5

TABLE 4. GROUP-AF BEARINGS-MANUFACTURING INSPECTION DATA

	Bearing Number						
	B/L	21	22	23	24	25	26
Bearing Assembly							
Cage Clearance, in.	0.0176	0.0172	0.0172	0.0170	0.0182	0.0173	0.0167
Roller End Clearance, in.	0.0012	0.0010	0.0095	0.00105	0.00105	0.0012	0.00115
Internal Radial Clearance (Unmounted), in.	0.0040	0.0041	0.0045	0.0046	0.0041	0.0044	0.0042
Rollers							
Length, in.	0.51175	0.51068	0.51194	0.51187	0.51194	0.51067	0.51196
Diameter, in.	0.51166	0.51089	0.51182	0.51183	0.51187	0.51085	0.51181
Surface Finish (AA), μ in.	—	2.75	2.25	2.25	2.25	3.0	2.25
Corner Radius R.O., in.	0.001	0.000175	0.0002	0.000175	0.000190	0.000175	0.0002
Crown Radius, in.	24	30	30	30	30	30	30
Cylinder Length, in.	0.209	0.2665	0.335	0.3355	0.327	0.276	0.326
Cylinder Flatness, μ in.	—	24	22	24	18	27	22
Cylinder Off-Set, in.	0.010	0.004	0.008	0.007	0.0055	0.010	0.0045
Crown Profile R.O., μ in.	—	—	—	—	—	—	—
End Squareness, μ in.	120	70	75	70	75	80	75
Crown Drop, in.	0.00085	0.00057	0.00018	0.00020	0.00015	0.0005	0.00020
Hardness (R)	60 min	61.5	63.0	63.5	63.5	61.5	62.5
Outer Ring							
OD Max, in.	6.7561	6.7558	6.7558	6.7558	6.7562	6.7566	6.7562
OD Min, in.	6.7350	5.7353	6.7353	6.7349	6.7353	6.7354	6.7353
OD Avg, in.	6.7456	6.7456	6.7456	6.7454	6.7458	6.7460	6.7458
ID, in.	6.4246	6.4245	6.4249	6.4247	6.4247	6.4247	6.4248
Eccentricity, μ in.	25	25	38	10	18	25	18
ID Flatness, μ in.	15	19.5	24	12	25	6	30
Surface Finish (AA), μ in.	4.0	3.5	4.0	4.0	4.0	3.0	4.8
Hardness (R)	62.0	63.5	63.0	63.0	63.0	63.0	63.0
Inner Ring							
Bore Diameter	4.8936	4.8937	4.8937	4.8937	4.8937	4.8936	4.8937
OD Overall, in.	5.6773	5.6769	5.6773	5.6772	5.6773	5.6773	5.6773
OD Roller Path, in.	5.3966	5.3981	5.3960	5.3957	5.3962	5.3980	5.3963
Roller Path Eccentricity, μ in.	18	18	18	20	20	18	18
Roller Path Taper, deg-min	0-0	0-0	0-0	0-0	0-0	0-0	0-0
Guide Flange Angle, deg-min	0-6	0-7.16	0-50.4	0-55.6	0-0.01	0-52.3	0-49.2
Guide Flange Finish (AA), μ in.	4.9	3.5	6.5	7.0	7.0	8.9	6.5
Roller Path Finish (AA), μ in.	3.0	3.5	2.5	3.5	3.0	3.5	3.5
Hardness (R)	63.0	64.0	62.0	62.0	62.5	63.0	63.0
Cage							
ID, in.	5.6977	5.6976	5.6974	5.6966	5.6985	5.6976	5.6971
Pocket Squareness, μ in.	450	380	110	330	150	510	410
Pocket Parallelism, in.	0.0011	0.001	0.0019	0.0013	0.0013	0.0013	0.0021
Unbalance, gram-centimeter	1.32	2.23	1.28	1.20	1.35	2.40	1.20
Hardness (R)	33.0	33.0	33.0	33.0	34.0	33.0	33.0

TABLE 5. GROUP-N BEARINGS — PRETEST WEAR RELATED MEASUREMENTS

Bearing No.	Avg Roller Weight (Grams)		Avg Skew Angle (Minutes)	
	Unflushed	Flushed	Unflushed	Flushed
Baseline	—	13.3875	—	—
1	13.2457	13.2474	14.94	15.29
2	13.2918	13.2924	11.95	11.79
3	13.2417	13.2377	14.19	14.19
4	13.2755	13.2736	13.71	13.62
5	13.2768	13.2786	13.43	13.76
6	13.2411	13.2421	14.98	14.22
7	13.2866	13.2853	10.87	10.87
8	13.2446	13.2486	14.47	14.59
9	13.2999	13.2938	13.96	13.85
10	13.3340	13.3317	15.10	14.78

Other pre-test work included in-house inspection measurements which were made and recorded during the process of installing each of the bearings in the test rig. These measurements included the fits of both the inner ring on the shaft and the outer ring in the support housing, the installed internal radial clearance of the test bearing, and the axial misalignment of the installed outer ring.

6.1.3 Experimental Program Plan

A 10-hour test program to be followed during the rig evaluation of each of the parametric bearings was prepared. The program, see Table 6, was designed to generate both calibration and endurance test data for each of the statistically designed bearings. At the completion of each 10-hour test, the experimental data is reduced in order to obtain the following bearing performance parameters:

- Heat generation
- Horsepower and torque
- Roller skid
- Inner and outer ring thermal stability
- Outer to inner ring thermal gradient
- Axial and circumferential thermal gradients

TABLE 6. CALIBRATION AND ENDURANCE TEST PROGRAM

	Supply Oil Flow (lb/min)			°F	Applied Bearing Load, (lb)	Bearing DN/Test Point No.						Test (hr)
	Under Race	Each Side Jet*	Total			1.0	2.0	2.5	2.75	2.9	3.0	
Calibration				225	250	1	4	7	10	13	16	
	10	5	20	225	500	2	5	8	11	14	17	3
				225	1000	3	6	9	12	15	18	
	5	4	13	225	500	19	20	21	22	23	24	1
	11	9	29	275	500	25	26	27	28	29	30	1
Steady State Endurance												
Group-N	5 or 11	4 or 9	13 or 29	225	500	Endurance at 3 MDN						4
Group-AF	10	5	20									
Cyclic Speed												
Group-N	5 or 11	4 or 9	13 or 29	225	250	2.0 ± 2.75 MDN Accels-Decels						1
Group-AF	10	5	20									

*Two jets, one directed at each side of bearing.

In addition, each roller element is weighed and also measured for the static angle of turn that is allowed within the inner ring guide flanges. Using the pretest and post-test measurements, roller wear as determined by weight loss, and roller and guide flange wear as determined by change in static skew angle is determined. Using statistical regression analysis techniques, the bearing parameters within each group of bearings is then ranked on the basis of roller element wear.

6.1.4 Baseline Bearing Test

Baseline experimental data was obtained on a 124.3 mm bearing which was similar to the TF-30 No. 5 position design for comparative use when analyzing the parametric test results. The bearing was rig evaluated in accordance with the 10-hour parametric test program as outlined in Table 6. A detailed tabulation of the pretest, test and post-test inspection results are presented in Reference 8.

6.1.5 Group-N Bearing Tests

As previously reported, parametric testing was completed on four of the ten Group-N bearings. The bearings tested are those identified in Figure 25 as No's. 7, 9, 6 and 2. Stable operation was noted on each bearing except No. 6 which failed during the calibration portion of the 10-hour program. A wide range of wear was observed during the testing of these four bearings. In general, similar thermal and power consumption results were obtained for each bearing. Although bearing No. 6 failed after only 1.58 hours of test and exhibited heavy eccentric roller end wear, the performance curves revealed no unusual thermal behavior. Bearing No. 6, which was the only unpreloaded bearing tested in this group, exhibited continuous skidding over the speed range of 1.0 MDN and no skidding at the 2.75 MDN level. No significant element skidding was apparent for either of the other three preloaded bearings or the preloaded baseline design. As shown in Figure 25, bearing No. 6 was the only bearing of the group tested that contained roller elements with a high level of coupled roller end radius runout. This coupled runout is tantamount to roller dynamic unbalance which is a prime cause of roller skewing. In the case of bearing No. 6, the skewing resulted in roller end wear of such an extent that a number of the rollers turned 90° in the raceway and resulted in the cage fracturing into several pieces.

6.2 Group-N Bearing Parametric Tests

During the current reporting period, testing was completed on five of the remaining six Group-N parametric bearings. The bearings tested were those identified in Figure 25 as No's. 4, 5, 1, 3, and 8. Stable operation was observed with bearings No's. 4 and 5. The remaining bearings failed during the calibration phase of the 10-hour program. As in the case of bearing No. 6 which had failed previously, bearings No's. 1, 3, and 8 also contained rollers with a high level of coupled roller end radius runout or unbalance as noted in Figure 25. Bearing No. 10, the remaining bearing from Group-N will be tested at a later date but not before the rollers are replaced. This repeat bearing, similar in design to bearing No. 8 which is one of those that failed in previous testing, presently contains roller elements with a high level of corner radius runout. Thus, a failure of similar severity would be expected to occur if this bearing were tested as is. Such a test is considered to be of little value to this program. As a result, bearing No. 10 is now being re-fitted with a new set of rollers that contain a minimum level of corner radius runout. This roller set will also feature a tighter tolerance on flat centrality which, when tested, will provide end wear data that will allow separation of the effects of this parameter from that of roller end radius runout.

6.2.1 Pretest Inspection and Preparation

Detailed dimensional measurements of the five Group-N bearings tested during this report period are provided in Table 3. In addition, the pretest roller weight and static skew angle measurements are shown in Table 5. Preparation of the bearings for test, including the strain gauging of the outer rings in order to provide roller pass frequency measurements and the copper flashing of alternate rollers for the purpose of highlighting end wear, was completed earlier as reported in Reference 8. Inspection measurements were made and recorded during installation of the parametric bearings into the test rig. These measurements included the fits of the inner ring on the shaft and the outer ring in the support housing, the installed internal radial clearance of the test bearing and the axial misalignment of the installed outer ring.

The measurements recorded for the five Group-N bearings that were tested during this report period are shown in Table 7.

TABLE 7. GROUP-N BEARINGS -- PRETEST RIG RELATED INSPECTION MEASUREMENTS

	Bearing Numbers				
	4	5	1	3	8
Inner Ring/Shaft Fit, in.	0.0012T	0.0013T	0.0012T	0.0012T	0.0012T
Internal Radial Clearance Installed, in.	0.0026	0.0039	0.0037	0.0034	0.0039
Outer Ring/Housing Fit, in.	0.0006L	0.0006L	0.0009L	0.0005L	0.0009L
Outer Ring Misalignment, deg.	0.487	0	0	0.487	0.487

6.2.2 Experimental Evaluation of Bearing No. 4

The first Group-N bearing tested was bearing No. 4 and, as shown in Figure 25, this design was not preloaded. At assembly the outer ring axial misalignment was adjusted to 0.487 degrees. Testing proceeded following the program outlined in Table 6. Roller pass frequency measurements indicated that roller skid was occurring in the speed range of 1.0 to 2.5 MDN. At speeds of 2.75 MDN and higher, the rollers did not skid, as indicated by the frequency measurements. The magnitude of the skid, see Figure 27, was the greatest at 2.0 MDN, with the maximum amount of skidding occurring at the lowest applied radial load. After completing the calibration portion of the program, the test was interrupted to inspect the bearing. Each roller was found to exhibit some light concentric wear on both ends, but no eccentric wear was in evidence. No skid damage to the bearing components was visible. The rollers were then weighed and their static skew angles measured. There was no significant change in the weight or skew angles based on pre-test measurements. The bearing was reinstalled in the rig and the steady state endurance and cyclic portions of the program were completed. Total oil flow to the bearing was metered at 25.6 lb/min. during the endurance testing.

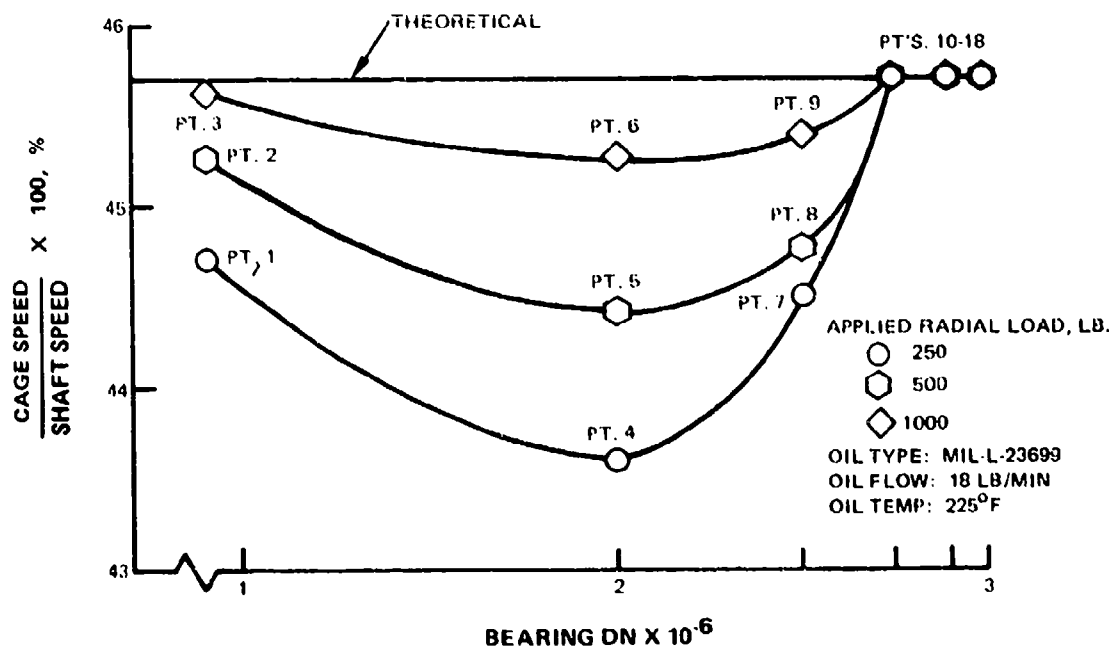


Figure 27. Test of Group-N Bearing No. 4 Shows Increased Skid as Load Is Decreased but With No Skid at Any Load Beyond 2.75 MDN

Stable operation was noted throughout the steady state endurance testing. Post-test inspection revealed all of the bearing components to be in good condition as shown in Figure 28. No distress or unusual wear of the components was noted. All of the rollers were found to be free of eccentric wear. However, they did exhibit the same light concentric rubbing patterns on both ends as was noted previously after the first 5 hours of calibration testing. Roller weight measurements indicated a weight loss of 0.002 grams for both the flashed and unflashed rollers. The static skew angle increased an average of $0^{\circ} 1.73'$ for the flashed rollers, and an average of $0^{\circ} 1.67'$ for the unflashed rollers.

6.2.3 Experimental Evaluation of Bearing No. 5

The next bearing tested was No. 5. As shown in Figure 25, this design did not provide for roller element preloading but did feature a high level of inner raceway axial taper. The bearing was installed in the test rig with zero outer ring misalignment, and completed the 10-hour program without interruption. Roller pass frequency measurements indicated that roller skid was occurring in the speed range of 1.0 to 2.5 MDN, as was also noted with bearing No. 4. Again, roller skidding was absent at speeds of 2.75 MDN or above. The skid map, Figure 29, shows the magnitude of skid again to be greatest at 2.0 MDN, with the maximum amount of skidding occurring at the lowest applied load. Stable operation was noted throughout the steady state and cyclic speed endurance testing which was conducted at a total bearing oil flow of 12.3 lb/min. Post-test inspection revealed all of the bearing components to be in good condition as depicted in Figure 30. No significant distress or unusual wear of the components was noted. All of the rollers were free of eccentric end wear, however, they did exhibit light concentric wear on one end. This wear was most likely due to the $0^{\circ} 3.25'$ inner raceway axial taper and the reduced oil flow of 12.3 lb/min during the steady state endurance testing. Roller weight measurements indicated a weight loss of only 0.0001 grams for both the flashed and unflashed rollers. The static skew angle increased an average of $0^{\circ} 1.40'$ for the flashed rollers, and an average of $0^{\circ} 1.84'$ for the unflashed rollers.

6.2.4 Experimental Evaluation of Bearing No. 1

The next bearing design tested was No. 1. As shown in Figure 25 this design is preloaded and Table 3 indicates that the maximum coupled roller end radius runout was determined to be an average 0.0037 inch. The bearing was installed in the rig without outer ring misalignment and testing was initiated in accordance with the 10-hour parametric program. Bearing performance was stable from the onset, but while running at point No. 9, 2.5 MDN and 1000 lb radial load, the bearing failed without warning. Total test time at failure was only 1.43 hours. During removal of the bearing from the test rig it was noted that the cage siderails were broken at one of the roller pockets. This allowed the siderails to flare out locally causing a groove to be machined into the outer raceway. Also, severe eccentric wear was noted on all of the roller ends. A photograph of the cage failure and several of the worn rollers is shown in Figure 31. Post-test measurements indicated the average weight loss of all rollers to be 0.0349 grams with the roller static skew angle increasing an average of $1^{\circ} 13.59'$.

6.2.5 Experimental Evaluation of Bearing No. 3

The fourth-Group-N bearing tested was bearing No. 3. As shown in Figure 25, this design did not provide for roller preloading, but did include a high level of inner raceway axial taper. The average coupled roller end radius runout was determined to be 0.00335 inch, see Table 3. At rig assembly, the outer ring was installed with the axial misalignment adjusted to an angle of 0.487° .

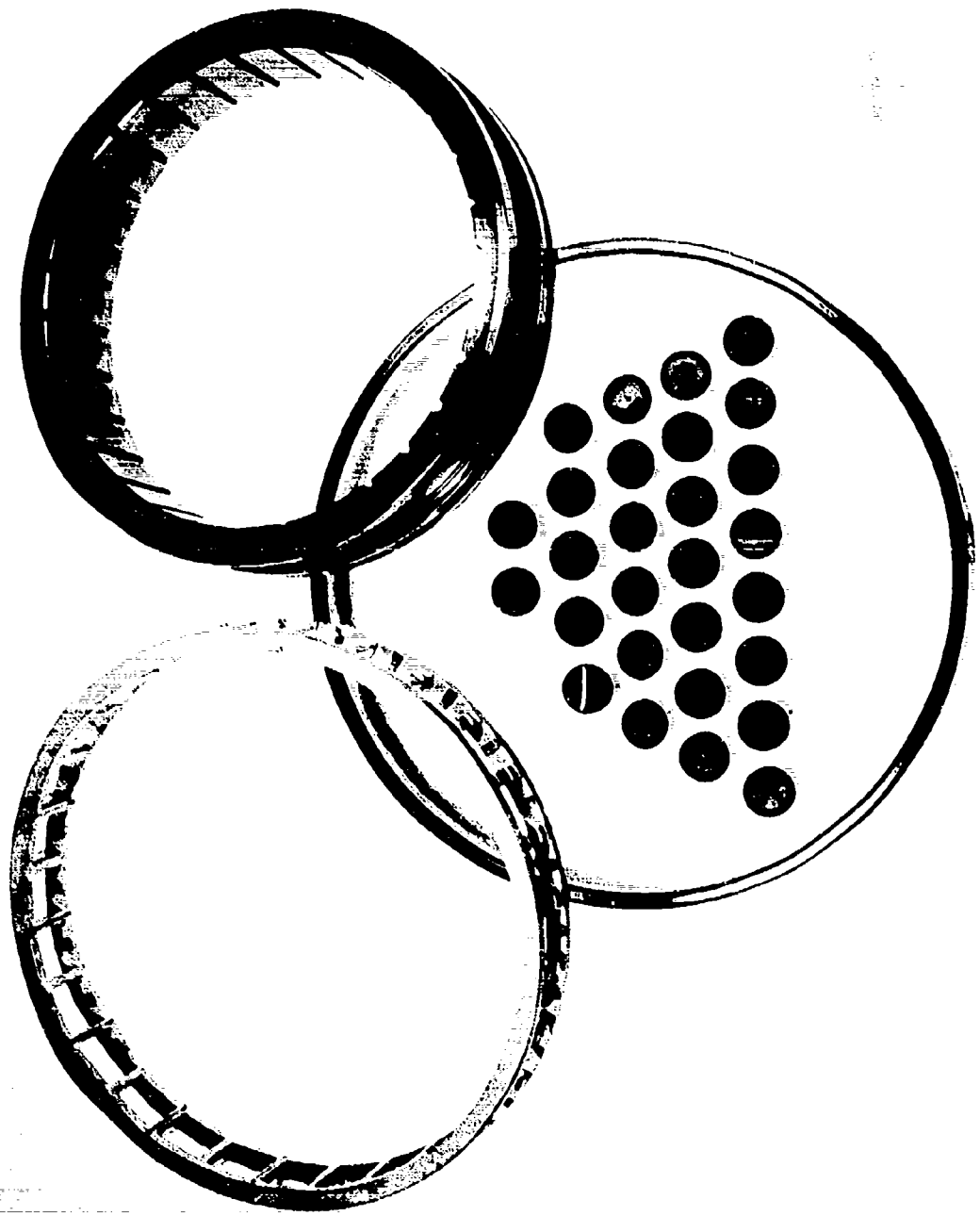


Figure 28. Group-N Bearing No. 4 Shows No Distress or Unusual Wear After Test

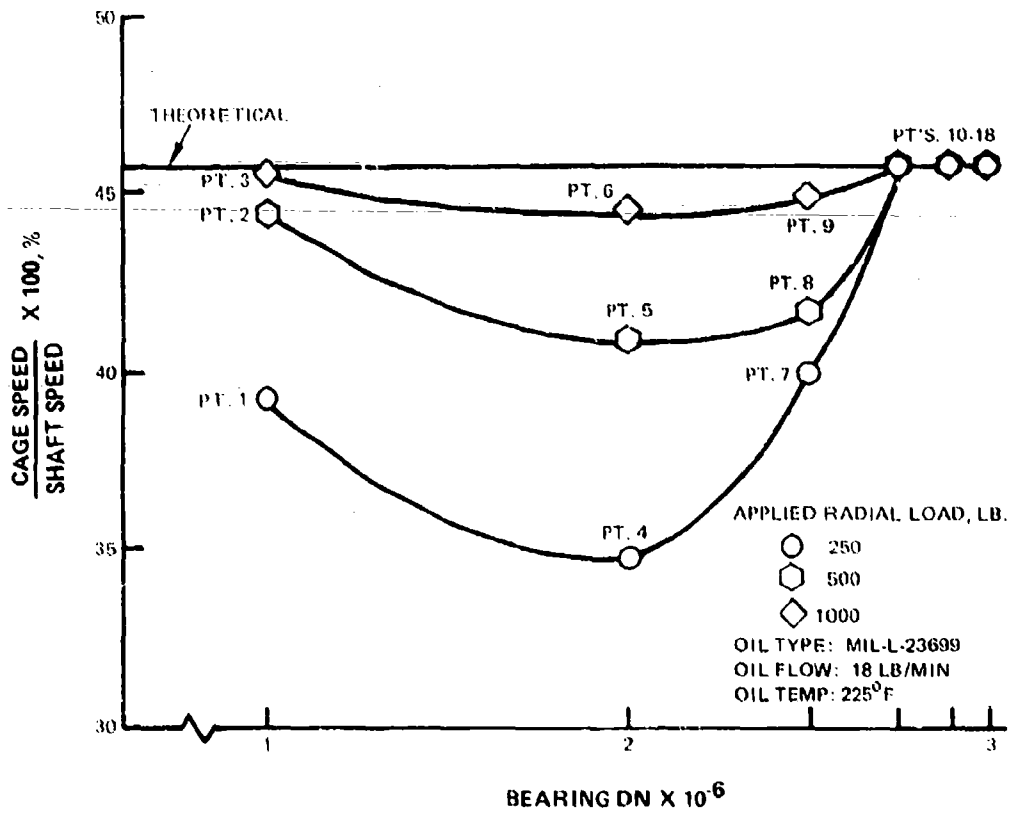


Figure 29. Test of Group-N Bearing No. 5 Shows Increased Skid as Load Is Decreased but With No Skid at Any Load Beyond 2.75 MDN

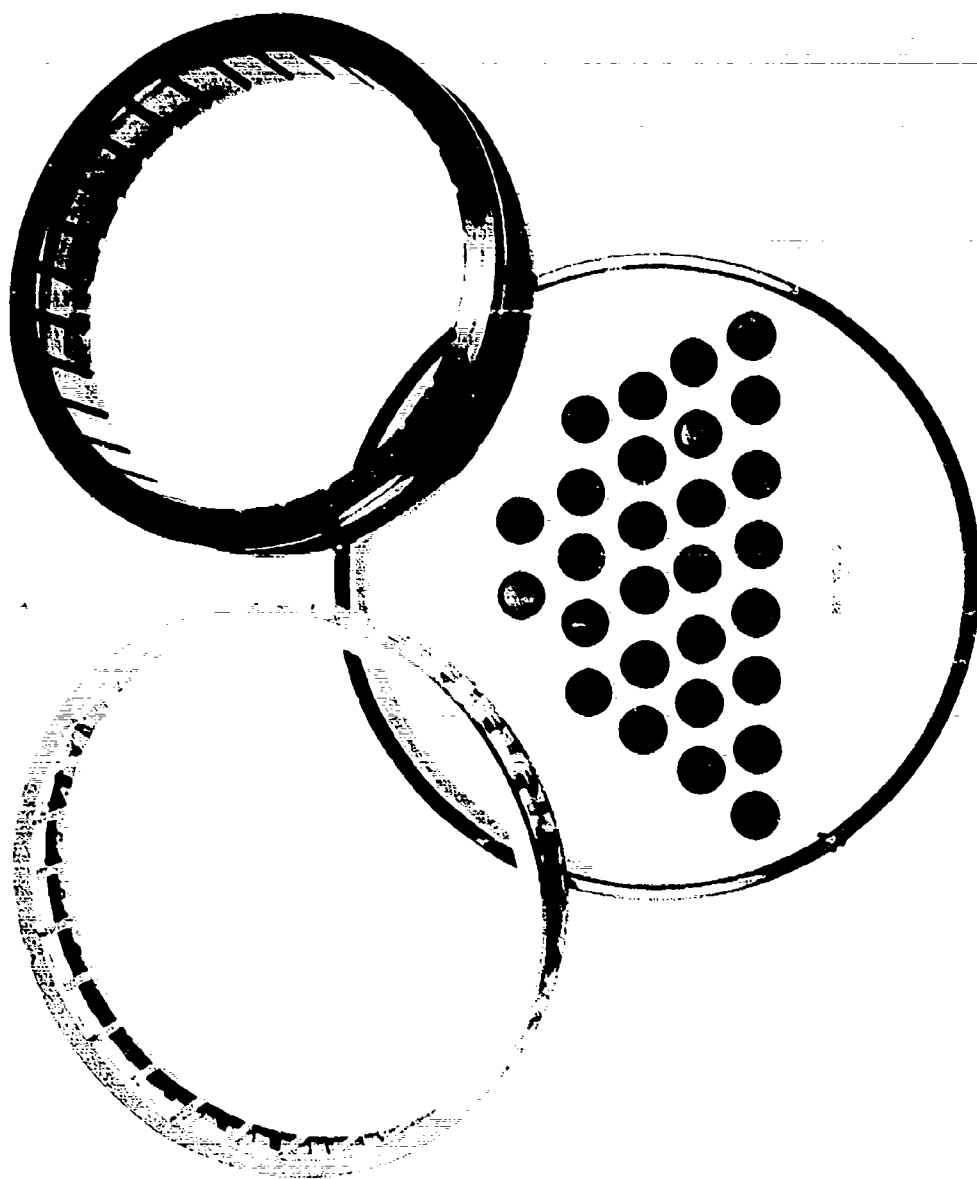


Figure 36. Group-N Bearing No. 5 Shows No Distress or Unusual Wear After Test

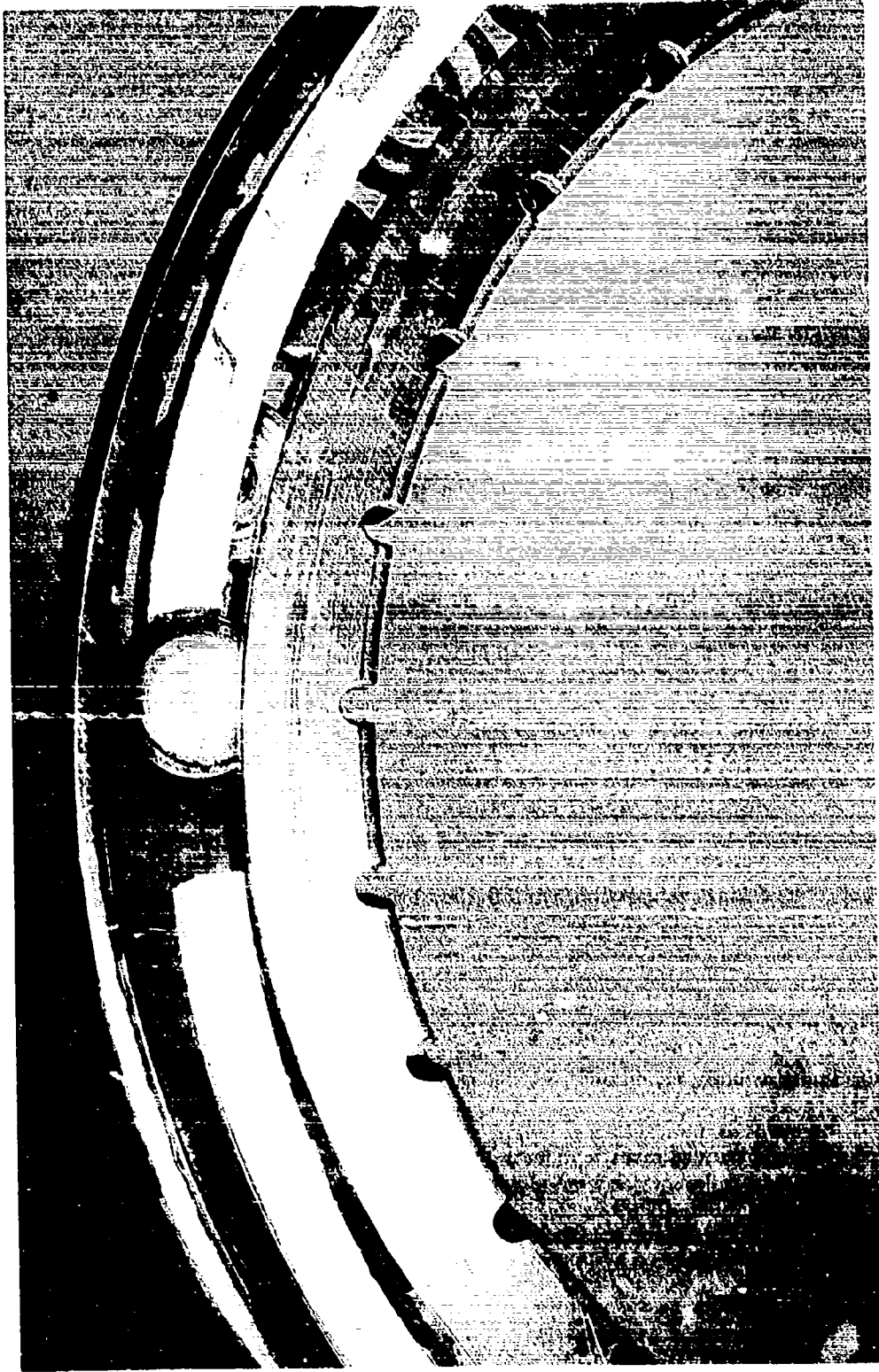


Figure 31. Testing of Group-N Bearing No. 1 Terminated as a Result of Cage Failure

Testing was initiated in accordance with the standard 10-hour program. From the onset, roller pass frequency measurements indicated that roller skid was occurring over the speed range of 1.0 to 2.5 MDN, as was also the case for the previously tested bearings No. 4 and 5. No skidding occurred at speeds of 2.75 MDN and above which had also been observed for bearings No. 4 and 5. The magnitude of skid was again seen to be the greatest at 2.0 MDN, with the maximum amount of skidding occurring with the lowest load. After completing point No. 9 in the schedule, the test was interrupted for inspection of the bearing. Total test time at this point was only 1.5 hours. Crescent or eccentric end wear was evident on both ends of all rollers as typified by the two rollers shown in Figure 32. The bearing was reinstalled in the rig and the test program was continued from point No. 10. While running at 2.5 MDN, point No. 21, the bearing failed without warning. The total test time at failure was 3.53 hours. During removal of the bearing from the rig it was noted that the cage siderails were broken and a section of one rail was separated from the remainder of the cage as shown in Figure 33. Eccentric end wear had progressed to the point where many of the rollers exhibited conical end shapes. Post-test measurements showed the average roller weight loss to be 0.0267 grams and the roller static skew angle increase to be an average of $1^{\circ} 7.5'$.

6.2.6 Experimental Evaluation of Bearing No. 8

The last Group-N bearing design tested was bearing No. 8 which is described in Figure 25. This design included roller preloading and a high level of inner raceway axial taper. From Table 3 it can be seen that the coupled roller end radius runout for this bearing averaged 0.0037 inch. Bearing No. 8 was installed in the rig with the outer ring axially misaligned 0.478° . Testing followed the program outlined in Table 6 with stable performance observed throughout the first 18 test points. After completing point No. 18, at which time 3.0 hours of testing were completed, the test bearing was removed from the rig for inspection as planned. As shown in Figure 34 it was discovered that a cage section had broken and separated from the remainder of the cage as a result of roller skewing. All rollers showed severe end wear, with the heaviest wear exhibited on the roller located in the pocket with the failed cross piece. Post-test measurements showed the average roller weight loss to be 0.0233 grams while roller static skew angle was shown to have increased an average of $1^{\circ} 25.1'$.

6.3 Summary of Group-N Bearing Tests

A summary of the wear results obtained on the Group-N bearings tested thus far is shown in Table 8. The average values of both roller weight loss and static skew angle change for both the flashed and unflashed rollers are presented for each bearing.

Of the five bearings tested during this report period, three of the bearings, No.'s 3, 4 and 5, were designed without roller preload, as shown in Figure 25. Each of these bearings exhibited roller skid in the speed range of 1.0 to 2.5 MDN, however, no skidding was noted in the speed range of 2.75 to 3.0 MDN. No distress or damage was observed from the operation of these bearings under skidding conditions.

Of the eight Group-N bearing designs tested, four contained rollers with a high level of coupled roller end radius runout or roller unbalance. The four bearings, No.'s 1, 3, 6 and 8, each experienced a cage failure which was judged to be the result of high roller skewing forces created by the unbalanced rollers. The four bearings that were designed with rollers having a low level of coupled corner radius runout successfully completed the 10-hour parametric program with a minimum of roller weight loss and static skew angle change.

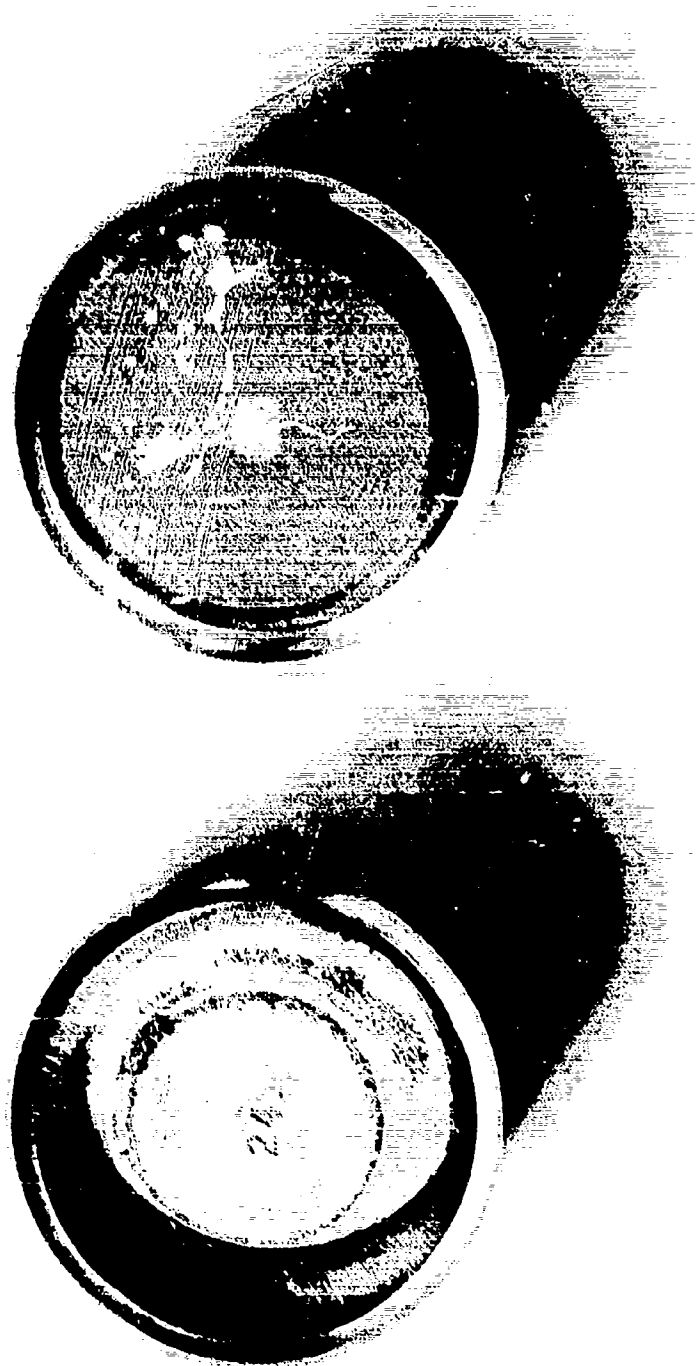


Figure 32. Eccentric Roller End Wear Noted on Group-N Bearing No. 3 Prior to Failure

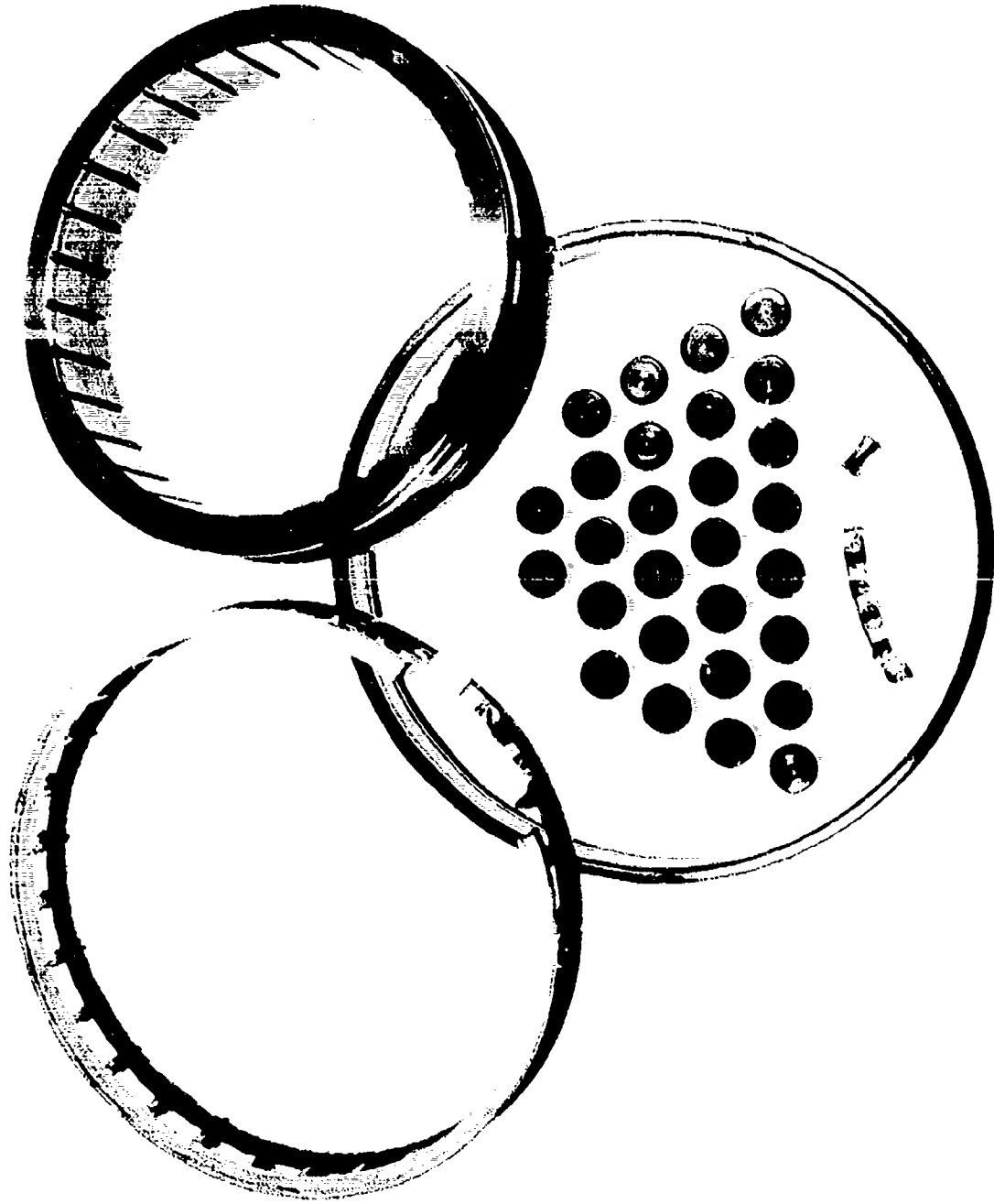


Figure 33 Testing of Group-N Bearing No. 3 Results in Roller Skew Related Failure at 2.5 MDN



Figure 31. Groove X Bearing No. 8 Cage Failure Results from Roller Skewing

TABLE 8. ROLLER WEIGHT AND SKEW ANGLE WEAR DATA FOR GROUP-N BEARINGS

Bearing No.	Average Weight Loss, Grams			Average Skew Angle Increase			Remarks
	Flashed	Unflashed	All Rollers	Flashed	Unflashed	All Rollers	
Baseline	0.0004		0.0004				
1	0.0349	0.0289	0.0349	1 deg 13.44 min.	1 deg 13.74 min.	1 deg 13.59 min.	Failed
2	0.0001	0.0001	0.0001	0 deg 1.09 min.	0 deg 1.32 min.	0 deg 1.20 min.	
3	0.0355	0.0180	0.0267	1 deg 16.53 min.	0 deg 58.38 min.	1 deg 7.46 min.	Failed
4	0.0002	0.0002	0.0002	0 deg 1.73 min.	0 deg 1.67 min.	0 deg 1.70 min.	
5	0.0001	0.0001	0.0001	0 deg 1.40 min.	0 deg 1.84 min.	0 deg 1.62 min.	
6	1.6145	1.7532	1.6838				Failed
7	0.0005	0	0.0003	0 deg 0.98 min.	0 deg 1.53 min.	0 deg 1.26 min.	
8	0.0287	0.0178	0.0233	1 deg 29.87 min.	1 deg 20.38 min.	1 deg 25.12 min.	Failed
9	0.0010	0.004	0.0007	0 deg 2.04 min.	0 deg 1.55 min.	0 deg 1.79 min.	

6.4 Statistical Analysis of Group-N Wear Results

The statistical analysis of the Group-N test data was completed for the purpose of determining the effects of both the changes in certain bearing geometry factors and certain tolerances on bearing wear, life, roller weight loss, and roller skew angle change. Regression and correlation analysis of the results were utilized to rank the important bearing parameters affecting each output response. The Group-N testing included the evaluation of seven independent bearing variables which are identified as follows:

- VAR 1 — Preload
- VAR 2 — Roller corner radius runout
- VAR 3 — Roller end circular runout
- VAR 4 — Inner raceway taper
- VAR 5 — Roller flat offset
- VAR 6 — Outer Ring Angular Misalignment
- VAR 7 — Lubrication

The above factors were considered the controlled variables of the test program and were varied as shown in Figure 25. Two levels for each variable were preselected and represent the range of possible extremes expected or allowed by the manufacturing or design process. A total of eight bearing designs containing the seven controlled variables were defined which would allow the linear contribution of each variable on bearing life to be examined statistically.

The main parameters affecting roller bearing life in this program are considered to be average roller weight loss and static skew angle change per hour of testing. Therefore, these two variables, considered as dependent in the statistical analysis of the test data, are expressed as follows:

$$Y_1 = \ln \left(\frac{\text{Average Weight Change}}{\text{Test Hours}} \right)$$

$$Y_2 = \ln \left(\frac{\text{Average Skew Angle Change}}{\text{Test Hours}} \right)$$

The natural logarithm (ln) of the outputs, Y_1 and Y_2 , was used in order to reduce the impact of extreme data points on the results of the analysis. Multiple regression equations were developed from the data by the method of least squares. Each equation yields the mean value of

one of the dependent variables. The equations therefore yield expected performance of a roller bearing under stated conditions. Prior to the development of the actual regression equations, a mathematical model was in each instance formulated relating the independent variables to the dependent variable. The general form of the mathematical model is a multivariate polynomial in which the coefficients appear linearly. The terms in each model are candidates for inclusion in the fitted regression equation.

The general model takes the form:

$$Y = b_0X_0 + b_1X_1 \dots + b_NX_N + e = \hat{Y} + e$$

where Y is the observed value of a particular dependent variable, either Y₁ or Y₂, \hat{Y} is the corresponding value of the dependent variable computed from the expression involving the X's and the b's, where the X's are the values of the independent variables, the b's are the coefficients to be estimated from the experimental data, and e represents the differences between observed and computed values of the dependent variable due to residual variation or experimental error in the observations.

The data set appropriate for each model was computer analyzed to determine the values of the regression coefficients and other relevant statistics. The regression models determined for each dependent variable, Y₁ and Y₂, are shown in Tables 9 and 10. The information presented includes:

- Variable name
- COEFFICIENTS: calculated values of regression coefficients, b_i
- CONF BAND: Confidence Band calculated as a function of t Table value for a given level of confidence, b_i, and S_{b_i}
- STD ERR: Stand error coefficient, S_{b_i}
- T-VALUE: calculated t value which is b_i/S_{b_i}

TABLE 9. GROUP-N BEARINGS -- ROLLER WEIGHT CHANGE

	Multivariate Linear Regression			
	Coefficient	Conf Band	Std Err	T-Value
Constant	-6.9350			
Var 1	0.40526E-03 +/-	0.739398E-02	0.171845E-02	0.24
Var 2	2.2332 +/-	1.16202	0.269885	8.27
Var 3	-0.17674E-01 +/-	0.261209E-01	0.606669E-02	-2.91
Var 4	-1.0112 +/-	1.11721	0.259477	-3.90
Var 6	-0.62936 +/-	7.48857	1.73925	-0.36
Var 7	-0.11593E-02 +/-	0.230405	0.535127E-01	-0.02

Percent Variability Explained = 97.505 SEE = 1.2581
 Correlation Between Y OBS and Y CALC = 0.98745 N = 9 T = 4.31
 Dependent Variable is Y₁

TABLE 10. GROUP-N BEARINGS -- ROLLER STATIC SKEW ANGLE CHANGE

Variable	Coefficient	Conf Band	Std Err	T-Value
Constant	-1.2123			
Var 1	= 0.99760E-03 +/-	0.261748E-02	0.607907E-03	-1.58
Var 2	= 1.7176 +/-	0.411071	0.954730E-01	17.99
Var 3	0.30283E-02 +/-	0.924037E-02	0.214612E-02	1.41
Var 4	0.24912 +/-	0.395218	0.917910E-01	-2.71
Var 6	1.0588 +/-	2.64911	0.615268	-1.72
Var 7	0.11403E-01 +/-	0.315068E-01	0.189303E-01	0.60

Percent Variability Explained = 99.462 SEE = 0.44505
 Correlation Between YOBS and YCALC = 0.99731 N = 9 T = 4.31
 Dependent Variable is Y₁

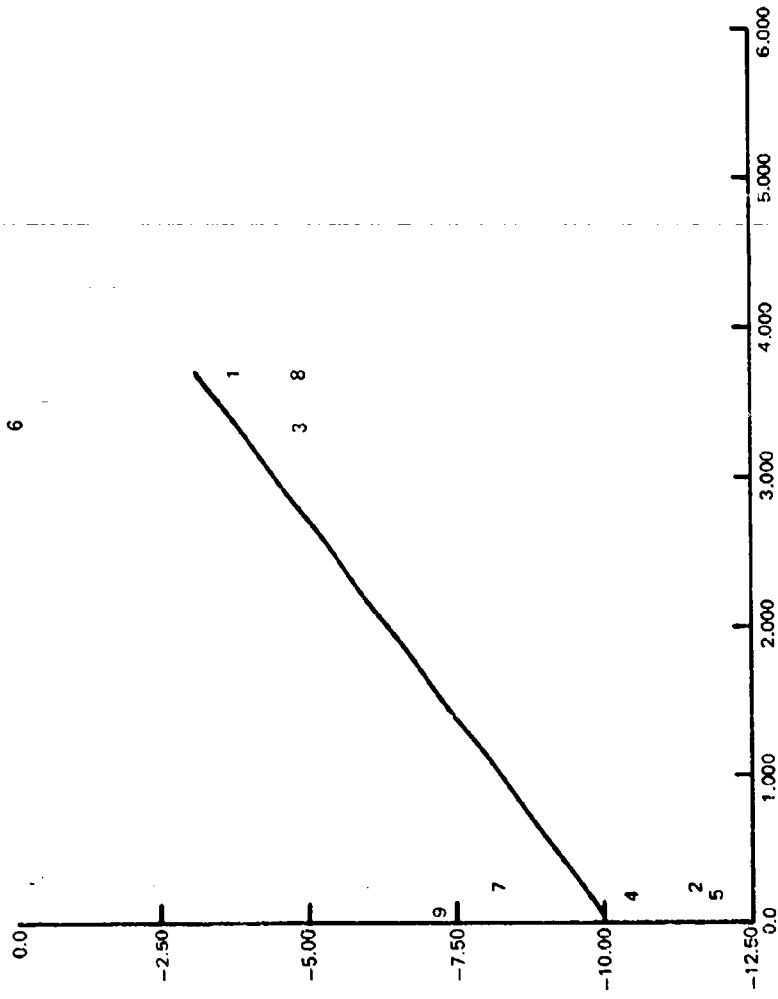
The T-value parameter permits the evaluation of each term in the response regression equation with the largest absolute value indicating that which is the strongest, or most important, bearing variable in the group. The sign indicates the direction of the effect, i.e., a positive sign signifies that an increase in the magnitude of the controlled variable results in an increase in roller weight loss and/or skew angle change, whereas a negative sign means that an increase of the magnitude of the controlled variable results in a decrease in roller weight loss and/or skew angle change.

Other statistics of interest are presented in Tables 9 and 10 and are the following:

- PERCENT VARIABILITY EXPLAINED, R^2 , which is the square of the multiple correlation coefficient R, is a measure of the proportion of variation in the dependent variable accounted for by the regression equation.
- The SEE or Standard Error of Estimate, is the magnitude of the error in predicting the output parameter.
- CORRELATION BETWEEN Y OBS AND \hat{Y} CAL. R, is an index indicating the degree of association between Y and \hat{Y} , where a value of 1.0 indicates a perfect fit, i.e., no experimental error, and a value of 0.0 indicates no association, i.e., large experimental error.
- N is the sample size.
- T is the Table T-value at 95% confidence which is to be exceeded by the calculated t-value in order to define a statistically important factor.

The statistical analysis of dependent variable 1; that is, roller weight change, indicates that the ln (average weight change/test hours) is affected primarily by roller corner radius runout or roller unbalance, VAR 2. As shown in Figure 35, the effect is positive as indicated by the upward slope of the curve. Secondary effects are shown for roller end circular runout, VAR 3, and/or roller flat offset, VAR 5, and inner raceway taper, VAR 4. These secondary effects are all indicated to be negative. The remaining variables of preload, VAR 1, outer ring angular misalignment, VAR 6, and lubrication, VAR 7, are shown to have no significant effect on roller weight change. Figure 35 exhibits the effect of dependent variable 1 versus VAR 2. Figures 36, 37, and 38 demonstrate the effect of VAR 3, 4, and 5 respectively, with the effect of VAR 2 removed from the data set.

Also, in Figures 36 and 38 it can be seen that VAR's 3 and 5 exhibit the same trends. This was due to the fact that bearings No. 2, 3, 6, 7, and 9 were all tested at the low levels of VAR's 3 and 5 and bearings No. 1, 4, 5, and 8 were evaluated at the high level for each variable.



VAR 2 - ROLLER CORNER RADIUS RUNOUT - INCHES FIR X 10³

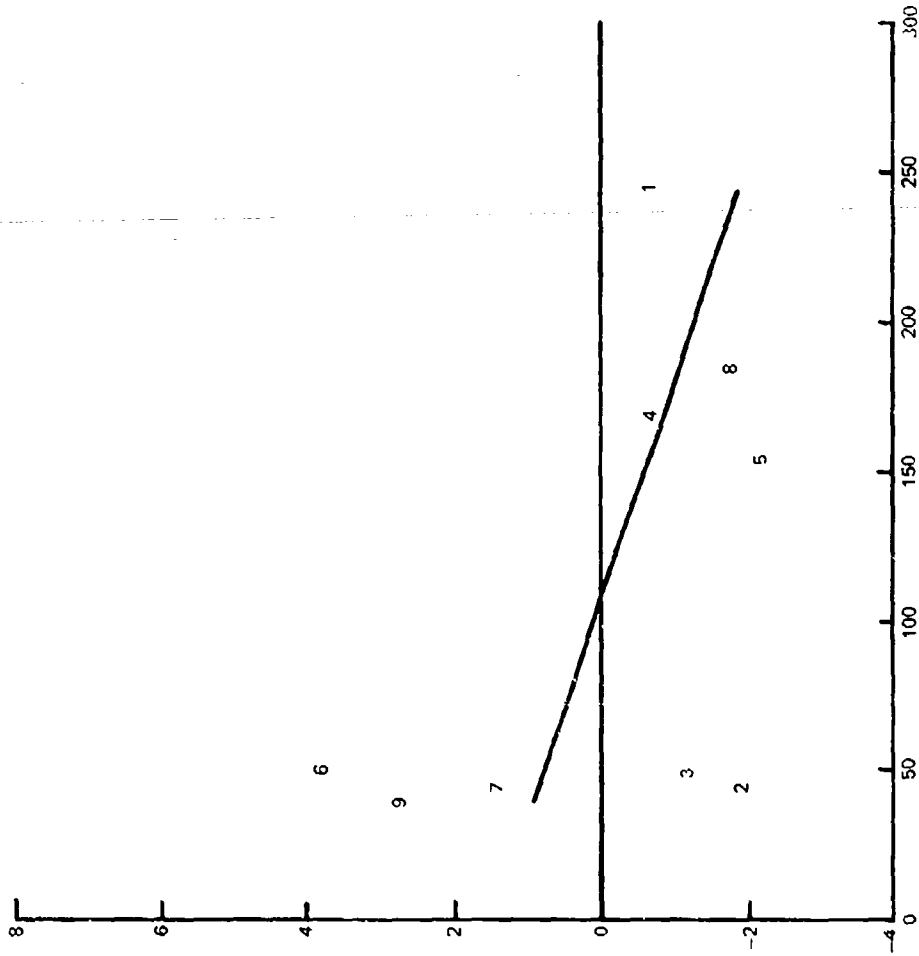
Figure 35. Roller Weight Loss Results from an Increase in Roller Corner Radius Runout

$$Y_1 = 1n \left(\frac{\text{AVG. WT. CHANGE}}{\text{TEST HRS.}} \right)$$

$$1_n \left(\frac{\text{AVG. WT. CHANGE}}{\text{TEST HRS}} \right) - \hat{y}$$

WHERE

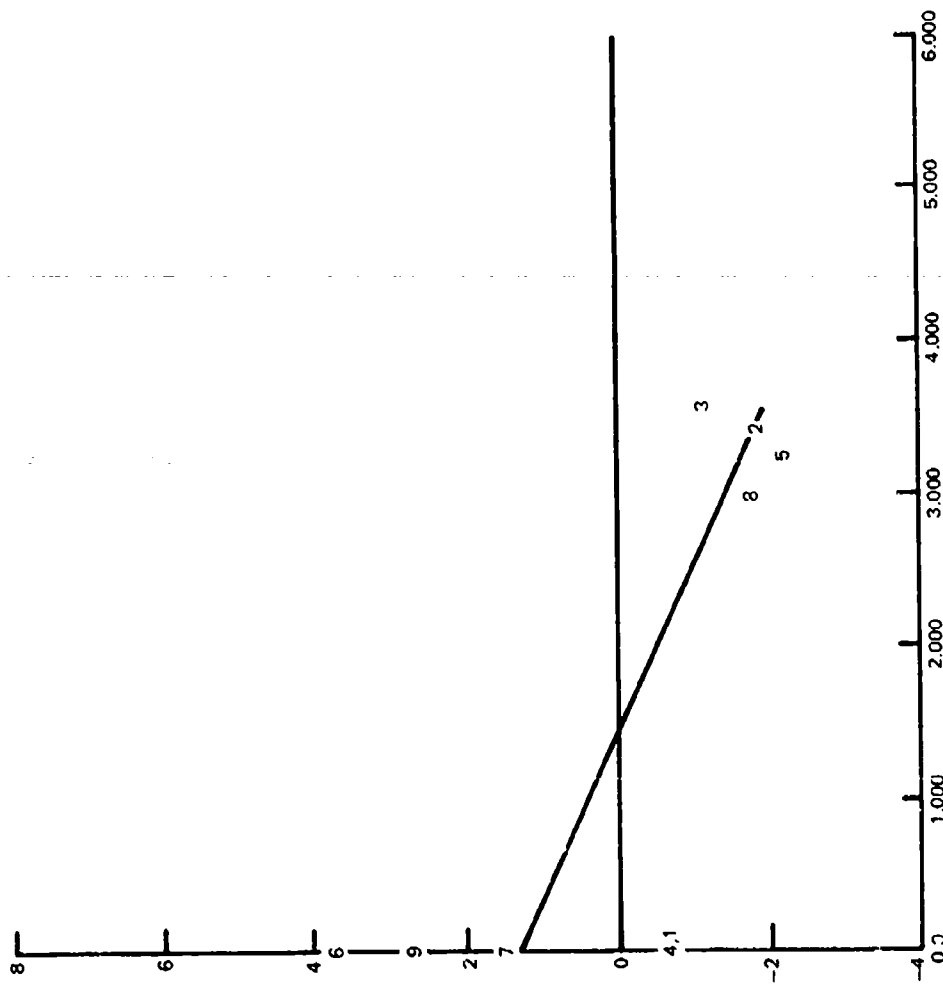
$$\hat{y} = 10.092 + 1.8867 \text{ ROLLER UNBALANCE}$$



VAR 3 - ROLLER END SQUARENESS RUNOUT -- INCHES FIR X 10⁵

Figure 36. Roller Weight Loss Results from a Decrease in Roller End Squareness

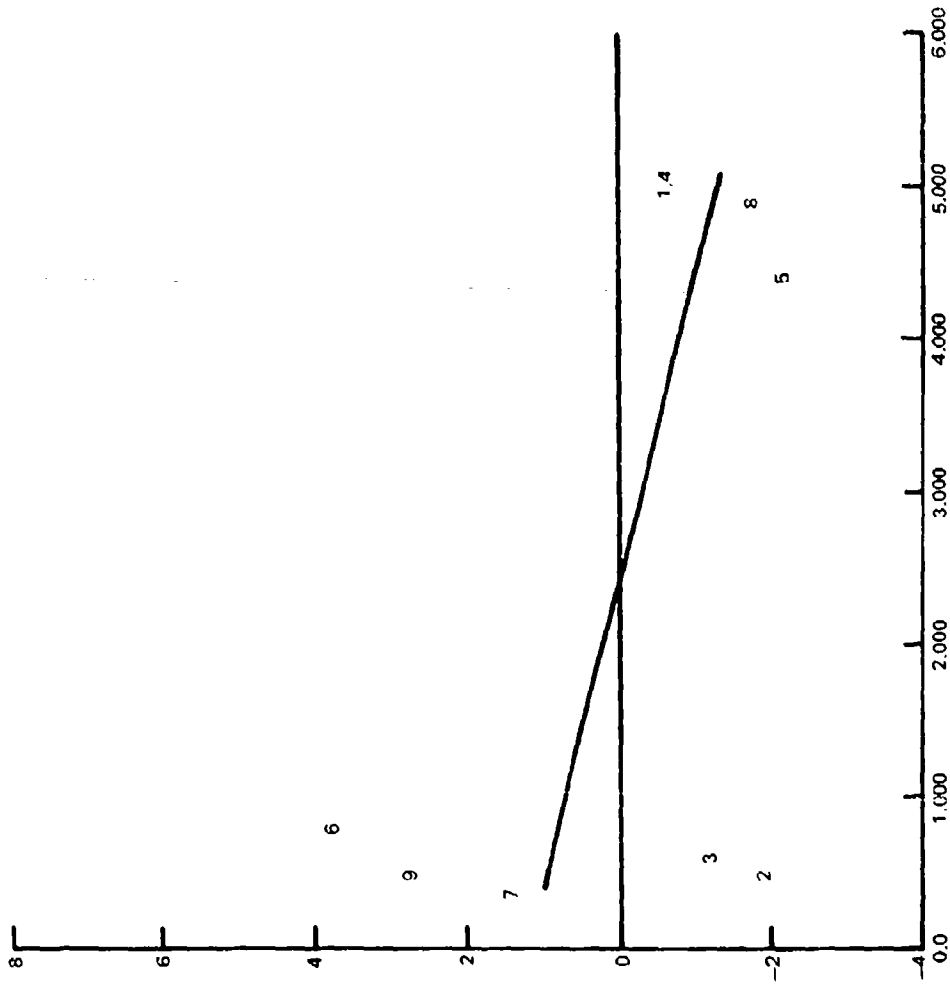
$$\ln \left(\frac{\text{AVG. WT. CHANGE}}{\text{TEST HRS.}} \right) - \bar{y}$$



VAR 4 - INNER RACE TAPER - MINUTES

Figure 37. Roller Weight Loss Results from a Decrease in Inner Race Taper

$$\ln \left(\frac{\text{AVG. WT. CHANGE}}{\text{TEST HRS.}} \right) - \diamond$$



VAR 5 - ROLLER FLAT OFFSET - INCHES X 10²

Figure 38. Roller Weight Loss Results from a Decrease in Roller Flat Offset

The statistical analysis of dependent variable 2, roller skew angle change, shows that the ln (average skew angle change/test hours) is affected only by VAR 2, the roller corner radius runout, with the remaining parameters from Group-N not significantly affecting the output. Again, VAR 2 demonstrates a positive effect as shown in Figure 39.

A summary of the statistically analyzed roller wear results and skew angle change for Group-N is presented in Table 11. Also presented are the results of seven additional bearing parameters evaluated and analyzed in a similar manner in a separate Pratt & Whitney Aircraft program.

6.5 Group-AF Bearing Tests

Testing was also completed on five of the six parametric bearings from Group-AF. The five designs tested are shown in Figure 26. Stable operation and performance was observed with each design except for No. 21 which experienced an inner ring fracture. The sixth Group-AF bearing, No. 26, which is a repeat of bearing No. 22, will be tested later in the program.

6.5.1 Pretest Inspection and Preparation

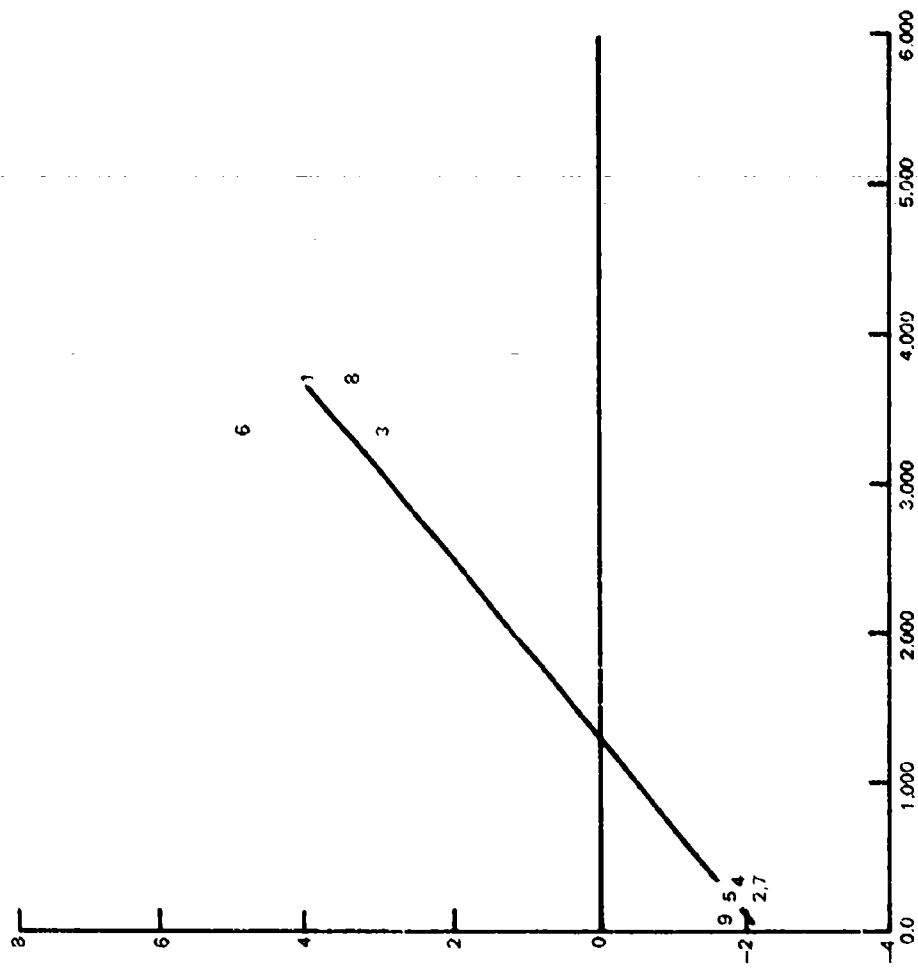
Detailed dimensional measurements of the six Group-AF bearings were taken and the results are provided in Table 4. The pretest roller weight and static skew angle measurements are shown in Table 12.

In-house inspection measurements were made and recorded during the process of installing the bearings in the test rig. These measurements included; the fits of both the inner ring on the shaft, the outer ring in the support housing and the installed internal radial clearance of the test bearing. Axial misalignment of the outer ring was maintained at zero for each of the Group-AF bearing tests. The measurements recorded are shown in Table 13.

6.5.2 Evaluation of Bearing No. 22

The first Group-AF bearing tested was bearing No. 22. As shown in Figure 26, this design included extended roller cylindrical flat length and increased guide flange layback. As indicated in Table 4, the guide flange angle was measured to be $0^{\circ} 50.4'$. The bearing was installed in the test rig and completed the 10-hour parametric program with stable operation noted throughout. During calibration testing, the slipping used for monitoring inner ring temperatures failed while running at point No. 10. The test was interrupted in order to remove the slipping and the program was then continued to completion. For the endurance testing portion of the program the total oil flow to the bearing was set at 20 lb/min. Bearing heat generation results as a function of speed, with variations in radial load and oil flow, are shown in Figure 40. It can be seen that a variation in applied radial load over the range of 250 to 1000 lb has only a slight effect on bearing heat generation whereas bearing oil flow is shown to have a direct and significant effect on bearing heat generation. Post-test inspection revealed all of the bearing components to be in good condition as can be seen in Figure 41, with no significant distress or unusual wear patterns noted. All of the rollers were found to be free of eccentric wear and inspection measurements indicated an average roller weight loss of only 0.0001 grams and an average static skew angle increase of $0^{\circ} 0.79'$.

$$Y_2 = 1^n \left(\frac{\text{AVG. WT. CHANGE}}{\text{TEST HRS}} \right)$$



VAR 2 - ROLLER CORNER RADIUS RUNOUT - INCHES FIR X 10³

Figure 39. Roller Static Skew Angle Incr Results from an Increase in Roller Corner Radius Runout

TABLE 11. ROLLER WEAR RESULTS FROM GROUP-N AND P&WA TESTS

Variable	Levels Tested			Avg. Roller Weight Change	Avg. Roller Skew Angle Change
	Low	High	Baseline		
<i>Group-N Test</i>					
Pre-load	0	2 Point O.R.	2 Point O.R.	—	—
Roller Corner Radius R/O, in.	0.0008	0.006	0.0008	↓*	↓*
Roller End Squariness, in. × 10 ⁻⁶	60	180	120	↑*	—
Inner Race Taper, min.	0.8	3.68	0.8	↑*	—
Roller Cylindrical Offset, in. × 10 ⁻⁶	10	50	10	↑*	—
Raceway Misalignment, deg.	0	0.5	0	—	—
Lubrication, lb/m.in.	13	29	20	—	—
<i>P&WA Test</i>					
Roller L/D Ratio, in./in.	0.77	1.0	1.0	↓	↓
Cage Unbalance, gram-centimeter	1.0	8.0	3.0	—	—
Roller End Clearance, in. × 10 ⁻⁶	1	5	1	↓*	↓*
Roller End Shape, Max. Protrusion, in. × 10 ⁻⁶	50	400	50	↑	↑
Flange Height, % of Roller dia.	20	30	25	↓*	↓*
Roller Dia. Variation, in. × 10 ⁻⁶	50	500	50	↓	↓
Roller Flat Length, % Roller Length	0	50	40	—	—
— No effect on output, either level or baseline value can be selected. ↓ Trend with output is positive, select a lower level for minimum roller weight change and static skew angle change. ↑ Trend with output is negative, select a higher level for minimum roller weight change and static skew angle change. * Indicates a significant roller bearing variable.					

TABLE 12. PRETEST ROLLER WEAR RELATED MEASUREMENTS FOR THE GROUP-AF BEARINGS

Bearing No.	Avg Roller Weight (Grams)		Avg Skew Angle (Minutes)	
	Unflashed	Flashed	Unflashed	Flashed
	21	13.3265	13.3270	14.28
22	13.3174	13.3202	33.73	33.45
23	13.3197	13.3261	22.47	20.41
24	13.3222	13.3180	17.12	16.93
25	13.3222	13.2209	20.88	21.22
26	13.3183	13.3195	31.40	31.02

TABLE 13. PRETEST RIG RELATED INSPECTION MEASUREMENTS FOR THE GROUP-AF BEARINGS

	Bearing Numbers				
	21	22	23	24	25
Inner Ring Fit on Shaft, in.	0.0013T	0.0010T	0.0023T	0.0023T	0.0024T
Internal Radial Clearance Installed, in.	0.0034	0.0038	0.0037	0.0033	0.0043
Outer Ring Fit in Housing, in.	0.0008L	0.0008L	0.0010L	0.0006L	0.0006L
Outer Ring Misalignment, deg	0	0	0	0	0

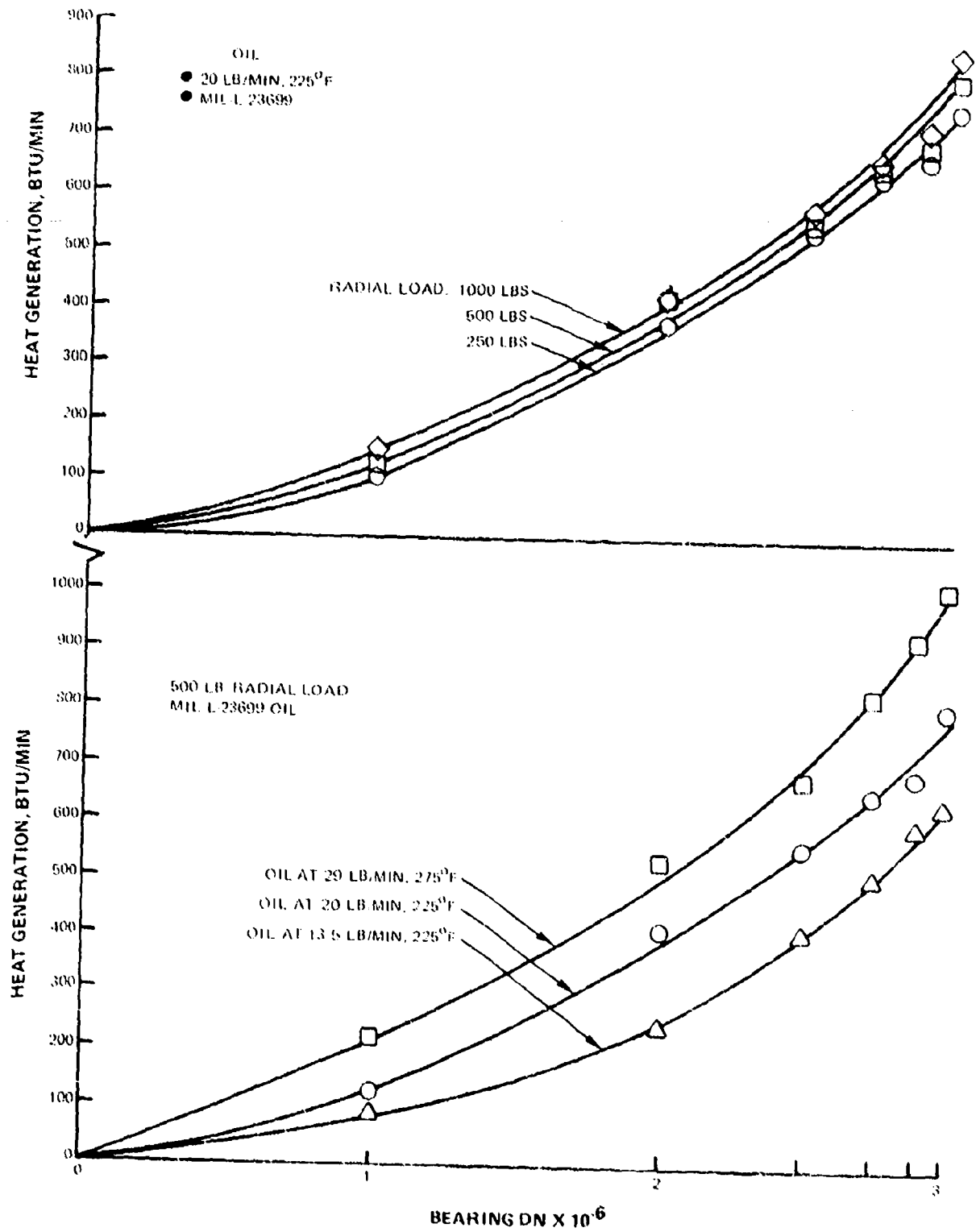


Figure 40. Group-AF Testing Shows That Increasing Load Has a Slight Effect on Bearing Heat Generation Whereas Increasing Oil Flow Significantly Increases Bearing Heat Generation

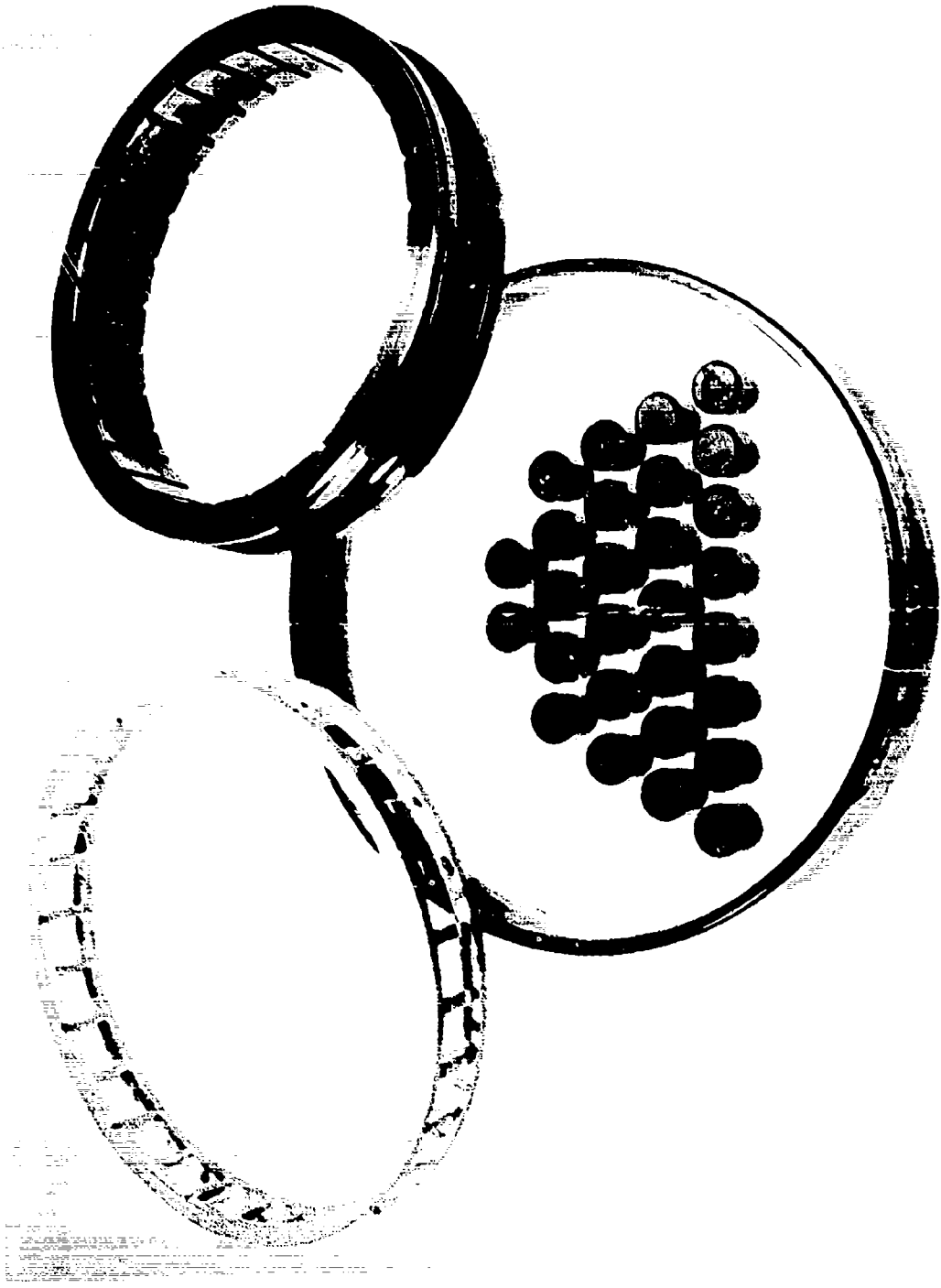


Figure 41. Group-AF Bearing No. 22 Shows No Distress or Unusual Wear After Test

6.5.3 Experimental Evaluation of Bearing No. 21

The second Group-AF bearing tested was bearing No. 21. As shown in Figure 26, this design provides for a low level of both roller flat length and guide flange layback. Pretest measurements, as presented in Table 4, indicated a roller cylinder length of 0.2665 inch and a guide flange layback angle of $0^{\circ} 7.16'$. The bearing was installed in the rig without outer ring misalignment and testing proceeded in accordance with the 10-hour parametric program outlined in Table 6. Stable operation of the bearing was noted from the onset of the testing. While running at 2.75 MDN, point No. 11, a failure occurred without warning which terminated the test. The total test time at failure was only 1.75 hours. Removal of the bearing from the rig revealed that the inner ring had fractured as shown in Figure 42. It also can be seen in Figure 42 that the outer ring and cage were both intact but damaged. The rollers were severely edge damaged but free of eccentric end wear. Post-test roller weight measurements indicated an average loss of 0.2094 grams. The static skew angle increased an average of $1^{\circ} 0.84'$ for all rollers. An extensive metallurgical analysis was conducted at the site of the inner ring break and the results indicated a transverse fracture which had progressed in a tensile manner. It was concluded that the fracture originated at the inner diameter of the ring in the vicinity of an intersection of a radial oil hole and an axial oil slot.

6.5.4 Experimental Evaluation of Bearing No. 23

Bearing No. 23 was tested next. As can be seen in Figure 26, this design is identical to No. 22 and features both extended roller flat length and increased guide flange layback except that the guide flange surface in this design is convex for the purpose of improving hydrodynamic lubrication between the roller end and the guide flange. As shown in Table 4, the guide flange angle was measured to be $0^{\circ} 55.6'$. The bearing completed the 10-hour parametric program with stable operation noted throughout. During the endurance portion of the program the total oil flow to the test bearing was maintained at 20.0 lb/min. Heat generation performance data was similar to that obtained earlier for bearing No. 22. Test data for outer to inner ring temperature differential and horsepower as functions of speed with oil flow as a parameter are shown in Figure 43. Rig horsepower data for bearing No. 23 is compared to rig horsepower data obtained earlier without a test bearing. In this latter case the rig bearing was therefore run without applied radial loading and without normal lubrication. It can also be seen in Figure 43 that a decrease in oil flow increases the temperature differential between the outer and inner rings, and decreases the rig horsepower. Post-test inspection of bearing No. 23 revealed all of the bearing components to be in good conditions as shown in Figure 44. No significant distress or unusual wear of the components was noted and all of the rollers were found to be free of eccentric wear. Roller weight measurements indicated an average weight loss of 0.0002 grams while it was determined that the skew angle increased an average of only $0^{\circ} 1.75'$.

6.5.5 Experimental Evaluation of Bearing No. 24

Bearing No. 24, as shown in Figure 26, features both extended roller flat length and a low level of flange layback. The guide flange of this design, like bearing No. 23, has a convex surface and, as shown in Table 4, its layback angle is $0^{\circ} 0.01'$. The bearing was installed in the test rig with zero outer ring misalignment and completed the 10-hour program with stable operation noted throughout. During the endurance portion of the program the total oil flow to the test bearing was again maintained at 20.0 lb/min. Performance data was similar to that obtained earlier for bearings No. 22 and 23 and post-test inspection revealed all of the components to be in good condition as shown in Figure 45. No significant distress or unusual wear of the components was noted and all of the rollers were found to be free of eccentric wear. Roller weight measurements indicated an average weight loss of 0.0002 grams while skew angle measurements indicated an average increase of $0^{\circ} 2.09'$.

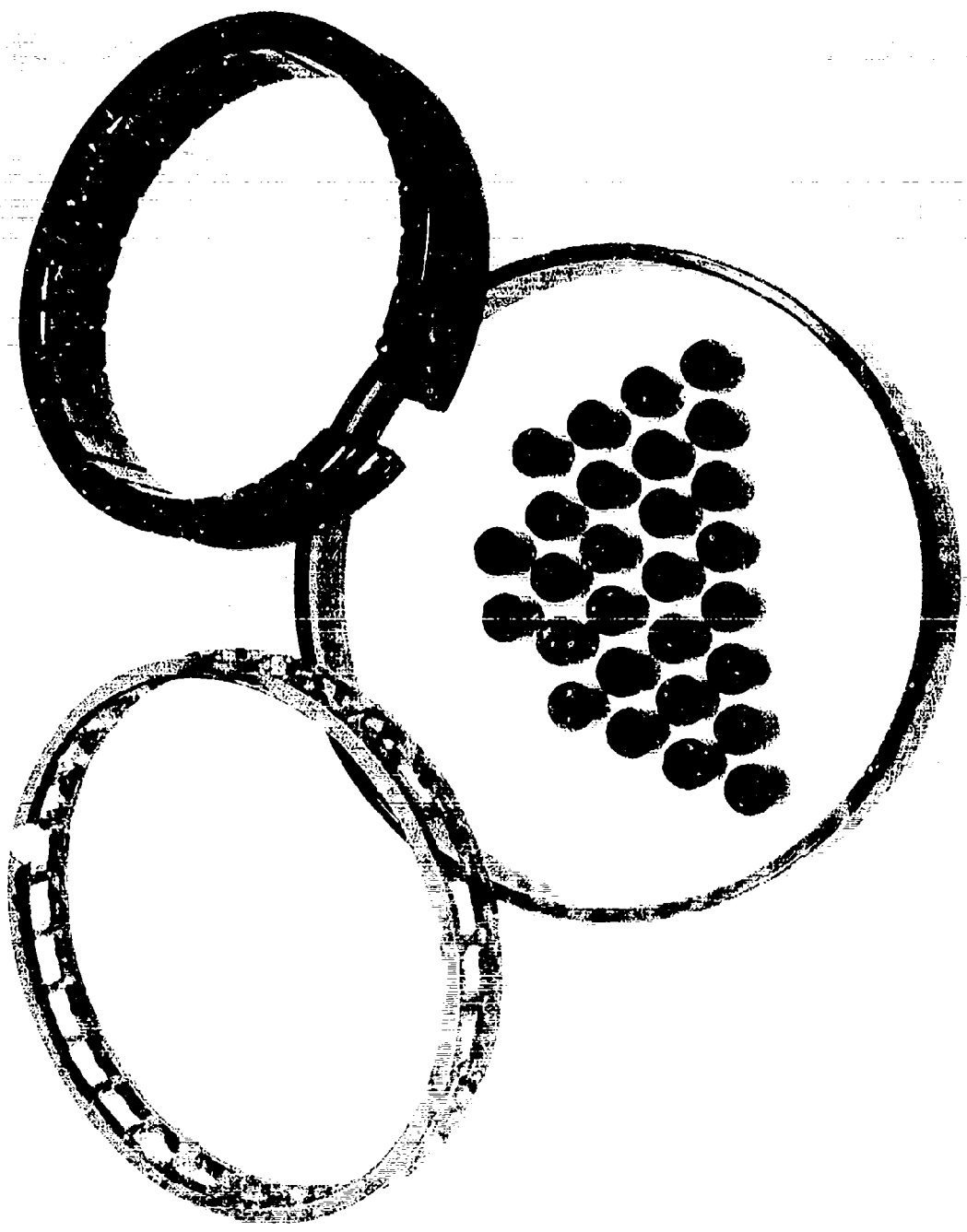


FIGURE 19. Inner Ring of Group-AF Bearing No. 21 Fractures During Testing at 275 MPa

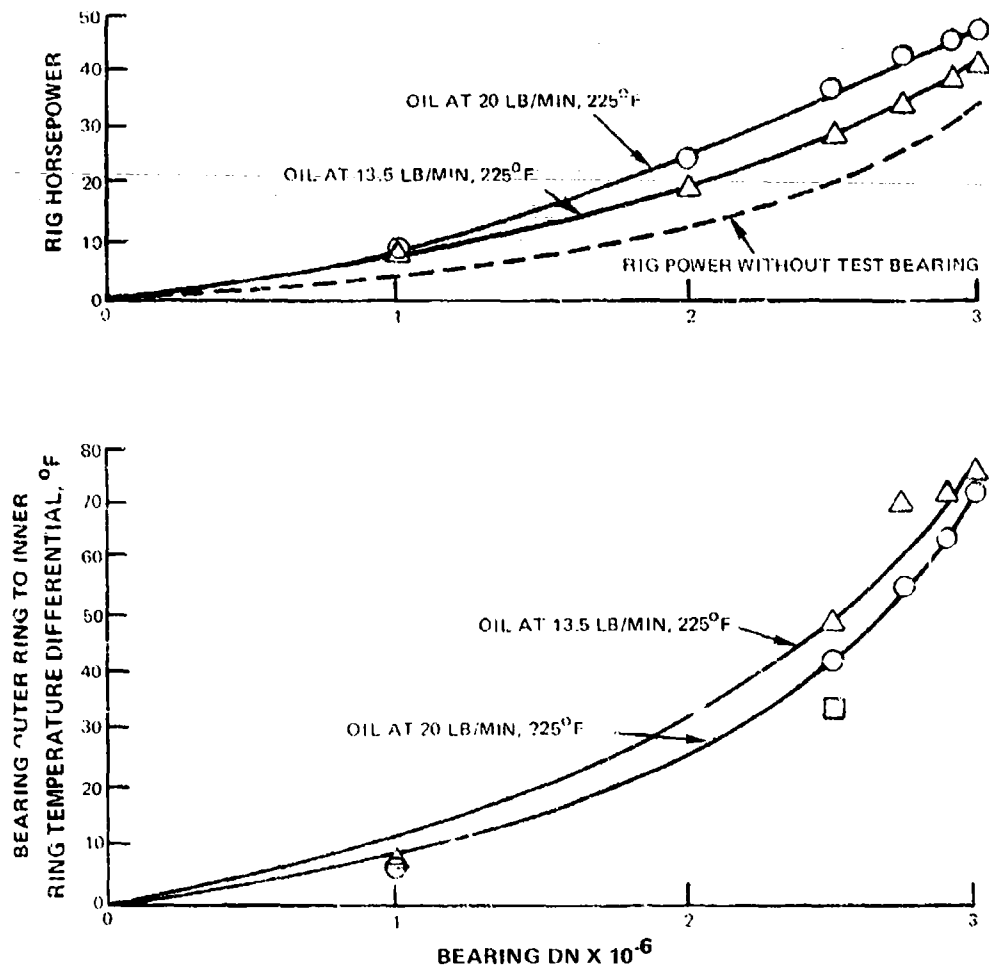


Figure 43. Increasing Oil Flow of Group-AF Bearing No. 23 Increases Rig Horsepower and Decreases Outer Ring to Inner Ring Temperature Differential

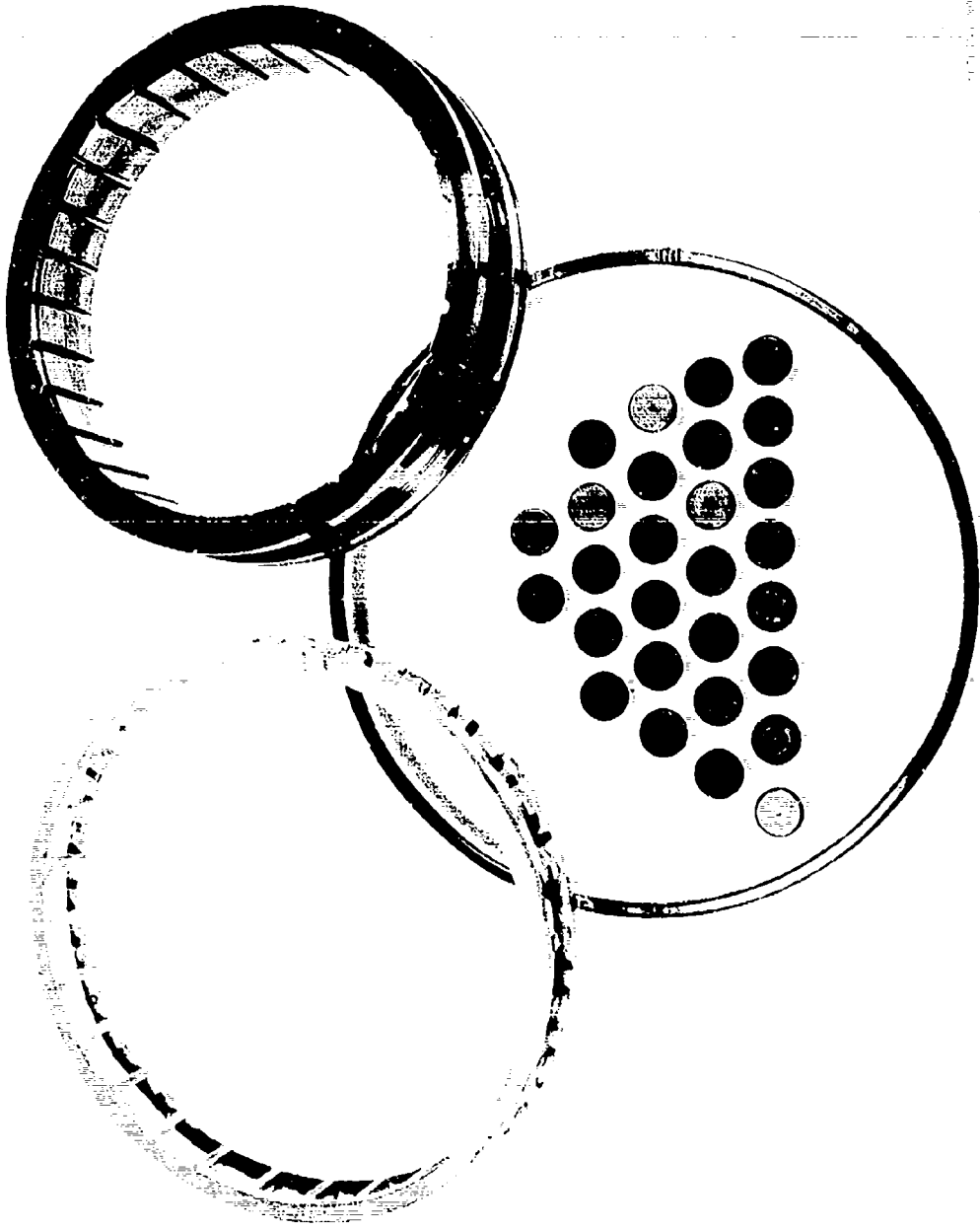


Figure 44. Group-AF Bearing No. 23 Shows No Distress or Unusual Wear After Test

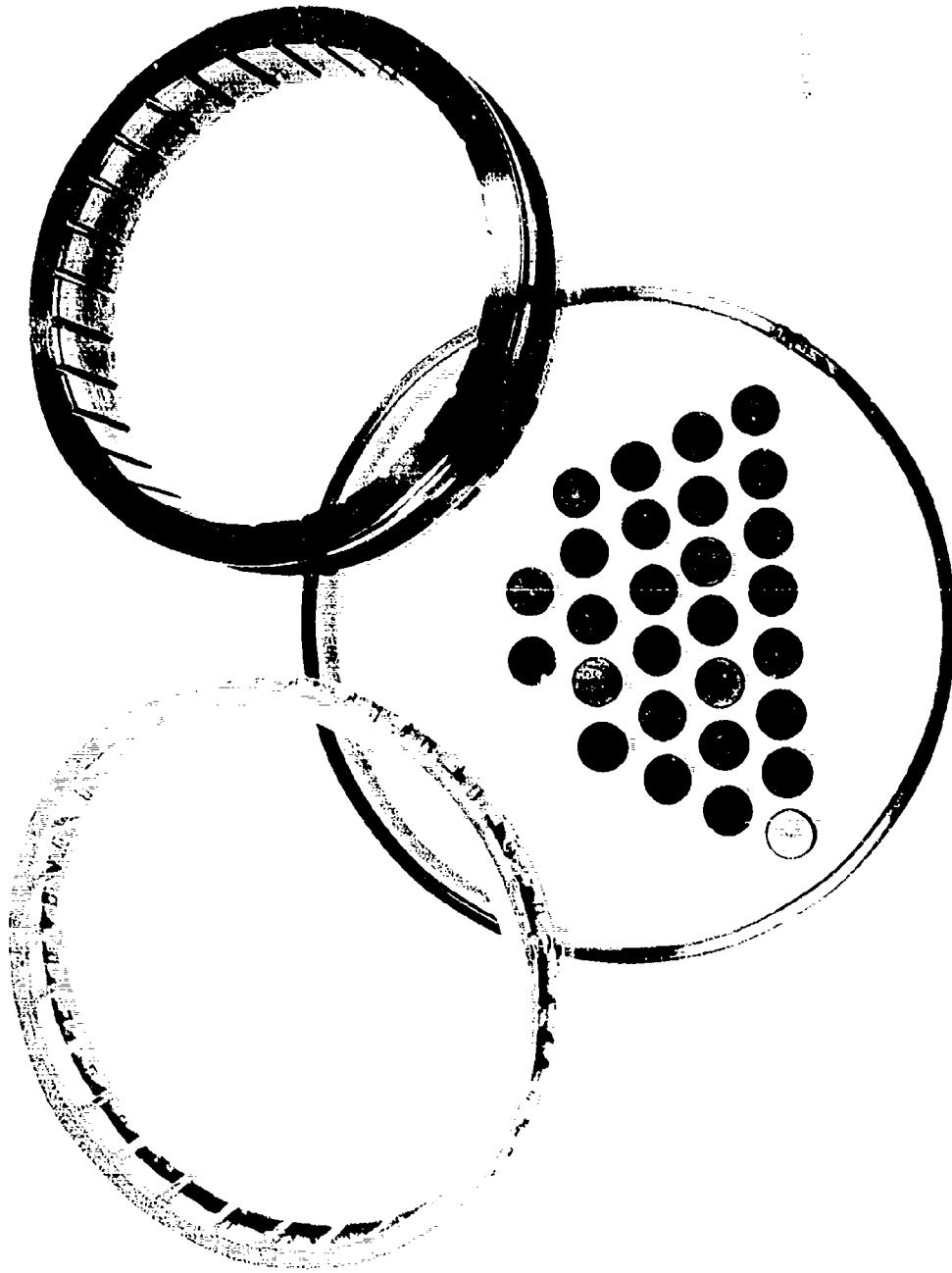


Figure 45. Group-AF Bearing No. 24 Shows No Distress or Unusual Wear After Test

6.5.6 Experimental Evaluation of Bearing No. 25

The fifth and last of the Group-AF bearings tested was bearing No. 25. As shown in Figure 26, this design features both a low level of roller flat length and increased guide flange layback. The guide flange surface, as in bearings No. 23 and 24, is also convex. As shown in Table 4, the guide flange layback angle was measured to be $0^{\circ} 52.3'$. The bearing was installed in the test rig without outer ring misalignment and completed the 10-hour parametric program with stable operation noted throughout. During the endurance portion of the program the total oil flow to the test bearing was again maintained at the 20 lb/min level. Performance data was similar to that obtained during the evaluation of bearing No's. 22, 23, and 24. Post-test inspection revealed all of the components to be in good condition as shown in Figure 46. No significant distress or unusual wear of the components was noted and all of the rollers were found to be free of eccentric end wear. Roller weight measurements indicated an average weight loss of 0.0001 grams while skew angle measurements showed an average increase of $0^{\circ} 1.10'$.

6.6 Summary of Group-AF Testing

Figures 47 and 48 provide a summary presentation of the operational data for the Group-AF bearings tested. The test data obtained for all bearings in this group generate similar curves as shown in these figures, testifying to their consistent thermal performance. The data obtained for bearing No. 21, which failed abruptly after only 1.75 hour of running, is also similar to that obtained for the other Group-AF bearings and falls within the range of these curves. A summary of the wear results obtained is shown in Table 14. Average values of roller weight loss for both the flashed and unflashed rollers are presented. Also shown as a wear parameter is the average skew angle change for the flashed as well as the unflashed rollers of each bearing.

6.7 Statistical Evaluation of the Group-AF Bearing Wear Results

Statistical techniques were used to determine the effect on roller end wear on the following four study parameters from Group-AF:

- Extended roller flat length
- Inner ring guide flange layback
- Inner ring guide flange contour
- Inner ring guide flange runout

It was concluded that the failure of bearing No. 21 was not related to the fact that it featured controlled levels of the above four study parameters. Post-test evaluation of this bearing indicated that this failure was most likely a result of local overstressing of the inner ring ID area due to lack of a proper blend at the intersection of a bore slot and a radial oil hole. Therefore, the extreme roller wear results associated with this test were not included in the analysis of the wear data for Group-AF. The evaluation of the above four parameters was then limited to that based on the wear data provided by the four remaining test bearings. The analytical procedures used were essentially the same regression and correlation analysis techniques used previously to process the Group-N wear data. It was concluded that the indicated levels of changes in the four independent study parameters for Group-AF did not cause a significant change in the average weight or skew angle. Therefore, the baseline levels for the four Group-AF parameters can be considered acceptable for use in future designs and have a low associated risk of producing unacceptable wear rates.

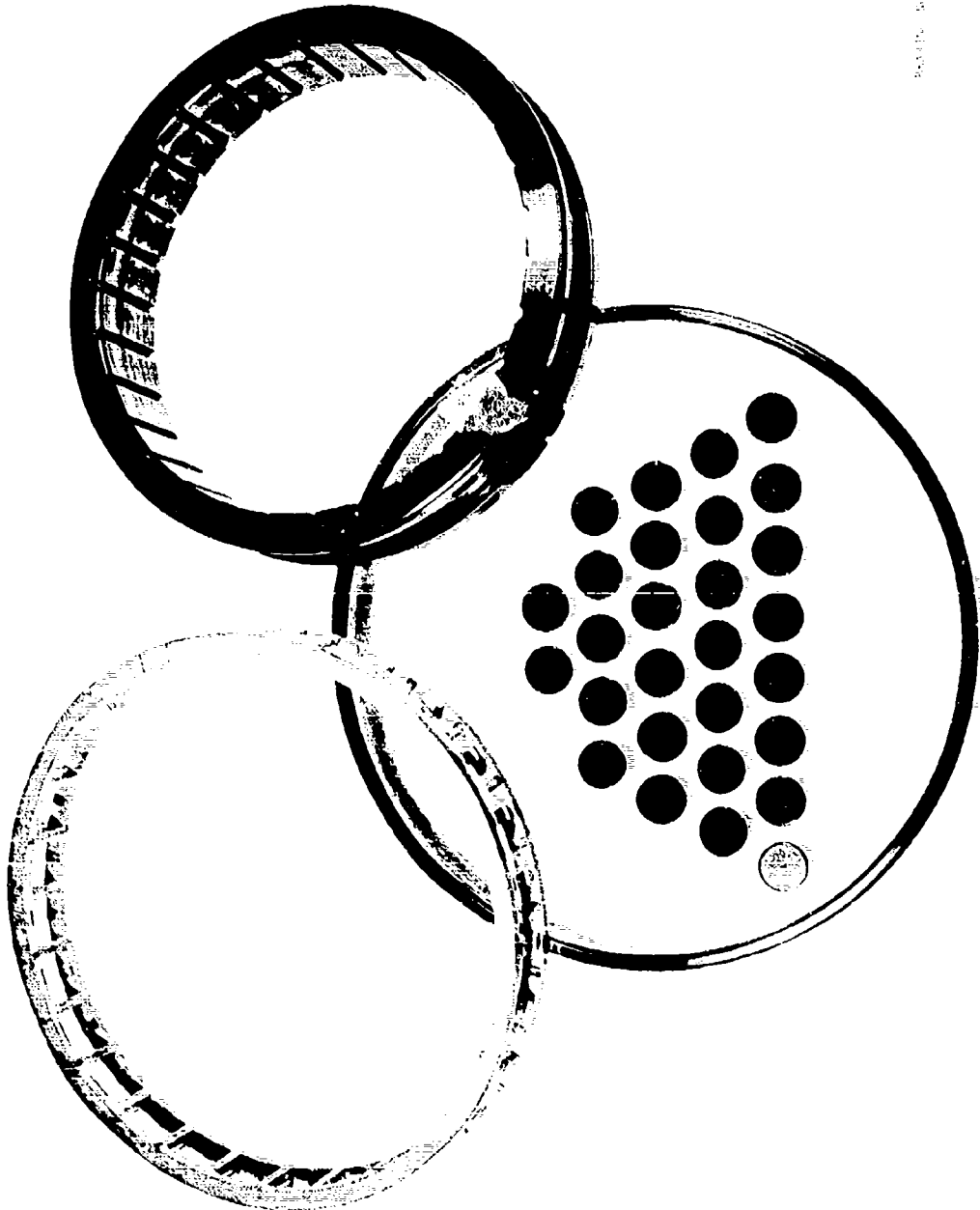


Figure 46. Group-AF Bearing No. 25 Shows No Distress or Unusual Wear After Test

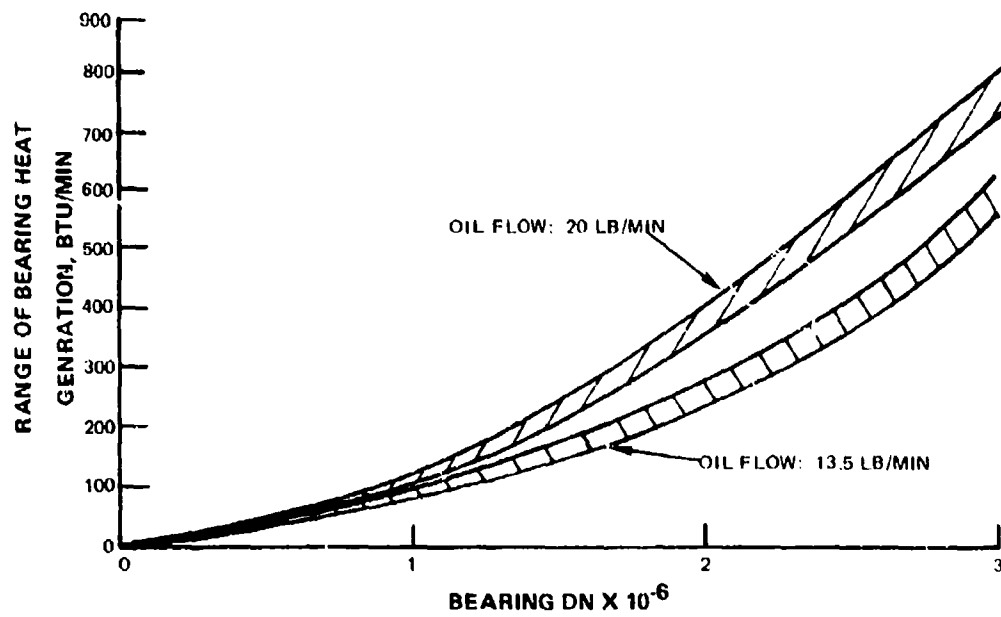
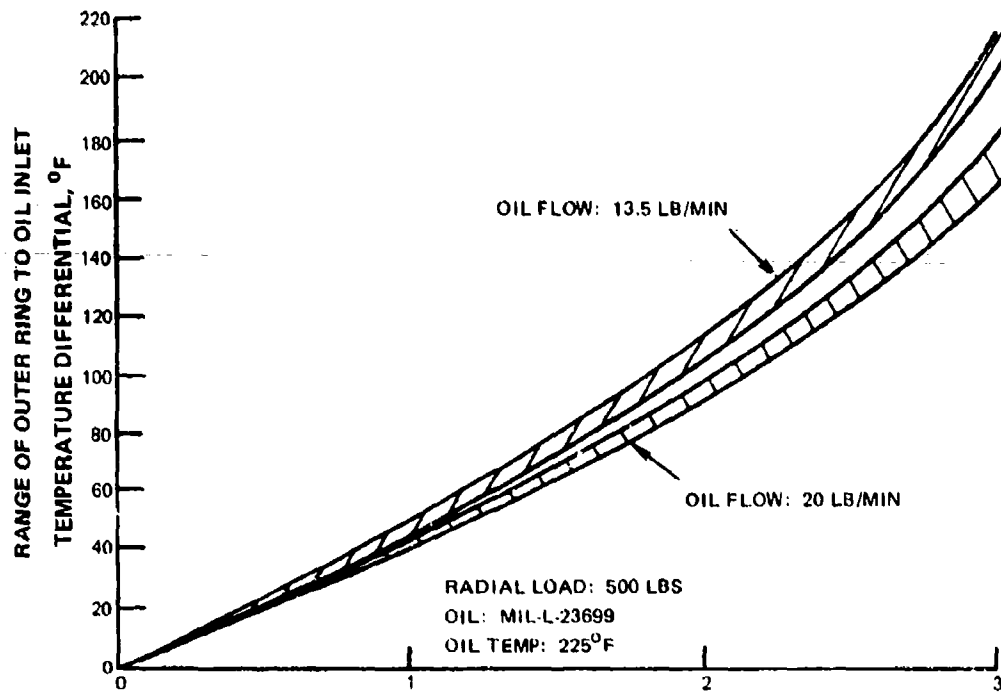
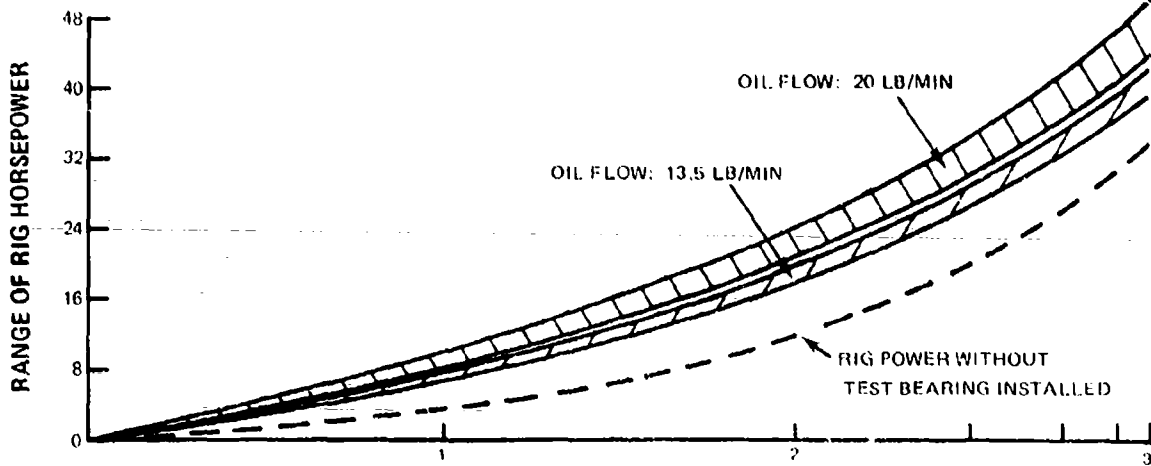


Figure 47. Group-AF Bearing Testing Indicates Similar Heat Generation and Outer Ring to Oil Inlet Temperature Differential for All Designs



RADIAL LOAD: 500 LBS
 OIL: MIL-L-23699
 OIL TEMP: 225°F

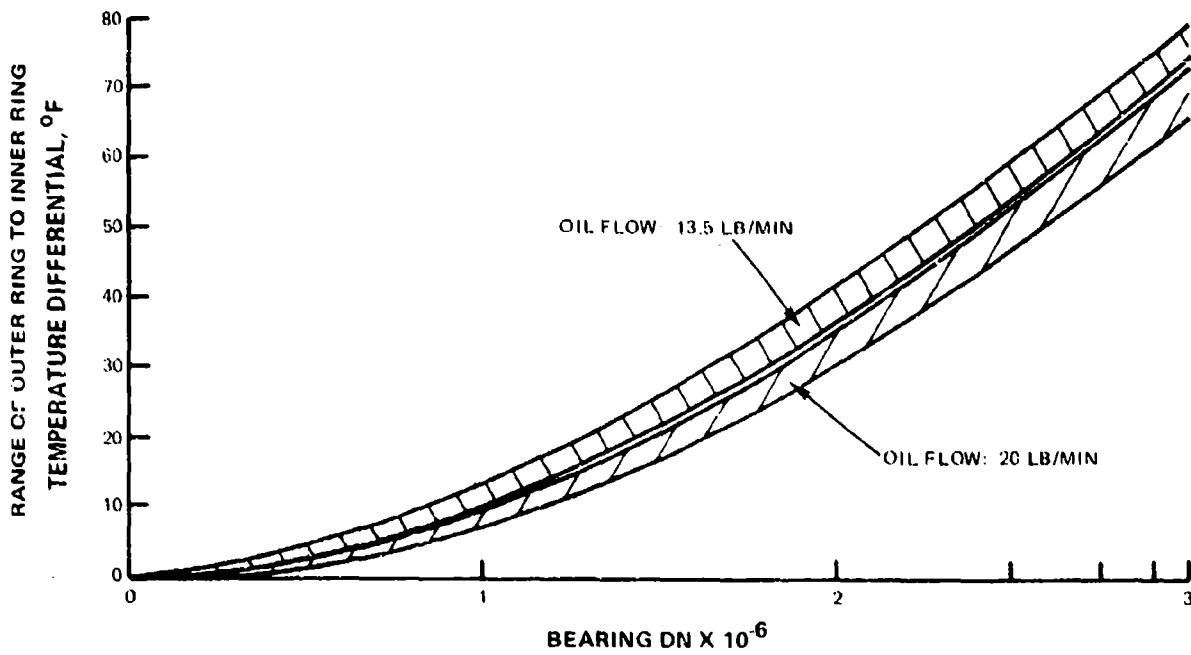


Figure 48. Group-AF Bearing Testing Indicates Similar Rig Horsepower and Outer Ring to Inner Ring Temperature Differential for All Designs

TABLE 14. ROLLER WEIGHT AND SKEW ANGLE WEAR DATA FOR GROUP-AF BEARINGS

Bearing No.	Average Roller Weight Loss, Grams			Average Skew Angle Increase		
	Flashed	Unflashed	All Rollers	Flashed	Unflashed	All Rollers
21	0.2139	0.2060	0.2094	1 deg 0.84 min.	1 deg 1.04 min.	1 deg 0.84 min.
22	0.0000	0.0002	0.0001	0 deg 0.88 min.	0 deg 0.72 min.	0 deg 0.79 min.
23	0.0002	0.0002	0.0002	0 deg 1.94 min.	0 deg 1.57 min.	0 deg 1.75 min.
24	0.0002	0.0002	0.0002	0 deg 2.40 min.	0 deg 1.78 min.	0 deg 2.09 min.
25	0.0002	0.0000	0.0002	0 deg 0.88 min.	0 deg 1.32 min.	0 deg 1.10 min.

6.8 Statistical Analysis of Composite Group; Groups N and AF Wear Results Combined With P&WA Data

The test results from the experimental test programs for Group N, AF, and P&WA bearings were statistically analyzed, i.e., changes in both roller weight and skew angle at accelerated test conditions. Figure 49 identifies all of the variables investigated, in the composite group while Table 15 presents the P&WA Group statistical test matrix and indicates the test levels for the variables evaluated in this group.

Two bearings were omitted from the analysis of this composite data set. Bearing No. 6 from Group-N was omitted because of the excessive wear response of the rollers that occurred after the bearing failed. Bearing No. 21 from Group-AF was deleted since it had been concluded that the inner ring failure which generated excessive bearing wear had not been influenced by the variation of any one of the four parameters being studied. The wear results from the remaining twenty tests, which is comprised of seven of Group-N, four of Group-AF, eight of Group-PWA, and the baseline bearing were included in the statistical analysis.

A ranking of the importance of the controlled variables as to their relative influence on both dependent wear parameters was defined using regression and correlation analysis. The results of this analysis are presented in Table 16 with the relative effect of the parameters identified in categories ranging from "very important" to "no consequence." For the dependent variables of both weight loss and skew angle increase the coupled roller end radius runout is the only parameter ranked as "very important." The effects of roller end clearance and L/D are considered as being next most significant in that they had an "important" effect on both wear parameters.

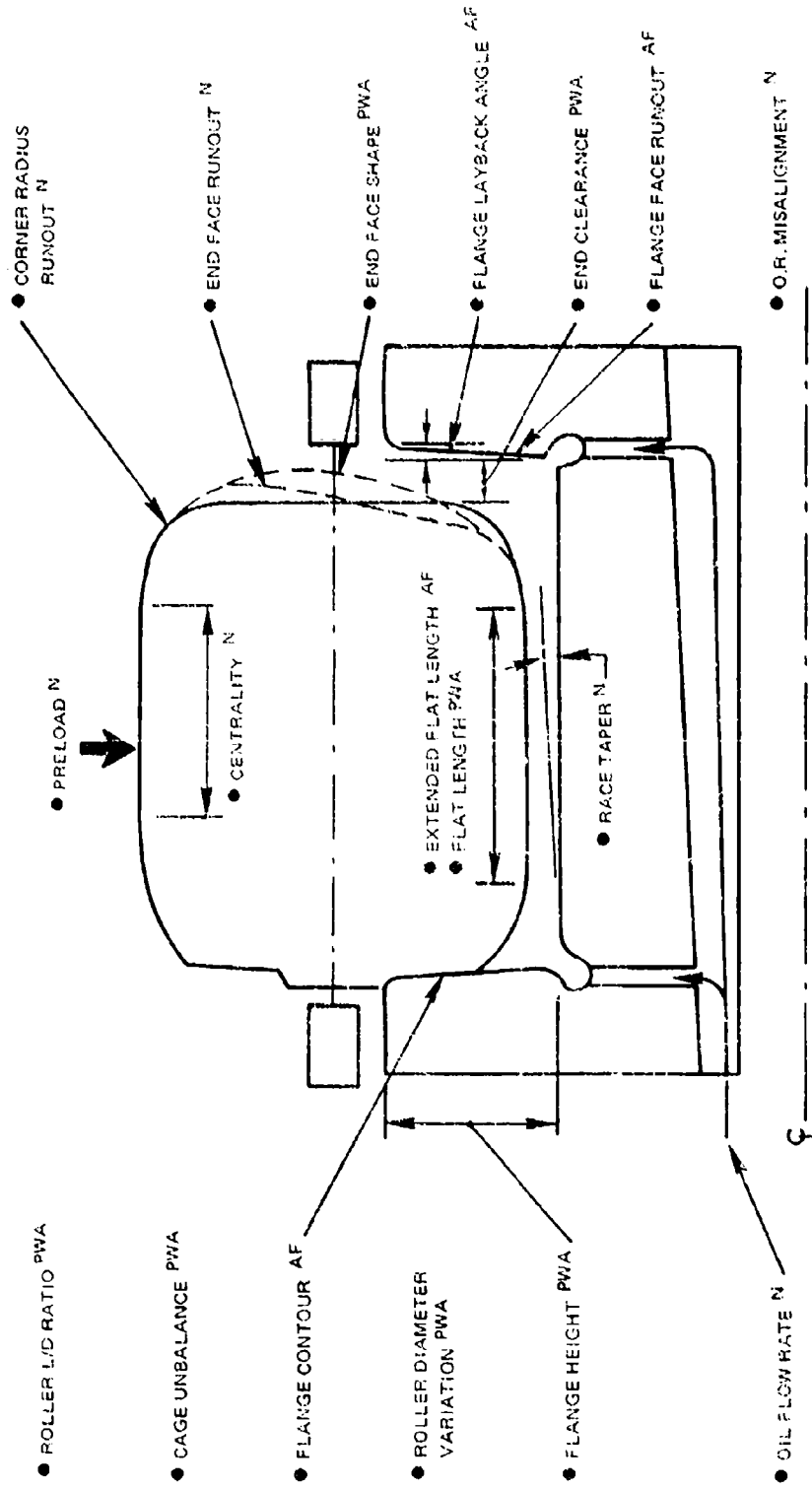
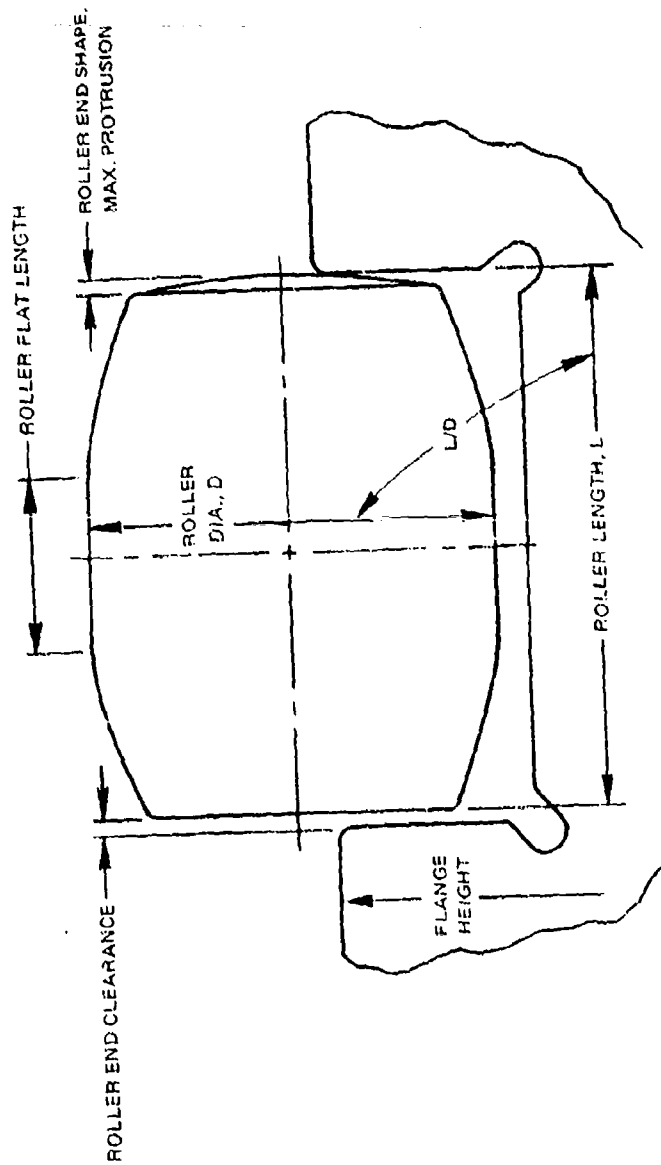


Figure 49: Roller Bearing Variables Experimentally Evaluated in Full-Scale Bearing Tests

TABLE 15. P&WA PARAMETRIC BEARING DESIGNS TESTED



BEARING SERIAL NO.	ROLLER LENGTH/DIA. RATIO, IN./IN.	CAGE UNBALANCE GRAM-CENTIMETER	ROLLER END CLEARANCE INCH	ROLLER END SHAPE, MAX. PROTRUSION, INCH	FLANGE HEIGHT % OF ROLLER DIAMETER	ROLLER DIA. VARIATION PER BEARING, INCH	ROLLER FLAT LENGTH, PERCENT OF ROLLER LENGTH
BASELINE	1.0	3.0	0.001	0.000050	25	0.000050	40
11	1.0	2.0	0.001	0.000050	20	0.000050	0
12	1.0	1.0	0.001	0.000400	20	0.000050	50
13	0.77	2.0	0.001	0.000400	20	0.000500	0
14	0.77	1.0	0.005	0.000050	30	0.000500	50
15	0.77	1.0	0.005	0.000400	30	0.000050	0
16	0.77	2.0	0.005	0.000050	30	0.000500	0
17	1.0	1.0	0.005	0.000400	30	0.000500	50
18	1.0	2.0	0.005	0.000400	30	0.000500	50

TABLE 16. EFFECT OF INDEPENDENT ROLLER BEARING VARIABLES ON WEAR

<i>Level of Significance</i>	<i>Roller Weight Change</i>	<i>Roller Skew Angle Change</i>
Very Important	<ul style="list-style-type: none"> ● Roller End Radius R/O 	<ul style="list-style-type: none"> ● Roller End Radius R/O
Important	<ul style="list-style-type: none"> ● Roller I/D ● Outer Ring Misalignment, O/R ● Inner Race Taper ● Preload 	<ul style="list-style-type: none"> ● Roller End Clearance ● Roller I/D ● Roller Diameter Variation
Moderate	<ul style="list-style-type: none"> ● Roller End Clearance 	
Slight	<ul style="list-style-type: none"> ● Roller End Shape, Max. Protrusion ● IR Guide Flange R/O to Face ● Roller End Squareness 	<ul style="list-style-type: none"> ● Preload ● Outer Ring Misalignment, O/R ● Roller End Squareness ● Inner Race Taper
No Consequence	<ul style="list-style-type: none"> ● Inner Ring Guide Flange Contour ● Roller Flat Centrality ● Lubrication ● Cage Unbalance ● Flange Height ● Roller Diameter Variation ● Roller Flat Length ● Inner Ring Guide Flange Layback 	<ul style="list-style-type: none"> ● Roller Flat Centrality ● Lubrication ● Cage Unbalance ● Roller End Shape, Max. Protrusion ● Flange Height ● Roller Flat Length ● Inner Ring Guide Flange Layback ● Inner Ring Guide Flange Contour ● Inner Ring Guide Flange R/O to Face

7. SIXTY HOUR DEMONSTRATION TEST — TASK III

A 3.0 MDN prototype roller bearing was designed and will be evaluated in a demonstrator rig test with a goal of 60 hours operation over a range of DN values from 2.2 to 3.0M. The information developed under Tasks I and II of the Contract was used in the design of this bearing which incorporates the best levels of both the seven Group-N parameters tested under Task II as well as the seven parameters evaluated under the separate P&WA program. The basis for selecting the parameter levels for use in this prototype bearing was the results of the statistical analysis as summarized in Table 16. In addition, the prototype bearing design incorporates certain other features deemed optimum as based on the analytical studies made under Task I of the Contract. These features include; reduced preload to prevent or minimize the probability of inner ring fractures, tighter fit of the inner ring on the shaft to prevent or minimize the extent of inner ring creep, and decreased roller crown radius as a consequence of selecting a reduced roller L/D ratio.

The levels of the key design parameters for the prototype bearing are presented in Table 17 and were determined as part of this Task III effort. In the design process, the bearing variables that had no effect on roller end wear were maintained at the baseline level. For those variables that showed a positive effect on roller wear, the lower level was selected for the prototype design and for those variables that indicated a negative effect the higher level was selected. An exception to the above procedure was made for the selection of the flange height level. The wear results as shown in Table 16 indicate that the lower level of flange height will result in lower roller wear and should be selected for the prototype design. However, the results as influenced by this variable are confounded with those of roller end clearance in that both of these factors were varied simultaneously in the P&WA test program. Thus, the influence of one cannot be separated from the other. Previous test experience at P&WA, however, indicates that improved roller skew control would result with the 25% baseline value of flange height as compared to that associated with the lower 20% level. Therefore, a 25% flange height was selected for the prototype design. Since the lower level for the other confounded variable of this group, which is roller end clearance, was the same as the baseline value, it was maintained at this level in the prototype design.

Fabrication of two prototype bearings is now in process. It is intended to rig test one bearing for sixty hours over a speed range of 2.2 to 3.0 MDN and the second bearing will be retained as a spare for future use should the first fail to complete the program.

TABLE 17. LIMITS OF THE 3.0 MDN PROTOTYPE BEARING DESIGN COMPARED TO BASELINE BEARINGS

<i>Parameters Evaluated by Test</i>	<i>Prototype Bearing</i>	<i>Baseline Bearing</i>
1. Preload — Outer Ring Out-of-Round	2 Point	2 Point
2. Roller Corner Radius R.O. — Inch	0.0008 Max.	0.001 Max.
3. Roller End Squareness — Inch	120 × 10 ⁻⁶ Max.	120 × 10 ⁻⁶ Max.
4. Inner Race Taper — Minute	0.8 Max.	0.8 Max.
5. Roller Flat Centrality — Inch	0.010 Max.	0.010 Max.
6. Outer Ring Misalignment — Degree	0	0
7. Lubrication Flow — lb/Min.	20	20
8. Roller Length/Dia. Ratio	0.77	1.00
9. Cage Unbalance — Gm-Cm	3.0 Max.	3.0 Max.
10. Roller End Clearance — Inch	0.0008 - 0.0015	0.0008 - 0.0018
11. Roller End Shape, Max. Protrusion — Inch	0 - 400 × 10 ⁻⁶	Not Defined
12. Flange Height — % of Roller Dia.	25	25
13. Roller Dia Variation — Inch	50 × 10 ⁻⁶ Max.	50 × 10 ⁻⁶ Max.
14. Roller Flat Length — % of Roller Length	49 - 60	33 - 49
<i>Parameters Evaluated Analytically</i>		
1. Outer Ring O.D. Out-of-Round — Inch	0.006 - 0.008	0.020 - 0.012
2. Inner Ring Bore — Inch	4.8920 - 4.8917	4.8939 - 4.8936
3. Roller Crown Radius — Inch	18	24

8. PLANNED EXPERIMENTAL PROGRAM

8.1 Prototype Bearing Test

The 3.0 MDN prototype bearing, described in Section 7 and Table 17, will be experimentally evaluated to assess its durability for a period of up to 60 hours. Testing will be conducted over a speed range of 2.2 to 3.0 MDN, with a goal being to obtain at least 30 hours of operation at 3.0 MDN. It is planned to run the 60 hours in the following sequence:

- Ten hours at 2.2 MDN
- Ten hours at 2.5 MDN
- Ten hours at 2.75 MDN
- Thirty hours at 3.0 MDN

It is also planned to periodically interrupt the test to visually inspect the bearings. Should a visual inspection provide evidence of premature distress, the bearing components will be measured which will include determination of both roller weights and static skew angles. These measurements would be compared to those measurements obtained earlier during the pretest inspection. A wear rate vs. time map would then be established.

8.2 Experimental Evaluation of Bearing No. 10

As shown in Figure 25, roller bearing No. 10 is similar in design to bearing No. 8 with both designs containing rollers with a high level of end radius runout. As shown in Table 3, this runout averages 0.0035 inches. Since severe cage failures were obtained with all four of those bearings tested that had high levels of roller and radius runout, bearing No. 10 will be refitted with a new set of rollers which have a minimum level of corner radius runout. The remaining roller geometries and tolerances will be maintained at those levels shown for bearing No. 10 in Figure 25 with the exception of roller flat centrality which will be controlled within 0.010 inch instead of 0.050 inch. This change will provide additional wear data necessary to separate the wear effects of roller end circular runout from those associated with roller flat centrality. The fabrication of the new rollers is in process and when completed bearing No. 10 will be assembled and rig evaluated following the established 10-hour parametric program.

8.3 Model Check Bearing Test

Bearing No. 26 of Group-AF, which is identical in design to bearing No. 22 shown in Figure 26, will be tested for the purpose of verifying the 3.0 MDN analytical model developed under Task I. The bearing will be experimentally evaluated and the data obtained will be analyzed and compared to predictions generated by the 3.0 MDN analytical model. If any sizeable discrepancy is found between the test data and the prediction then the analytical model will be accordingly modified to affect agreement.

8. PLANNED EXPERIMENTAL PROGRAM

8.1 Prototype Bearing Test

The 3.0 MDN prototype bearing, described in Section 7 and Table 17, will be experimentally evaluated to assess its durability for a period of up to 60 hours. Testing will be conducted over a speed range of 2.2 to 3.0 MDN, with a goal being to obtain at least 30 hours of operation at 3.0 MDN. It is planned to run the 60 hours in the following sequence:

- Ten hours at 2.2 MDN
- Ten hours at 2.5 MDN
- Ten hours at 2.75 MDN
- Thirty hours at 3.0 MDN

It is also planned to periodically interrupt the test to visually inspect the bearings. Should a visual inspection provide evidence of premature distress, the bearing components will be measured which will include determination of both roller weights and static skew angles. These measurements would be compared to those measurements obtained earlier during the pretest inspection. A wear rate vs. time map would then be established.

8.2 Experimental Evaluation of Bearing No. 10

As shown in Figure 25, roller bearing No. 10 is similar in design to bearing No. 8 with both designs containing rollers with a high level of end radius runout. As shown in Table 3, this runout averages 0.0035 inches. Since severe cage failures were obtained with all four of those bearings tested that had high levels of roller and radius runout, bearing No. 10 will be refitted with a new set of rollers which have a minimum level of corner radius runout. The remaining roller geometries and tolerances will be maintained at those levels shown for bearing No. 10 in Figure 25 with the exception of roller flat centrality which will be controlled within 0.010 inch instead of 0.050 inch. This change will provide additional wear data necessary to separate the wear effects of roller end circular runout from those associated with roller flat centrality. The fabrication of the new rollers is in process and when completed bearing No. 10 will be assembled and rig evaluated following the established 10-hour parametric program.

8.3 Model Check Bearing Test

Bearing No. 26 of Group-AF, which is identical in design to bearing No. 22 shown in Figure 26, will be tested for the purpose of verifying the 3.0 MDN analytical model developed under Task I. The bearing will be experimentally evaluated and the data obtained will be analyzed and compared to predictions generated by the 3.0 MDN analytical model. If any sizeable discrepancy is found between the test data and the prediction then the analytical model will be accordingly modified to affect agreement.

REFERENCES

1. Schlichting, Hermann, *Boundary Layer Theory*, 4th Ed., McGraw-Hill, N.Y., 1951.
2. Timoshenko, S., *Theory of Elasticity*, 2nd Ed., McGraw-Hill, N.Y., 1951
3. McGrew, J.M., "Design For Wear of Sliding Bearings," ASME Paper No. 74-DE-15.
4. Engel, Peter A., *Impact Wear of Materials*, Elsevier Scientific Pub. Co., Amsterdam, 1976.
5. Koelle, H.H., *Handbook of Astronautical Engineering*, 1st Ed., McGraw-Hill, N.Y., 1961.
6. Thomson, W.T., *Introduction to Space Dynamics*, John Wiley & Sons, N.Y., 1961.
7. Gould, Philip, "Parallel Surface Squeeze Film: The Effect of the Variation of Viscosity with Temperature and Pressure," *Journal of Lubrication Technology*, ASME Transactions, Vol. 89, No. 3, July 1967, pp. 373-382.
8. P&WA Interim Report FR-8615, "Development of Mainshaft High Speed Cylindrical Roller Bearings For Gas Turbine Engines," April 1977.

DISTRIBUTION LIST

	<u>Copies</u>
Commander, Naval Air Systems Command, Department of the Navy, Washington, DC 20361	16
<u>Intra-Command Addressees</u>	
AIR-50174 (2)	AIR-52032 (1)
AIR-06 (1)	AIR-52031 (1)
AIR-536 (1)	AIR-330 (1)
AIR-5364 (1)	AIR-330A (1)
AIR-5364C (1)	AIR-310 (1)
AIR-53645 (1)	AIR-340E (1)
AIR-5362 (1)	AIR-320A (1)
AIR-41117B (1)	
Chief of Naval Material, (Code MAT 08T234 - W. Greenert) Washington, DC 20361	1
Commander Naval Air Development Center (Code 30212 - L. Stallings), Warminster, PA 18974	1
Commanding Officer, Naval Research Laboratory, (Code 6170 - H. Ravner), Department of the Navy, Washington, DC 20375	1
Chief, Office of Naval Research, (Code 473 - R. S. Miller), Arlington, VA 22217	1
Commander, Naval Air Engineering Center, Naval Air Station Lakehurst, (Code 92724 - P. B. Senholz), Lakehurst, NJ 08733	1
Commanding Officer, Naval Air Rework Facility, Naval Air Station North Island (Code 341 - D. Stanley), San Diego, CA 92135	1
Superintendent, Naval Postgraduate School, Monterey, CA 93940	1
Commander, Naval Ship Engineering Center, (Code 6107 - D. C. Metcalf and G. F. Rester), Washington, DC 20362	2
Commander, David W. Taylor Naval Ship Research and Development Center, (Code 2832 - N. Glassman), Annapolis, MD 21402	1
Commander, Naval Weapons Support Center, (Code 70513 - J. A. Parkes), Crane, IN 47522	1
Commanding Officer, Naval Air Propulsion Center, P.O. Box 7176 Trenton, NJ 08628	
	PE4 6
	PE72 20
	AD1 5

	<u>Copies</u>
Defense Documentation Center for Scientific and Technical Information (DDC), Building No. 5, Cameron Station, Alexandria, VA 22314	12
Commander, Robbins Air Force Base, (WRALC/MMIRDA - W. G. Webb) Robbins AFB, Georgia 31093	1
Director, Applied Technology Laboratory, U. S. Army Research and Technology Laboratories (AVRADCOM) (Code - DADL-E-TAP, W. Hudgins) Ft. Eustis, VA 23064	1
Director, U. S. Army Ballistic Research Laboratories, (Code AMXBR-VL/W. Thompson), Aberdeen Proving Ground, MD 21005	1
Director, U. S. Army Air Mobility R&D Lab-Lewis, (Code MS-77-5 E. Bailey), 21000 Brookpark Rd., Cleveland, Ohio 44135	1
Commanding General, Corpus Christi Army Depot, (Code DRSAB-FESI H. Bull), Mail Stop 29, Corpus Christi, TX 78419	1
Commander, U. S. Army Aviation Systems Command (Code DRSAD-LEP Stewart Chen), Box 209 Main Office, St. Louis, MO 63166	1
AFSC Liaison Office, NASA-Lewis Research Center, 21000 Brookpark Rd., MS-501-3, Cleveland, Ohio 44149	1
Administrator, NASA-Lewis Research Center, 21000 Brookpark Rd., Cleveland, Ohio 44135 (Attn: Messrs R. Sliney, L. P. Ludwig and E. Zaretsky)	3
Ampex Corporation, Advanced Technology Division, Attn: Dr. W. A. Gross, MS 3-08, 401 Broadway, Redwood City, Calif. 94063	1
Avco-Lycoming Division, Attn: Peter Lynwander, 550 S. Main Street, Stratford, Conn. 06497	1
The Barden Corporation, Attn: Harold R. Berglund, Dept. 76, 200 Park Ave., Danbury, Conn. 06810	1
Battelle's Columbus Labs, Engineering Systems Department, Attn: Mr. J. Kannel, 505 King Ave., Columbus, Ohio 43201	1
Bell Aerospace Company, Technical Library, Attn: Mrs. Eunice P. Hazleton, P.O. Box 1, Buffalo, New York 14240	1 1
The Bendix Corporation, Research Laboratories, Attn: Dr. W. M. Spurgeon, 20008 Civic Center Dr., Southfield, MI 48076	1 1

Copies

The Boeing Company, Aerospace Group, Attn: Mr. Jan W. Vanwyk, 205540, Box 3999, Seattle, Washington, 98124	1
The Boeing Company, Vertol Division, Attn: A. Lenski, Boeing Center, P.O. Box 16858, Philadelphia, PA 19142	1
Borg-Warner Corporation, Research Center, Attn: Research Library, Wolf and Algonquin Rds., Des Plaines, Ill. 60018	1
Catholic University of America, Attn: Prof. T. Litovitz, Department of Physics, Vitreous State Laboratory, Washington, DC 20017	1
CBS Laboratories, Attn: R. J. Roper, 227 High Ridge Rd., Stamford, Conn. 06905	1
Chevron Research Company, Attn: Mr. Neal W. Furby, P.O. Box 1627, Richmond, California. 94804	1
Coordinating Research Council, Attn: Ms. Lorri Tobman 219 Perimeter Center Parkway; Atlanta, GA 30346	1
Curtiss-Wright Corporation, Wood-Ridge Facility, 1 Passaic Street, Woodridge, N.J. 07075	1
Detroit Diesel Allison, Div. of General Motors, Attn: Library (R. Mallott), P.O. Box 894, Indianapolis, Ind. 46202	1
Eastman Kodak Company, Engineering B-23 Attn: Mr. J. W. John, Kodak Park, Rochester, New York 14650	1
The Fafnir Bearing Co., Attn: H. B. Vandorn, New Britain, Conn. 06050	1
Fairchild Industries, Inc., Fairchild Republic Div., Attn: Henry W. Kleindienst, Conklin St., Farmingdale, New York 11735	1
Ford Motor Company, Scientific Research Labs, Attn: Mrs. L. B. Phillips, P.O. Box 2053, Dearborn, Michigan 48121	1
The Franklin Institute Research Labs., Attn: Mr. John Rumbarger, 20th & The Parkway, Philadelphia, PA 19006	1
The Garrett Corp., AiResearch Manufacturing Div., Attn: Peter Lemstra, 402 S. 36th Street, Phoenix, Arizona 85034	1

Copies

General Dynamics, Convair Aerospace Division, Attn: U. J. Swenney, CH Librarian, P.O. Box 80986, San Diego, Calif. 92112	1
General Dynamics, Convair Aerospace Div. Attn: Technical Library, P.O. Box 748, Fort Worth, Texas 76101	1
General Electric Co., Aircraft Engine Group, Attn: Mr. D. Hester, MS M87, Evendale, Ohio 45215	1
General Electric Co., Aircraft Engine Group, Attn: Mr. John Clark, MS H62, Evendale, Ohio 45212	1
General Electric Co., Corporate Research and Development, Attn: G. R. Fox, Bldg. 57, RM 365, P.O. Box 43, Schenectady, New York 12301	1
General Motors Corporation, Research Laboratories, Attn: Mr. Fred Rounds, 12 Mile and Mound Rds., Warren, MI 48090	1
Georgia Institute of Technology, Attn: Mr. W. O. Winer, Department of Mechanical Engineering, Atlanta, Georgia 30332	1
Robert P. Grey Consulting Engineers., Inc., Attn: M. R. Chasman, Vice President, 200 Grey Creek Drive, Athens, GA 30601	1
Hughes Aircraft Company, Attn: B. W. Campbell, Bldg. 6, MS E110, Centinela and Teale Street, Culver City, CA 90034	1
IIT Research Institute, Attn: Document Library, 10 West 35th Street, Chicago, Ill 60616	1
Industrial Tectonics, Inc., Bearings Division, Attn: H. Signer, Chief Engineer, 18301 S. Santa Fe, Compton, CA 90224	1
International Harvester Company, Solar Division, Attn: Mr. P. A. Pitt, 2200 Pacific Highway, San Diego, CA 92112	1
Jet Propulsion Laboratory, California Institute of Technology, Attn: Library Oper. Gr. (ACQUIS) 4800 Oak Grove Drive, Pasadena, CA 91103	1
Kaman Aerospace Corporation, Attn: R. B. Bossler, Old Windsor Road, Bloomfield, Conn 06002	1
LTV Aerospace Corporation, Vought Aeronautics Co., Attn: Thomas P. McGinty, P.O. Box 5907, Dallas, TX 75222	1

	<u>Copies</u>
LTV Missile & Space Division, Technical Information Center, Attn: T. M. Rozelle, MS B2, P.O. Box 909, Warren, MI 48090	1
Marlin-Rockwell Div. TRW, Attn: MR. H. Munson, 402 Chandler Street, Jamestown, NY 14701	1
The Marquardt Corporation, Attn: Al Malek, MS 3-D8M 16555 Saticoy Street, Van Nuys, CA 91409	1
Massachusetts Institute of Technology, Mechanical Engineering Department, Attn: Prof. B. G. Rightmire, 77 Massachusetts Ave., Cambridge, MA 02139	1
McDonnell Aircraft Co., Attn: Mr. J. M. Sinnett, MS 331, P.O. Box 516, St. Louis, MO 63166	1
Mechanical Technology Inc., Attn: P. Gupta, 968 Albany-Shaker Road, Iatham, New York 12110	1
Midwest Research Institute, Attn: Mr. Vern Hopkins, 425 Volker Blvd., Kansas City, MO 64110	1
Miniature Precision Bearings, Inc., Product Engineering Attn: C. G. Beecher, Dept. 511, Keene, New Hampshire 03451	1
Monsanto Company, Attn: Richard Green, 800 North Lindberg Boulevard, St. Louis, Missouri 63166	1
MSA Research Corporation, Attn: J. W. Mausteller, Evans City, PA 16033	1
Northrup Corporation, Aircraft Division, Attn: Library - H. W. Jones, 3901 West Broadway, Hawthorne, CA 90250	1
North American Rockwell Corp., Rocketdyne Division, Attn: Robert Spies, 6633 Canoga Ave., Canoga Park, CA 91303	1
North American Rockwell Corp., Attn: B. E. White, D/41-096 AJ01, 12212 Lakewood Blvd., Downey, CA 90241	1
North Carolina State University, Attn: Mr. N. W. Comer, P.O. Box 5356, 208 Daniels Hall, Raleigh, North Carolina 27607	1
Oak Ridge National Laboratory, Union Carbide Corporation Attn: A. G. Grindell, P.O. Box Y, Oak Ridge, Tenn 37830	1
PPG Industries, Inc., Tribology Lab., Engineering Div., Attn: Mr. H. R. Gorman, P.O. Box 11472, Pittsburgh, PA 15238	1

	<u>Copies</u>
Pratt & Whitney Aircraft, Attn: Library (L. T. Kress), 400 Main Street, E. Hartford, Conn. 06108	3
Rochester Institute of Technology, Department of Mechanical Engineering, Attn: Dr. Neville Rieger, Gleason Professor, Rochester, NY 14623	1
Rensselaer Polytechnic Institute, Attn: Mr. F. F. Ling, Department of Mechanics, Troy NY 12181	1
Rex Chainbelt, Inc., Bearing Division, Attn: W. G. Looft, P.O. Box F, Downers Grove, Ill. 60515	1
Rocketdyne Division, North American Rockwell, Attn: L. J. Rainey - Head Librarian, 6633 Canoga Ave., Canoga Park, CA 91304	1
Rose-Hulman Institute of Technology, Attn: John J. Coy, Terre Haute, Indiana 47803	1
Shaker Research Corp., Attn: J. M. McGrew, Northway 10 Executive Park, Ballston Lake, NY 12019	1
SKF Industries, Inc., Attn: L. Sibley, Engineering and Research Center, 1100 First Ave., King of Prussia, PA 19406	1
Southwest Research Institute, Attn: Mr. B. B. Baber, 8500 Culebra Rd., San Antonio, Texas 78284	1
Sperry Rand Corporation, Vickers Division, Attn: Mr. Sam Jamieson, Engineering Library, Troy Michigan 48084	1
Sundstrand Aviation, Attn: R. Allen, Dept. 759, 4747 Harrison Ave., Rockford, Ill. 61101	1
TRW, Inc., Engineering Library, Attn: Elizabeth Barrett, 23555 Euclid Ave., Cleveland, Ohio 44117	1
Technological Institute, Attn: H. S. Cheng, Department of Mechanical Engineering, 2145 Sheridan Rd., Evanston Ill 60201	1
Teledyne CAE, Attn: G. Hamburg, 1330 Laksey Rd., Toledo, Ohio 43697	1
The Timken Company, Physical Laboratories, Attn: Pete Orvis, 1835 Dueber Ave., S.W., Canton, Ohio 44706	1

	<u>Copies</u>
Union Carbide Corporation, Attn: Tech. Librarian, P.O. Box 24166, 1500 Polco Street, Indianapolis, Ind. 46224	1
United Technologies Corp., Hamilton Standard Division, Attn: Library, Windsor Locks, Conn 06096	1
University of Virginia, Department of Mechanical Engineering Attn: Dr. E. J. Gunter, Jr., Charlottesville, VA 22903	1
Westinghouse Electric Corp., R&D Laboratories, Attn: Research Library, Beulah Rd., Churchill Borough, Pittsburgh, PA 15235	1
Westinghouse Electric Corp., Aerospace Electrical Div., P.O. Box 989, Attn: A. E. King, Lima, Ohio 45802	1
Westinghouse R&D Center, Attn: Mr. D. J. Boes, Bldg. 501 Rm 3Y68, Beulah Rd., Churchill Boro, Pittsburgh, PA 15235	1
Williams Research Corporation (Attn: J. Paletta), 2280 West Maple Rd., Walled Lake, Michigan 48088	1
Commanding General, Wright-Patterson Air Force Base, Dayton, Ohio 45433	
Code AFAL/TSR	1
AFAPL/CCN	1
AFAPL/DOE (STINFO)	15
AFAPL/DOY (Richard Motasney)	1
AFAPL/POP-1 (Mr. B. L. McFadden, Jr.)	1
AFAPL/POD-2 (Mr. K. E. Binns)	1
AFAPL/SFL	35
AFAPL/XP	1
AFML/LAE/J.J. Sullivan	1
AFML/INE W. Johnson	1
AFML/MBT R. Benzing	1
AFML/MBT Maj. L.L. Fehrenbacher	1
ASD/ENHEA Mr. Ray Bishop	1
ASD/ENJZ Mr. Jim Barrett	1
2750th ABW/SSL	1
FTD/PDTA-4	1
AF Rocket Propulsion Lab., Attn: L. Tepe/LKDS, Edwards Air Force Base, CA 93523	1
HQ AFSC/INA, Andrews Air Force Base, Washington, DC 20334	1
AFSC/DLE, Andrews Air Force Base Washington, DC 20334	1

	<u>Copies</u>
HQ U.S. Air Force, RDPS/Mr. A. Eaffy, Washington, DC 20350	1
Chemical Propulsion Information Agency, The Johns Hopkins University, Attn: Dr. Peter L. Nichols, 8621 Georgia Ave., Silver Spring, MD 20910	1
Defense Supply Agency, Office of Technical Services Dr. John A. Krynitsky, Director, Cameron Station, Alexandria, VA 22314	1
Department of Transportation, Library Service Div., FOB-10A, TAD-494/6, 800 Independence Ave., S.W. Washington, DC 20591	1
FAA HQ, GAO-1, H. Rothen, 800 Independence Ave., S. W. Washington, DC 20591	1
U.S. Atomic Energy Commission, Division of Reactor Development and Technology, Attn: Nicholas Grossman, F-309, Washington, DC 20545	1
Commander, Naval Material Industrial Resources Office, (W.J. Welsch/Code 224) Bldg. 537-2, Phila., PA 19112	1
Commanding Officer, Naval Air Rework Facility, Marine Corps Air Station (Code 332/Mr. M. A. Morgan), Cherry Point, N. C. 28533	1
Bell Helicopter Textron, Plant 5, P.O. Box 482, Attn: R. Battles, Fort Worth, Texas 76101	1
General Electric Co., Attn: Mr. C. Pineo, Bldg. 40 2nd Floor, 1000 Western, Lynn, MA 01905	1
Sikorsky Aircraft, Attn: A. Lemanski, Stratford, Conn. 06602	
Sikorsky Aircraft, Attn: K. Keller, Stratford, CT 06602	3